Longitudinal Analysis of Steel-Concrete Composite Box Girder Decks

Comparison between the Classical Formulations and the Generalized Beam Theory

Luís João Ferreira Vieira

Thesis to obtain the Master of Science Degree in

Civil Engineering

Supervisors: Prof. José Joaquim Costa Branco de Oliveira Pedro
Prof. Rodrigo de Moura Gonçalves

Examination Committee

Chairperson: Prof. António Manuel Figueiredo Pinto da Costa
Supervisor: Prof. José Joaquim Costa Branco de Oliveira Pedro
Member of the Committee: Prof. Pedro Manuel de Castro Borges Dinis

March 2017

ACKNOWLEDGEMENTS

Ao Professor José Oliveira Pedro desejo agradecer pela muita ajuda e grande interesse demonstrados nesta dissertação enquanto orientador e também por todos os ensinamentos valiosos que me deu ao longo do meu percurso universitário.

Ao Professor Rodrigo Gonçalves gostaria de expressar a minha gratidão por toda a disponibilidade e empenho que demonstrou na orientação deste trabalho, assim como pela sua preocupação pelo meu futuro académico e profissional.

Ao Professor Dinar Camotim quero manifestar o meu agradecimento pelos importantes esclarecimentos e úteis sugestões.

À minha mãe e aos meus irmãos quero reconhecer o apoio incansável, a compreensão e a motivação que sempre me transmitiram no decorrer deste trabalho.

Por último, quero agradecer profundamente ao meu pai que desde cedo suscitou em mim um tão grande interesse pela engenharia e me incutiu os valores de trabalho árduo e rigor segundo os quais me guiei.

ABSTRACT

Asymmetrical loads on box girder bridge decks cause not only bending but also torsion with warping and distortion of the cross-section. The latter two may prove to be relevant for the longitudinal analysis and design of the deck but their effects within the overall structural behaviour are difficult to assess using shell finite element models.

The present work is developed around two alternative methods for the longitudinal analysis of steel-concrete composite box girder decks that preserve the structural significance of each main type of cross-section deformation: bending, torsion with warping, distortion and shear lag. The first method covers the prismatic classical bar theories of bending and torsion with warping, the analogy of a beam on an elastic foundation for the analysis of distortion, known as folded plate action, and a simplified semi-empirical methodology for the consideration of the shear lag effect. The second refers to a finite element method based on the Generalized Beam Theory, which is geared towards the longitudinal analysis of homogenous/composite thin-walled prismatic bars.

Comparisons are established between the two methods in terms of theoretical background and numerical results, using two case studies.

Within the analysis of the numerical examples, the influence of intermediate diaphragms to the longitudinal behaviour is investigated, referring particularly to the participation of torsion and distortion deformation modes. Some insightful notes are given concerning the design effects of intermediate diaphragms, and the governing load configurations for box girders deck design.

KEYWORDS

Box girder bridges
Steel-concrete composite bridges
Longitudinal analysis
Classical formulations
Beam on elastic foundation analogy
Generalized Beam Theory

RESUMO

Cargas assimétricas em tabuleiros de pontes em caixão causam não só flexão, mas também torção com empenamento e distorção da secção transversal. Estes últimos podem ser bastante relevantes para a análise longitudinal de tabuleiros em caixão muito deformáveis, mas os seus efeitos não são fáceis de identificar utilizando modelos de elementos finitos de casca.

O presente trabalho desenvolve-se em torno de dois métodos alternativos para a análise longitudinal de tabuleiros em caixão mistos aço-betão que preservam o significado estrutural dos principais modos de deformação: flexão, torção com empenamento, distorção e *shear lag.* O primeiro relaciona-se com as teorias clássicas de barras para a flexão e a torção com empenamento, a analogia de viga em fundação elástica para análise da distorção e uma metodologia semi-empírica simplificada para consideração do efeito de *shear lag. O* segundo refere-se a um método de elementos finitos baseado na Teoria Generalizada de Vigas, que está orientado para a análise longitudinal de barras prismáticas homogéneas/mistas de parede fina.

São estabelecidas comparações entre os dois métodos em termos de fundamentos teóricos e de resultados numéricos para dois casos de estudo.

Na análise de exemplos numéricos é investigada a influência dos diafragmas intermédios para a análise longitudinal, com particular foco na participação dos modos de torção e distorção. São tecidas algumas considerações acerca dos efeitos dos diafragmas intermédios e das configurações de carga condicionantes para o dimensionamento do tabuleiro em caixão.

PALAVRAS-CHAVE

Ponte em caixão
Ponte mista aço-betão
Análise longitudinal
Formulações clássicas
Analogia de viga em fundação elástica
Teoria Generalizada de Vigas

CONTENTS

LIST OF TABLES

LIST OF FIGURES

LIST OF ABREVIATION AND SYMBOLS

ABREVIATIONS

DOF	Degree of freedom
FEM	Finite Element Method
GBT	Generalized Beam Theory

INDEXES AND SPECIAL SYMBOLS

cos	Cosine
$cosh$	Hyperbolic cosine
sin	Sine
$sinh$	Hyperbolic sine
$tanh$	Hyperbolic tangent
$d[\,]$	Infinitesimal portion
$\frac{d^n}{dx^n}[\,]$	n[th] order derivative with respect to variable x
$\int_K [\,]\, dk$	Integral in K with respect to k
$\int_0^s [\,]\, ds$	Integral around the mid-line
$\int_0^{s,cell} [\,]\, ds$	Integral around the cell mid-line
$\oint [\,]\, ds$	Closed integral around the cell mid-line
$[\,]_{,k}$ or $\frac{\partial [\,]}{\partial k}$	Partial derivative with respect to k
$\frac{d[\,]}{dk}$	Derivative with respect to k
$()_b, ()_{b,SL}, ()_w, ()_d$	With respect to bending according to Euler-Bernoulli beam theory for bending, bending accounting shear lag effect, torsion with warping and distortion
$()^L, ()^T$	With respect to longitudinal bending of the plates and to transverse deformation of the cross-section (for the problem of distortion)
$\sum [\,]$	Summation
$[\,]^M, [\,]^F$	With respect to membrane and flexural plate components
$[\,]^t$	Transpose
$\delta[\,]$	Virtual infinitesimal variation

LATIN LETTERS

A	Cross-sectional area; or Generic point along the mid-line of the cross-section
A_f	Cross-sectional area of a flange
A_r	Cross-sectional area of the longitudinal reinforcements within a respective flange width
A_w	Web cross-sectional area
A_0	Area enclosed by the mid-line of the closed contour walls
$\bar{A}, \bar{B}, \bar{C}, \bar{D}$	Auxiliary functions used in the definition of the solution for distortion
$\boldsymbol{B}, \boldsymbol{C}, \boldsymbol{D_1}, \boldsymbol{D_2}$	GBT linear stiffness matrices
B_A	Bimoment in point A (for a general case, index may be omitted)
$\boldsymbol{C_e}$	Constitutive relations operator
C_o	Constant defined in analysis of torsion
C_1, C_2, C_3, C_4	Constants of integration for the solution of torsion with warping
D	Number of GBT deformation modes
E	Young's modulus
E_c,E_s	Young's moduli for concrete and steel
$\boldsymbol{F}$	Force vector in GBT
F_1, F_2, F_3	Lagrange's linear and quadratic hierarchic polynomials
F_A, F_B	Vertical forces in point A and B defined in analogy of a beam on an elastic foundation
F_i	Shear forces between connecting plates
G	Shear modulus; or Centre of mass
G_c, G_s	Shear moduli for concrete and steel
G_k	Characteristic value for permanent loads
H_1, H_2, H_3, H_4	Hermite's cubic interpolation functions
I_x, I_y, I_Z	Moments of inertia with respect to x, y and z axes
I_{yz}	Product of inertia with respect to y and z axes
I_b, I_t, I_w	Cross-sectional moments of inertia of the bottom, top and web flanges
$\overline{I_b}, \overline{I_t}, \overline{I_w}$	Transverse moments of inertia, per unit length, of the bottom, top and web plates
I_c	Central second moment of inertia
$I_{w,e}$	Equivalent moment of inertia of the web plate for the problem of distortion
I_ω	Warping constant
J	Saint-Venant torsional constant
$\boldsymbol{K}$	Global stiffness matrix
L	Length of the beam
L_d	Characteristic length for distortion
M	Generic bending moment

M_A, M_B	Bending moments in point A and B
M_{oA}, M_{oA}	Particular nodal moments in point A and B of the infinite beam (in analogy of a beam on an elastic foundation)
M_t	Applied concentrated torsional moment
M_b, M_t, M_w	Bending moment on the bottom, top and web plates for the problem of distortion
M_y	Bending moment around the y axis (if related with a specific point of application, the index y is omitted and replaced by the designation of the given point)
N	Number of deformation modes
N_b, N_t, N_w	Axial force on the bottom, top and web plates for the problem of distortion
N_w	Number of warping deformation modes;
P	Point auxiliary to the positioning of the shear centre
Q	Concentrated applied load;
Q_k	Characteristic value for concentrated load in Load Model 1
R_b, R_t, R_w	Radius of curvature for longitudinal bending of bottom, top and web plates for the problem of distortion
R_A, R_B	Vertical forces in points A and B
R_{oA}, R_{oA}	Particular nodal vertical forces in point A and B of the infinite beam (in analogy of a beam on an elastic foundation)
R_Z	Radius of curvature around the z axis
S	Mid-line domain
S_d	Diagonal force which produces distortion of the cross-section
$S_{\omega y}, S_{\omega z}$	Sectorial product of inertia with respect to y and z axes
T	Torsional moment; or Concentrated Torsional moment
T_w	Warping torsion component
T_{SV}	Saint-Venant torsion component
$\boldsymbol{U}$	Displacement vector
U_x, U_y, U_z	Components of the displacement vector along x, y and z axes
V	Generic shear force; or Volume
W_{int}, W_{ext}	Internal and external work
X, Y, Z	Global coordinates used in the implementation of GBT finite element
a_0	Length for positioning of a concentrated load along a beam
${a_0}^*$	Complementary Length for positioning of a concentrated load along a beam defined for the solution to the problem of torsion with warping
a_1, a_2, a_3	Lengths for positioning of a distributed load along a beam
a_4, a_5	Auxiliary lengths for definition of the solution for bending according to Euler-Bernoulli beam theory.
b	Total width of the top flange

b_b	Width of the bottom flange
b_e	Effective width of a generic flange
$b_{e,1}, b_{e,2}, b_{e,3}$	Effective width of the interior top, projecting top and bottom flanges
b_t	Width of the top flange within web-flange intersections
b_w	Width of the web flange
c_1, c_2, c_3	Constants of integration for the solution of distortion
$d; \boldsymbol{d}$	Distance between centres of gravity of top and bottom flanges and vector of degrees of freedom
e	Vertical load eccentricity with respect to the web-flange intersection
e_y, e_z	Auxiliary coordinates for definition of the shear centre
$\boldsymbol{f}$	Generic load vector
f_i	Shear flows between connecting plates
f_x, f_y, f_z	Components of a generic load along x, y and z axes
g	Length of the cross-sectional diagonal
k	Additional coefficient for calculation of effectives widths of projecting flange portions; or Transverse stiffness of the frame defined for the problem of distortion
k_1, k_2	Dimensionless parameters defined for the definition of the distortion equilibrium equation
l	Span length
l_i	Length of element i
m_A	Generic moment applied in point A
m_{anti} , m_{sym}	Anti-symmetrical and symmetric parcels of the external bending moment
m_i, n_i	Components of displacement in node i along web mid-line and vertical directions due to deformation of the cross-section
$\overline{m_i}$	Transverse bending moment in point i due to diagonal load
$m^L_{b,d}, m^L_{t,d}, m^L_{w,d}$	Longitudinal bending moments caused by plate distortional loads in bottom, top and web plates, considering each isolated from the others
m_T	Distributed torsional load
n	Steel-concrete homogenisation coefficient
p	Generic vertical load
p_{anti} , p_{sym}	Anti-symmetrical and symmetric parcels of the external force
p_A	Generic force applied in point A
$p_{b,PureT}, p_{t,PureT}, p_{w,PureT}$	Forces of the torsional subsystem in bottom, top and web plates, considering pure torsion
$p_{b,d}, p_{t,d}, p_{w,d}$	Forces of the distortional subsystem in bottom, top and web plates
$p^L_{b,d}, p^L_{t,d}, p^L_{w,d}$	Component of the forces of the distortional subsystem in bottom, top and web plates, which produce longitudinal bending

$p_{b,d}^T, p_{t,d}^T, p_{w,d}^T$	Component of the forces of the distortional subsystem in bottom, top and web plates, which produce transverse deformation of the cross-section
p_d	Generic distortional plate load
p_d^L, p_d^T	Components of the forces of the distortional subsystem which produces longitudinal bending and transverse deformation of the cross-section
q	Uniformly distributed applied load; or shear flow in the walls of the cross-section due to torsion with warping
q_k	Characteristic value ofr the uniformly distributed load in Load Model 1
q_w	Shear flow in the walls of the cross-section due to warping torsion
q_{SV}	Saint-Venant shear flow
r	Tangential radius between shear centre and the mid-line of the cross-section walls
r_b, r_t	Dimensionless ratios defined for the problem of distortion
r_P	Tangential radius between point P and the mid-line of the cross-section walls
s	Coordinate measured along the mid-line of the cross-section walls
t	Thickness of a generic plate
t_b, t_t, t_w	Thicknesses of bottom, top and web plates
${t_t}^S$	Equivalent homogenised thickness of the top plate
u, v, w	Displacements along x, y and z axes
$\bar{u}_k, \bar{v}_k, \bar{z}_k$	Displacement components for mode k
$\widetilde{u_S}$	Normalized unit warping function
x	Longitudinal axis of the box-girder in Classical Formulations; or Coordinate in Classical Formulations; or Longitudinal local axes of the wall in GBT; or Coordinate in GBT
x^*	Complementary longitudinal coordinate defined for the solution to the problem of torsion with warping
y	Horizontal axis of the box-girder cross-section in Classical Formulations; or Coordinate in Classical Formulations; or Mid-line local axis of the wall in GBT; or Coordinate in GBT
y_b, y_t	Distances of the distortional neutral line to the mid-line of bottom and top flanges
z	Vertical axis of the box-girder cross-section in Classical Formulations; or Coordinate in Classical Formulations; or Thickness Local axis of the wall in GBT; or Coordinate in GBT

GREEK LETTERS

α	Stiffener ratio defined for the problem of bending with shear lag ; or factor defined in the constitutive relations of GBT
$\alpha_b, \alpha_t, \beta$	Dimensionless relations defined for the problem of distortion
γ	Shear strain brought by torsion with warping
γ_C, γ_S	Density for reinf steelShear strain brought by torsion with warping
γ_{SV}	Shear strain brought by San-Venant torsion
$\gamma_{xy}, \gamma_{yz}, \gamma_{xz}$	Shear strain components in xy, yz and xz planes
δ	Diagonal deformation of the cross-section
δ_i	Component of the diagonal deformation of the cross-section in node i
$\boldsymbol{\varepsilon}$	Strain vector
ε_w	Warping normal strain
$\varepsilon_{xx}, \varepsilon_{yy}, \varepsilon_{zz}$	Normal strains components along x, y and z axes
ζ	Characteristic length for the problem of torsion with warping
θ	Generic rotation; or Angle between cross-sectional diagonal and horizontal
λ	Parameter used in definition of the solution for the problem of distortion
μ	Warping shear parameter
ν	Poisson's coefficient
ν_C, ν_S	Poisson's coefficient for concrete and steel
ξ_I, ξ_{II}	Auxiliary functions used in the definition of the solution for the problem of distortion
σ_b	Bending normal stress as defined by Euler-Bernoulli beam theory
$\sigma_{b,SL}$	Bending normal stress accounting shear lag effect
$\sigma_{b,SL}^b, \sigma_{b,SL}^t$	Bending normal stress of the bottom and top flanges accounting shear lag effect
$\sigma_{b,SL}^{b,max}, \sigma_{b,SL}^{t,max}$	Maximum bending normal stress of the bottom and top flanges accounting shear lag effect
$\sigma_{i,d}$	Distortional warping normal stress in point i (location may be omitted)
σ_w	Torsional warping normal stress
${\sigma_b}^C, {\sigma_b}^S$	Bending normal stress of the homogenised flange in the heterogeneous and homogenous configurations
${\sigma_{b,SL}}^C, {\sigma_{b,SL}}^S$	Bending normal stress accounting shear lag effect of the homogenised flange in the heterogeneous and homogenous configurations
${\sigma_d}^C, {\sigma_d}^S$	Distortional warping normal stress of the homogenised flange in the heterogeneous and homogenous configurations
${\sigma_w}^C, {\sigma_w}^S$	Torsional warping normal stress of the homogenised flange in the heterogeneous and homogenous configurations
$\sigma_{xx}, \sigma_{yy}, \sigma_{zz}$	Normal stresses along x, y and z axes

τ_{xy}	Shear stress in xy plane
τ_{yz}	Shear stress in yz plane
τ_w	Shear stress due to warping torsion component
τ_{SV}	Shear stress due to uniform torsion component
ϕ	Angle of twist of the cross-section around the shear centre;
φ	Angle between webs and vertical direction
χ	Warping torsion amplitude function
ω_S, ω_P	Sectorial coordinates for the quasi-closed cross-section with respect to shear centre S and point P
$\widetilde{\omega_S}, \widetilde{\omega_P}$	Equivalent sectorial coordinates for the closed cross-section with respect to shear centre S and point P
Γ	Displacements along the intersection of cross-section with the mid-planes of bottom, top and web plates due to distortion
$\Delta_b, \Delta_t, \Delta_w$	Displacements along the intersection of cross-section with the mid-planes of bottom, top and web plates due to distortion
Ξ_U	Auxiliary matrix for definition of the displacement vector in GBT
Ξ_ε	Auxiliary matrix for definition of the strain vector in GBT
$\boldsymbol{\Phi}$	Mode amplitudes vector in GBT
Φ_k	Amplitude function for mode k in GBT
Ψ, $\boldsymbol{\Psi}$	Effective width coefficient for shear lag accountability and longitudinal shape functions matrix
Ω	Mid-plane surface of the girder walls

1. INTRODUCTION

Box girder decks have always been a very popular type of bridge superstructure, mostly due to their structural efficiency provided by high torsional and flexural stiffness with respect to self-weight (Schlaich & Scheef, 1982; Chen & Yen, 1980). In light of the modern-day economical demands, designers have progressively searched to reduce the overall weight and volume of concrete walls and steel plates, leading almost unavoidably to very slender and flexible cross-sections (Pedro, 1995). As a direct consequence, the effects of cross-section out-of-plane (warping) and in-plane deformation (distortion) have become more relevant and should be accounted for.

In unicellular steel-concrete composite box girders subjected to symmetric loads, the longitudinal stresses can usually be very accurately represented by considering the effects of longitudinal bending and, eventually, of shear lag effect if the flanges are wide. For asymmetrical loads, however, cross-section in-plane twisting and deformation take place and generate longitudinal deformation of the plates, leading to the development of additional longitudinal normal stresses. These effects can turn out to be very important to the design verifications of composite box-girders, given the high magnitude of asymmetrical traffic loads of NP EN 1991-2 (European Committee For Standardization, 2005b), especially in the cases of (i) high width-to-height slenderness of the deck cross-section and (ii) diaphragms which are flexible or fairly distanced throughout the span.

The study of torsion and distortion in composite bridge decks is therefore an important issue from a practical standpoint, which is why it has drawn interest by both researchers and designers. However, the analysis of these effects is relatively complex and is usually solved by resorting to shell finite element models that do not allow a clear identification of the different structural effects on the overall behaviour of the bridge deck.

The present work is developed around two alternative methods for the longitudinal analysis of a composite deck that maintain the structural significance of bending, torsion, distortion and shear lag. The first relates to the classical approaches to obtain the longitudinal equilibrium equations and is henceforth designated as the “Classical Formulations”. It encompasses the Euler Beam theory for bending, the warping torsion theory presented by Benscoter (1954) and the folded plate theory based on a beam on elastic foundation analogy first introduced by Wright, Abdel-Samed, & Robinson (1968) as a way of accounting for distortion in box girders. It also contains the simplified method for the determination of the non-linear stress distribution brought by shear lag effect in bending as presented in C; the second method involves the use of the Generalized Beam Theory (GBT), a recently emerging formulation for thin-walled prismatic members which has shown very promising results (Silvestre & Camotim, 2002; Camotim, Basaglia, & Silvestre, 2010; Henriques, Gonçalves, & Camotim, 2015), including for box-girder bridges (Gonçalves & Camotim, 2010), but is still generally unknown to designers. In this theory, it is considered that the overall response of the beam-type structure is described by the superposition of pre-defined cross-section deformation modes (including bending, torsion, distortion and others), whose amplitudes along the longitudinal span are the unknowns left to be determined in the structural analysis.

The aim of this dissertation is therefore to shed some light into these two methods used to perform the longitudinal analysis of box-girder decks, in terms of their formulations, and most especially into the results they provide both in terms of total longitudinal normal stresses and the participations of bending, torsion, distortion and shear lag. There is a specific focus on the analysis of steel-concrete composite box-girders with intermediate diaphragms, whose relevance on the longitudinal profile of the torsional and distortional stresses is well known but not simple to asses. A critical discussion shall be addressed, which will try to identify important aspects from a design point of view, namely the importance of torsion/distortion and of diaphragm spacing.

The work is divided into seven Chapters, namely the present “Introduction” and seven other Chapters:

- Chapter 2 – Reference is given to some of the main methods of analysis for box-girder bridges, namely the Classical Formulation, Finite Strip and Shell Finite Element Methods, and GBT.
- Chapter 3 – The Classical Formulations for bending, torsion with warping and distortion are presented, as well as a simplified methodology for accounting for the shear lag effect. The solutions of the equilibrium equations for the bending, torsion with warping and distortion problems are presented, considering concentrated and distributed loads for simply supported and fixed-end spans.
- Chapter 4 – Defines the fundaments of the GBT, as well as a GBT-enriched finite element and its implementation in MATLAB.
- Chapter 5 – Presents a theoretical comparison between the methods defined in Chapters 3 and 4.
- Chapter 6 – First order analyses are conducted on two numerical examples. The first, concerning a simply concrete box-girder bridge, and a second one, regarding a steel-concrete composite box-girder bridge subjected to standard roadway actions from NP EN 1991-2. For the second example three different situations are considered in terms of diaphragm spacing, to allow investigating their influence in the torsional and distortional stresses. A critical comparison of the two methods is finally presented, based on the results obtained for the two case studies.
- Chapter 7 – Presents the main conclusions of the work and some possible future developments.

2. STRUCTURAL ANALYSIS METHODS FOR STEEL-CONCRETE COMPOSITE BOX GIRDERS

2.1. GENERAL REMARKS

Box girders are currently amongst the most widespread types of bridge superstructures (Schlaich & Scheef, 1982). They are typically composed of an upper plate or deck, a lower plate and two or more web plates, forming a unicellular or multicellular configuration, respectively. In the particular case of steel-concrete composite box girders, the upper deck takes the form of a reinforced concrete slab whereas the webs and bottom flange are usually materialized through steel plates. The existence of a closed cross-section provides high torsional stiffness to these structures, which proves to be very useful in situations where torsional behaviour is a governing factor, such as curved or skewed support bridges. These superstructures are also characterized by having high longitudinal stiffness with respect to their self-weight, making it possible to achieve long spans with shallow depths, which are aesthetically pleasant and more economical solutions (Schlaich & Scheef, 1982, Pedro, 1995).

The behaviour of box girders usually involves significant cross-section in-plane deformation (distortion), thus requiring methods of analysis entailing the simultaneous consideration of both transverse and longitudinal behaviours. Several approaches have been proposed for this purpose, of which reference is made to the following:

1. Classical formulations
2. Finite strip and shell finite element methods
3. Generalized Beam Theory

The following sections briefly describe the main characteristics of the abovementioned methods.

2.2. CLASSICAL FORMULATIONS

Longitudinal stresses in box girders can be determined according to the so called “Classical Formulations” for bending, torsion and distortion. The method described here makes use of a procedure that subdivides the complex problem of “folded plate action” into simpler and more understandable structural analyses regarding bending, torsion and distortion. The method is considered valid for box beams whose length over height slenderness ratios (l/d) are around 4 or higher, if the span lengths l are 1.5 times higher than the deck width b and if local disturbance zones resulting from direct force application are considered separately (Schlaich & Scheef, 1982).

For loads applied symmetrically at the cross-section, transverse and longitudinal analyses can be carried out independently. Beam flexural behaviour is prominent and may or may not take into account the effect of shear deformation of wide flanges, commonly referred to as the shear lag effect.

On the other hand, in the case of asymmetrical transverse loadings, longitudinal and transverse analyses are connected. Eccentric forces cause cross-section in-plane deformation (distortion) and also longitudinal bending of the plates, thus generating longitudinal stresses. This effect is known as distortional warping.

Eccentric loads also induce torsion. Wherever the torsional moment changes, non-uniform torsion also adds up to the longitudinal stress profile. This is usually more relevant in sections near warping restraining supports or in the vicinity of concentrated eccentric loads.

Both distortional and torsional warping cause an increase of the maximum longitudinal stresses, which may or may not be negligible depending on the case at hand.

According to the work by Pedro (1995), and based on the IABSE publication by Schlaich & Scheef (1982), the analysis procedure for a thin-walled box beam subjected to a generic loading, such as the one presented in Figure 2.1, consists of first subdividing the loading according to the following steps:

1) Longitudinal analysis of the beam assuming a rigid cross-section. Vertical and torsional loadings derive from direct integration along the transverse direction. Torsional and bending moment diagrams are obtained, as well as the longitudinal stresses in the cross-section due to bending. If shear lag effects are to be considered, effective widths are calculated so as to determine the modified bending stress distribution.

2) Transverse analysis:
   2.1) Analysis of the top flange considering it to be rigidly fixed at the webs – see Figure 2.1a1. Vertical loads are henceforth replaced by equivalent forces and moments, applied at the top of the webs. In the case of dead loads and distributed live loads, correspondent forces and moments can be deemed uniform in the longitudinal direction. On the other hand, concentrated live loads like those caused by tandem systems are carried through the top flange plate in such a way that the longitudinal distribution of transverse flexural moments is non-linear. This distribution can be obtained by means of influence surfaces or shell/finite strip analysis. As a simplification, one can admit that the vertical load is equivalent to the action of a concentrated load plus a moment, applied at the nearest point of the web plate. If this approach proves to be excessively on the safe side, it is also possible to make use of other simplified models for in-plane load degradation according to the specific case study.[1]
   2.2) Analysis of a strip of longitudinal length $dx = 1$ as a frame subjected to eccentric reactions (m_A, p_A), (m_B, p_B) – Figure 2.1a2:
      2.2.1) Division of the applied point and line loads into symmetric and anti-symmetrical parts

$$p_{sym} = \frac{p_A + p_B}{2} \quad ; \quad p_{anti} = \frac{p_A - p_B}{2} \qquad (2.1)$$

$$m_{sym} = \frac{m_A + m_B}{2} \quad ; \quad m_{anti} = \frac{m_A - m_B}{2} \qquad (2.2)$$

[1] According to a practical example presented by Pedro (1995), it is possible to define the length of uniformly distributed vertical loads and moments, applied at the web and equivalent to the action of an eccentrically concentrated vertical load.

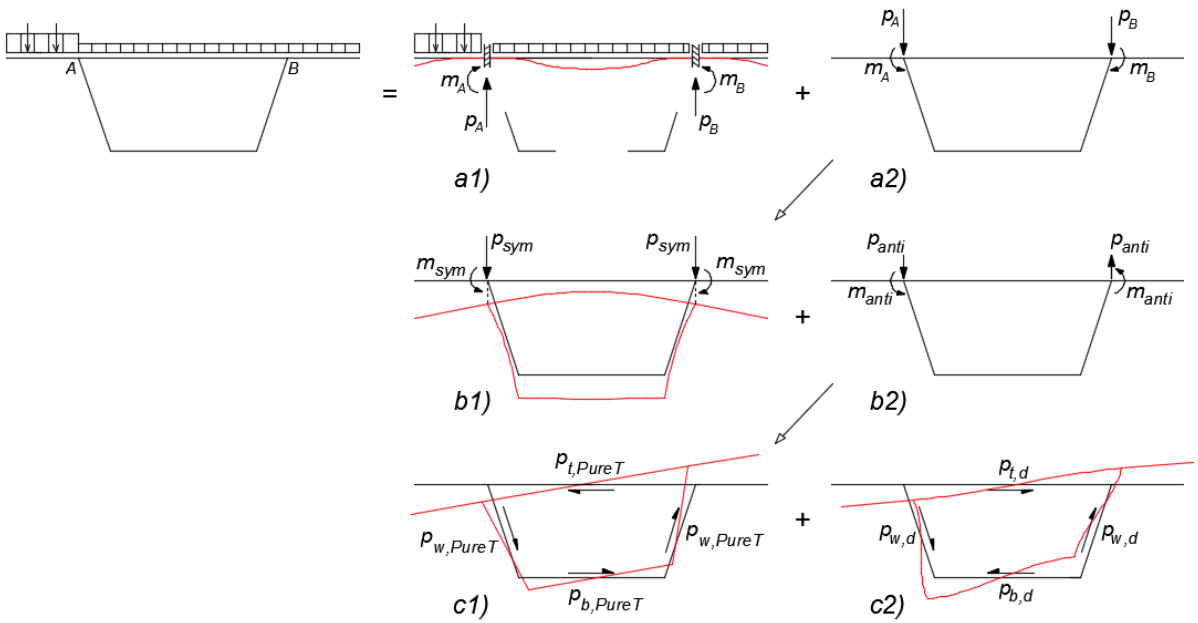

Figure 2.1 – Loading subdivision for a box girder bridge

2.2.2) Calculation of the cross-section symmetric transverse bending. For symmetrical loading, the distribution of the transverse bending moments is hereby obtained by adding these results to those derived in 2.1). The effect of longitudinal bending responsible for rigid body displacement of the cross-section was already taken into account in 1).

2.2.3) Division of the anti-symmetrical parcel into torsional and distortional subsystems. In addition to shear stresses described by St. Venant's uniform torsion theory, the non-uniform torsional component causes longitudinal stresses in the cross-section. These torsional warping stresses may be determined following Benscoter's torsion theory, which contemplates torsion bi-shear (Benscoter, 1954).

2.2.4) Finally, the effects of distortional subsystem must be accounted for. Results are far from exact if the single frame is analysed independently from the remaining structure, since part of the load is carried longitudinally, to the neighbouring frames. Therefore, there is a direct link between transverse deformation of the cross-section and longitudinal bending of the plates, which is obtained through equilibrium and compatibility. It is therefore possible to develop a theoretical model of a beam supported on elastic springs that is intended to replicate the effect of cross-section distortion throughout the span. This analogy was originally proposed by Wright, Abdel-Samed, & Robinson (1968). Analysing the web as a beam on an elastic foundation, one can simultaneously obtain transverse bending moments to be added up to those drawn from 1) and 2.2.2), and longitudinal stresses to be added up with the ones provoked by bending and torsional warping.

2.3. FINITE STRIP AND SHELL FINITE ELEMENT METHODS

Finite strip/shell element methods offer a different approach to the resolution of the problem at hand. The domain of analysis, in this case the box girder bridge, is subdivided into smaller components or 'elements' that are interconnected with each other through 'nodes' or, in the case of finite strips, 'nodal lines' (see Figure 2.2). In the classic displacement-based approaches, the problem degrees of freedom (DOFs) correspond to the displacements and rotations at these nodes/nodal lines. Then, employing interpolation functions for the displacements, elementary stiffness matrices can be constructed. In a similar manner, for each element, applied loads are substituted with equivalent nodal forces and moments, which can be obtained through either virtual work or minimum total energy principles. At this stage, elementary stiffness and load matrices are assembled to form a set of overall equilibrium equations, which can be solved with respect to the defined DOFs. Having determined the displacement field, longitudinal strains and stresses are calculated through differentiation of the displacement field and using the constitutive relations.

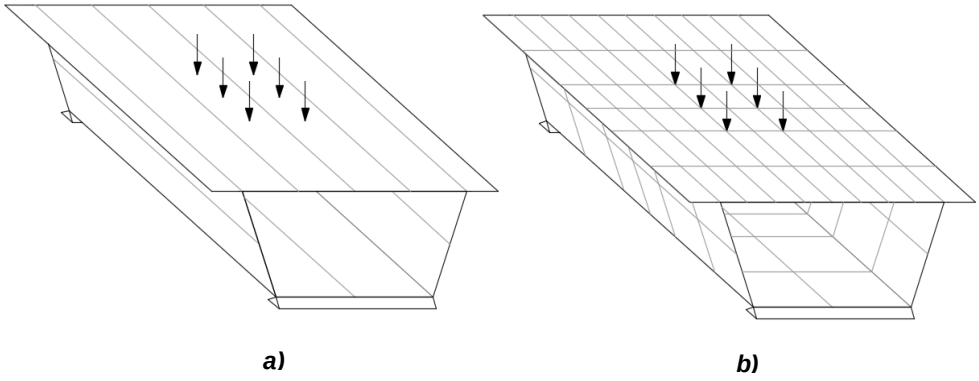

Figure 2.2 – a) Finite strip and b) shell finite element model schematizations

When dealing with shell finite elements, bridge models often involve a very large number of elements and generate a high volume of information to be analysed and post-processed. Moreover, a higher refinement of the mesh must be adopted in zones of higher disturbance, namely where geometry or loading vary rapidly, in order to capture accurately these effects.

Even for structures having regular geometries and simple boundary conditions, a full shell finite element model quickly becomes prohibitive as the DOF numbers increase. The finite strip method may be more adequate in some cases, as it takes advantage of the prismatic nature of the superstructure and, in some cases, of semi-analytical solutions, to reduce the computational effort. The bridge is divided into strips whose displacements along the longitudinal and transverse directions are described by trigonometrical (Fourier series) and polynomial functions, respectively.

Although it was initially meant for straight simply supported beams, it is now possible to apply the finite strip method to other cases such as, for example, continuous span bridges or even curved bridges, adopting some necessary simplifications. Nonetheless, it presupposes a constant cross-section along the longitudinal direction, which presents itself the method's greatest drawback.

Further information on the shell finite element method and the finite strip element method can be respectively found in Zienkiewicz, Taylor, & Zhu, (2005) and Y.K.Cheung (1976).

2.4. GENERALIZED BEAM THEORY (GBT)

Generalized Beam Theory, or GBT, provides an intermediate approach between those present in shell finite and finite strip element methods and classical beam formulations. It employs a set of plausible simplifying hypothesis that permit the development of an efficient thin-walled beam theory considering both cross-section in-plane and out-of-plane (warping) deformation. This theory is therefore valid for box girder bridges as long as their plates can be classified as thin-walled.

According to GBT, the deformed configuration of a beam is expressed as a linear combination of pre-established cross-section 'deformation modes' (see Figure 2.3) whose amplitude functions along the member axis are left to be determined. These may include global modes (as those commonly dealt with in classical beam theories: axial extension, major and minor axes bending and torsion around the shear centre) as well as other configurations such as for example distortion, local-plate, transverse extension or shear modes, which are often neglected in classical analyses.

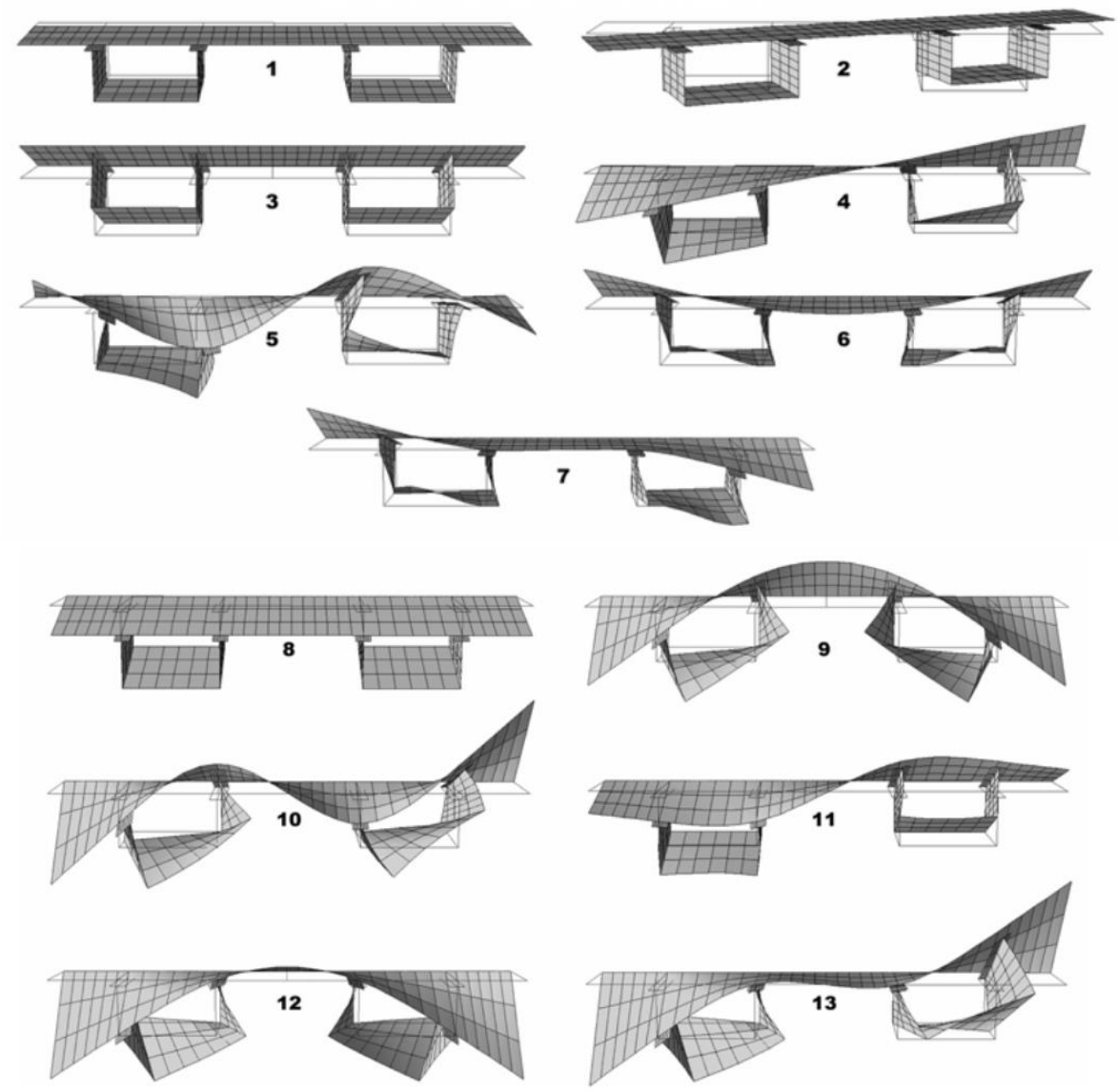

Figure 2.3 – Deformation modes for a Steel-Concrete composite multicellular box girder. (Gonçalves & Camotim, 2010)

Compared to the finite strip and shell finite element methods, GBT offers a clearer insight into the overall structural behaviour of a thin-walled beam, since the contribution of the individual modes and their relative importance can be readily assessed by inspecting the amplitude functions of the individual modes (see Figure 2.4). At the same time, for linear problems, one can usually arrive at sufficiently accurate solutions with a fraction of the computational effort involved in equivalent finite strip or shell finite element analysis. This is a direct consequence of the imposed simplifying hypothesis to the stress and strain fields, which reduce the number of admissible deformation modes and, consequently, the number of degrees of freedom.

Even so, GBT's simplifying hypothesis are less limiting than those in which Classical Formulations are set upon, making it a more general and accurate tool. Furthermore, even though the classical approach also offers the possibility to calculate the participation associated with each mode, it is somewhat restricted to those few standard deformation modes. A theoretical comparison between the two methods shall be addressed in more detail in chapter 5.

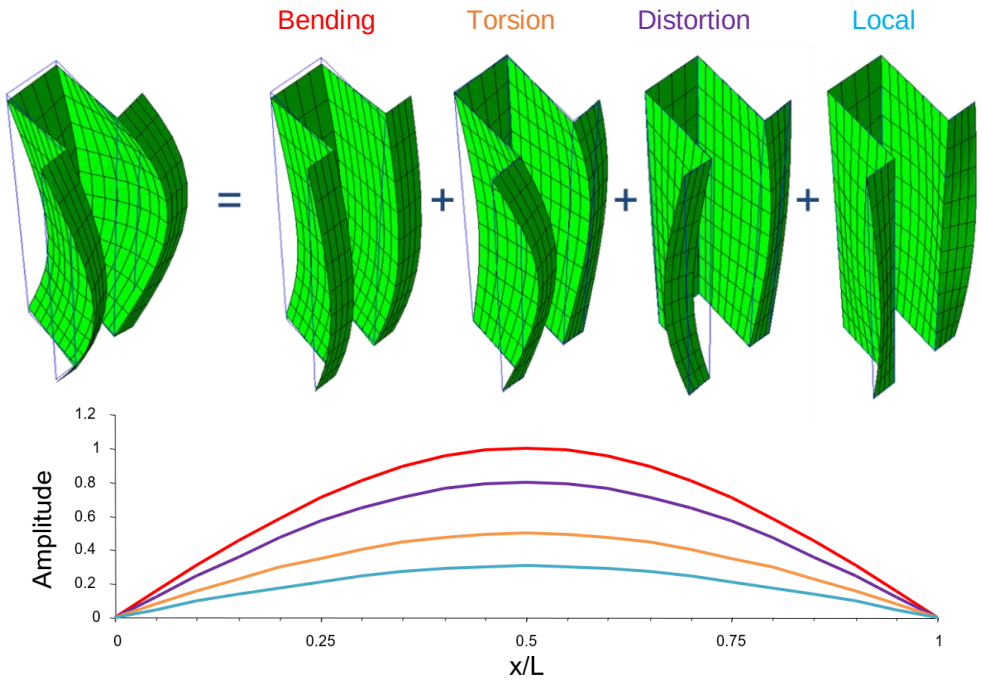

Figure 2.4 – GBT modal decomposition (adapted from Gonçalves (2014))

The first step of a GBT-based analysis is the definition of the deformation modes. Several papers have contributed in this field for polygonal shaped arbitrary cross-sections, (see for example Gonçalves, Ritto-Corrêa, & Camotim (2010), Gonçalves, Bebiano, & Camotim (2014) and Bebiano, Gonçalves, & Camotim (2015)). Having determined the deformation modes, as well as their associated stiffness properties, one is left to obtain the longitudinal amplitude functions of each mode. This can be done either analytically (in particular cases only) or by means of a finite element formulation, similar to the one described in Section 2.3. The deformed configuration of the structure is finally obtained by superposition of the deformation modes multiplied by their corresponding amplitude functions. Strains can be calculated by means of displacement field differentiation and stresses are then obtained using the constitutive relations.

3. CLASSICAL FORMULATIONS

3.1. INTRODUCTION

This chapter presents the analysis methods mostly based on theoretical classical formulations for bending, torsion and distortion. Despite the simplifications and complexity of the physical phenomenon, they can be more reliable and clearer at a pre-design stage than other methods such as finite strip and shell finite element methods which involve sorting through high volumes of data, and therefore are more likely to produce errors in the evaluation of their results (Schlaich & Scheef, 1982).

The chapter is divided in two distinct parts. The first refers to the longitudinal analysis of a box girder subjected to bending, where reference is made to the consideration of shear lag effects according to the definition of effective widths. Then, the longitudinal and transverse behaviours of the box girder acted by eccentric loads are deduced, examining the effects of torsion and distortion.

This type of approach is guided towards the analysis of homogenous box girders, i.e. box girders with a single material, for which steel-concrete composite box girders fall out of scope. The simplest and most common way to solve this problem is to use the concept of homogenisation through which the heterogeneous cross-section is substituted with one composed of a single material (see Figure 3.1). The process of homogenisation depends on the structural phenomenon at hand. Hence, the following subchapters include sections dedicated to the homogenisation rules for each separate sub-analysis.

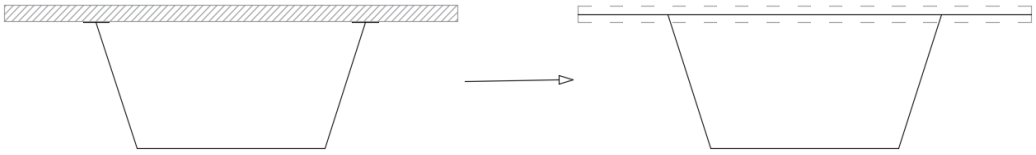

Figure 3.1 – a) Typical cross-section of a steel-concrete composite box girder and b) equivalent homogenised cross-section

The reinforced concrete deck is also, by itself, heterogeneous. The existence of reinforcement bars, distributed along both the longitudinal and transverse directions, alter the properties of the concrete plate. However, according to Chen & Yen (1980), the orthotropic properties of the concrete deck have little effect on the flexural stresses. Consequently, in the present dissertation, the upper flange will be taken approximately as a non-cracked and non-reinforced slab. This assumption is commonly accepted in service conditions of prestressed concrete decks, but it should be well evaluated for the case of composite decks, where the slab over the supports may be partially cracked. The behaviour of composite box girders is also highly influenced by slip in the steel-concrete interface. This connection is usually ensured by steel shear studs, welded to the steel flanges and distributed along the longitudinal and transverse direction. In the present study, it is assumed that longitudinal slip does not occur or its effect is negligible.

The following sections are mostly based on the work developed by Pedro (1995), who presented nearly identical formulations for the analysis of the distortional warping stresses and applied to concrete box girder bridge decks analysis. Additional references are given at each section.

3.2. BENDING ANALYSIS FOR BOX GIRDERS

3.2.1. Elastic bending

Acting loads on box girder bridges are responsible for the development of longitudinal stresses, mostly due to longitudinal bending. The ratio of the cross-sectional dimensions to the span length permit it to be considered as slender prismatic bar, thus allowing for elastic bending behaviour to be determined according to Euler-Bernoulli theory.

Following some simplifying hypotheses, it is possible to arrive at the differential beam equation for linear elastic bending. These results are valid only for the homogenised box girder in accordance to section 3.2.1.3.

3.2.1.1. Hypotheses

The hypotheses assumed when analysing the box girder are as follows:

A1. Prismatic girder;

A2. Homogenous and isotropic elastic material in accordance with Hooke's law;

A3. Plane sections remain plane and normal to the axis of the beam – Bernoulli's Hypothesis;

A4. Sections are free to deform in their own plane, i.e. $\sigma_{yy} = \sigma_{zz} = \tau_{yz} = 0$ – Navier's Hypothesis.

3.2.1.2. Bending equation

Let us consider a box girder subjected to a total symmetrical vertical load *p*(x), such as the one in Figure 3.2.

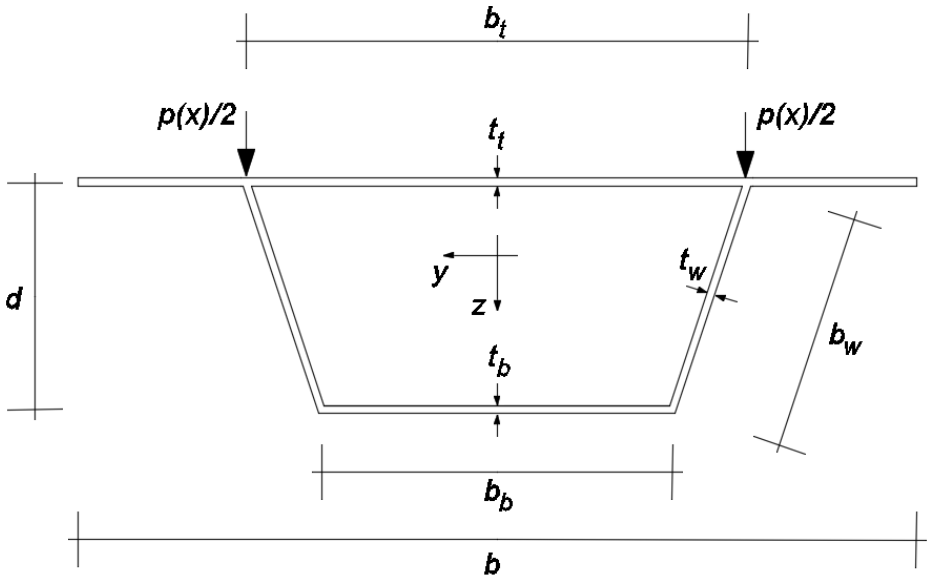

Figure 3.2 – Generic box beam cross-section subjected to symmetrical vertical loads on top of the webs

Based on Bernoulli's hypothesis, for an infinitesimal length the longitudinal deformation of any point of the cross-section is given by

$$\varepsilon_{xx} = \frac{z}{R_z} \ , \tag{3.1}$$

where z refers to the downwards vertical coordinate relative to the centre of gravity and R_z is the radius of curvature, positive as shown in Figure 3.3.

In accordance with Hooke's law, using Navier's hypothesis and making use of the Young's modulus E, the longitudinal stress due to bending derives as:

$$\sigma_b = \varepsilon_{xx} E = \frac{E}{R_z} z \ . \tag{3.2}$$

Considering that the vertical load will not produce any axial force, N, it can be shown that the cross-section region where strain is null, designated as neutral axis, passes through the centre of gravity, since

$$N = \int_A \sigma_b \, dA = \int_A \frac{E}{R_z} z \, dA = \frac{E}{R_z} \int_A z \, dA = 0 \ . \tag{3.3}$$

Hence, the longitudinal stresses should solely equilibrate the bending moment M_y produced by the external loading:

$$M_y = \int_A \sigma_b \, z \, dA = \int_A \frac{E}{R_z} z^2 = \frac{E I_y}{R_z} \ , \tag{3.4}$$

where I_y is hereby defined as the second moment of inertia around the y axis, expressed as

$$I_y = \int_A z^2 \, dA \ . \tag{3.5}$$

Combining (3.2) and (3.4), the equilibrium equation between bending moment and the longitudinal stress at any given point of the cross-section is therefore defined by

$$\sigma_b = \frac{M_z}{I_y} z \ . \tag{3.6}$$

Let us now consider the deformed shape of the beam as approximated by Figure 3.3a. From differential geometry and assuming that the displacements are small, it can be said that

$$\frac{1}{R_z} = -\frac{v_{,xx}}{\left[1 + v_{,x}{}^2\right]^{\frac{3}{2}}} \approx -v_{,xx} = \frac{M_y}{E \, I_y} \ , \tag{3.7}$$

in which v is the displacement of the centre of gravity along the vertical z axis and $v_{,x}$ and $v_{,xx}$ are the first and second derivatives along the axial direction, respectively.

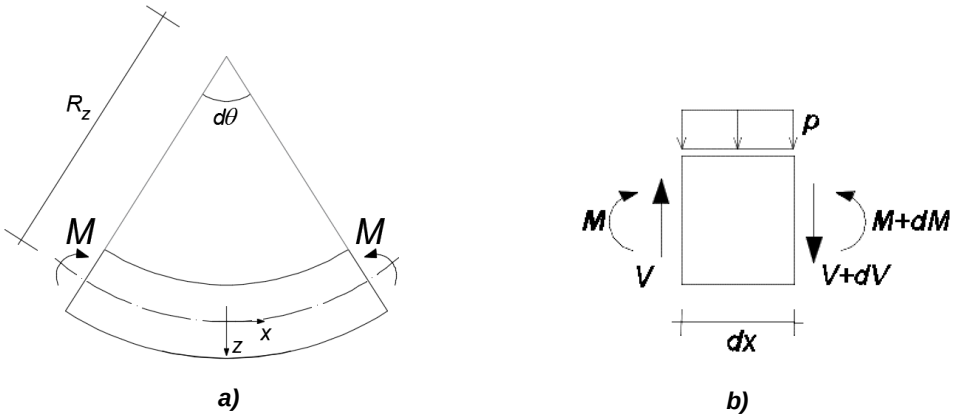

Figure 3.3 – a) Deformed shape of a beam subjected to bending moment and b) static equilibrium of a segment of beam subjected to vertical loads

Performing the static equilibrium of an infinitesimal segment of beam subjected to the generic vertical load $p(x)$ (see Figure 3.3b) comes

$$p(x) = -\frac{dV}{dx} \;\; ; \;\; V(x) = \frac{dM}{dx} \; . \tag{3.8}$$

Through equations (3.7) and (3.8), the simplified Euler-Bernoulli beam equation for bending is given as

$$\frac{d^4 v}{dx^4} \, EI_y = \; p(x) \; . \tag{3.9}$$

3.2.1.3. Homogenisation rules for elastic bending in steel-concrete composite box girders

The Euler-Bernoulli Beam Theory here presented presupposes that the beam is made of a homogenous material and therefore cannot be used directly for steel-concrete composite box girders. However, through correlation of material stiffness properties, it is possible to transform the steel-concrete box girder into an equivalent homogenous box girder in which reference is made to one of the materials. In common practice, the concrete deck of thickness t_t is usually replaced by a steel plate of thickness ${t_t}^S$, as previously shown in Figure 3.1. It is easy to show that (see Calgaro & Virlogeux (1988)), the homogenisation coefficient for bending is dependent on the ratio between Young's modulus of steel, E_s, and of reinforced concrete, E_c as follows

$$\left(\frac{t_t}{{t_t}^S}\right)_b = \frac{E_s}{E_c} = n \; . \tag{3.10}$$

For plates made from the reference material, in this case steel, equation (3.6) can be applied directly. For the concrete deck however, the homogenisation coefficient should take place such that:

$${\sigma_b}^C = \frac{{\sigma_b}^S}{n} = \frac{M_y}{n \, I_y} \, z \; . \tag{3.11}$$

3.2.2. Shear lag effect

The elastic bending theory is exact for pure bending, since the shear forces are null. For common situations, however, shear stresses exist that in turn are responsible for cross-section deformation, including warping. Plane cross-sections thus no longer remain plane so Bernoulli's hypothesis and consequently the theory are no longer exact, even though they provide a good first approximation.

When shear deformability of the cross-section is considered, the longitudinal stress diagram in wide flanges changes with respect to the one resulting from Euler-Bernoulli beam theory as a result of the so-called shear lag effect. As illustrated in Figure 3.4, the stresses increase in regions close to the web-flange junctions and decrease with the distance to these junctions. The ratio between the maximum and mean stresses in the cross-section has been proven to be sufficiently relevant in elastic analysis of cross-sections, in the vicinity of concentrated loads and with high ratios of the flange width-to-span length (Chen & Yen, 1980)[2]. It may eventually prove to be especially meaningful for fatigue and serviceability verifications (Salama & Nassif, 2011).

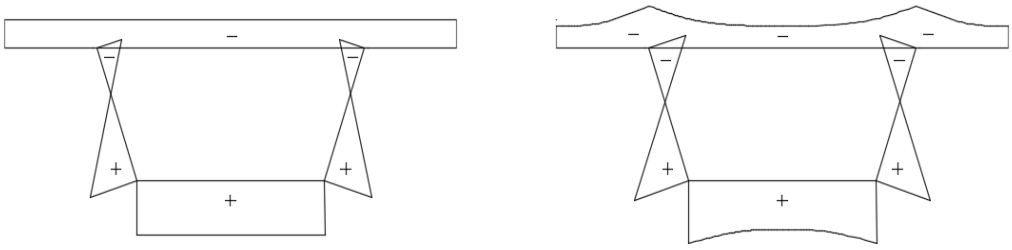

Figure 3.4 – Longitudinal bending stresses a) without shear lag effect and b) with shear lag effect

The traditional method of accounting for the effect of shear lag consists in calculating the cross-section properties using effective (reduced) widths for the wide flanges. More than one definition can be used for evaluating these parameters. In this work, reference is made to the approach followed in (B.S.I., 2004), which is related with the stress distribution. Here, the effective width is considered to be the width that sustains a force equal to that in the actual flange, assuming the longitudinal stresses to be at the same time constant and equal to the maximum longitudinal stress of the non-linear stress distribution (Castro, Elghazouli, & Izzuddin, 2007). Having evaluating these maximum values, one can obtain the stresses in the whole cross-section through analytical expressions (Lamas, 1982).

Calculating effective widths offers a much more practical approach in comparison to determining analytical solutions for the normal stress distribution[3]. These usually involve complex equations and use several approximations that limit their application to some typical cases.

[2] While assessing effective slab widths in composite beams, Castro, Elghazouli, & Izzuddin (2007) presented clear evidence that, if material nonlinearity is taken into account, stress redistribution occurs and the shear lag effect is significantly diminished. Similar conclusions were obtained in Henriques, Gonçalves, & Camotim (2015).

[3] Some analytical expressions for the determination of longitudinal stress distributions in composite steel-concrete box girders may be found in Chen & Yen (1980).

3.2.2.1. Effective Width

The determination of the longitudinal stresses in a span of a box girder considering the shear lag effect may be achieved by first considering an equivalent cross-section (see Figure 3.5) with flanges reduced to their effective widths, such that

$$\frac{b_e}{b} = \frac{\sigma_b}{\sigma_{b,SL}^{max}} = \Psi \ , \qquad (3.12)$$

in which Ψ is the effective width coefficient or ratio, and σ_b and $\sigma_{b,SL}^{max}$ are the mean and maximum longitudinal stresses, respectively.

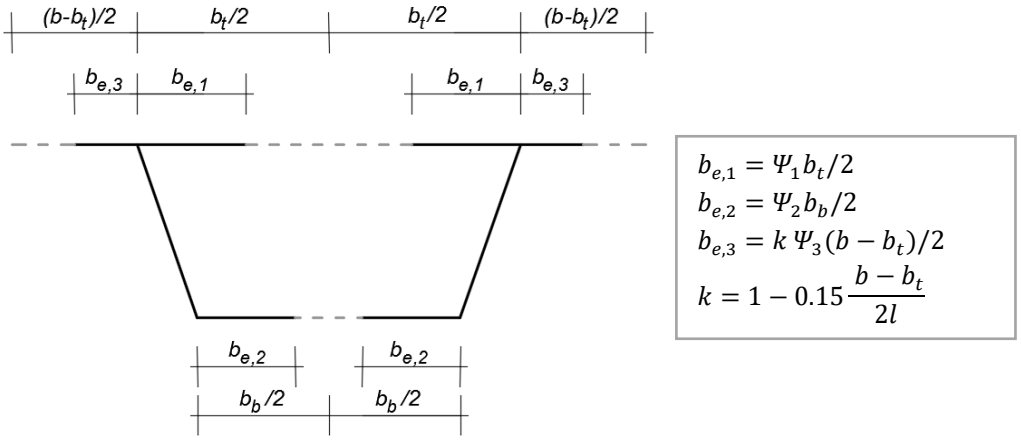

Figure 3.5 – Effective cross-section for a box girder bridge

The effective width coefficient mainly depends on the following aspects:

1. Ratio width/length of the flange segment $(b_t; b_b; b - b_t)/(2\,l)$
2. Type of load (concentrated or distributed)
3. Support conditions
4. Stiffener ratio α[4] defined by

$$\alpha = \frac{A_r}{A_f} \ , \qquad (3.13)$$

in which A_r and A_f are the cross-sectional areas of the longitudinal stiffeners and of the corresponding flange, respectively, along the width $\left(\frac{b_t}{2}; \frac{b_b}{2}; \frac{b-b_t}{2}\right)$.

Taking into account the previous parameters, c proposes a set of effective width coefficients Ψ which are presented in Table 3.1 and Table 3.2[5]. Although they were obtained for distributed uniform loads along the entire span, the code indicates that they should also be employed for standard highway or railway loads, including wheel and axle loads. For flange portions projecting beyond an outer web, these should also be affected of an additional coefficient $k = [1 - 0.15\ (b - b_t)/(2\,l)]$.

[4] Research has shown that the extent of shear lag within a flange plate is dependent on the ratio between the axial stiffness and the shear stiffness of the plate. The introduction of longitudinal stiffeners increases the axial stiffness without changing the shear stiffness so that there is a consequent increase in shear lag (Křistek, 2004).

[5] For composite box girders, the effective cross-section should be calculated in accordance with the same effective width coefficients with the exception of concrete flanges under tension which are assumed to be cracked. In such cases, the mean effective width Ψ should be modified by adding $(1 - \Psi)/3$ (B.S.I., 2005).

The effective width ratios Ψ for intermediate values of $(b_t; b_b; b - b_t)/(2\,l)$ and α may be obtained by linear interpolation. The same can be done for intermediate positions in the span.

Table 3.1 – Effective width ratio Ψ for simply supported beams. (B.S.I., 2004)

$\frac{b}{L}$	Mid-span		Quarter-span		Support	
	$\alpha = 0$	$\alpha = 1$	$\alpha = 0$	$\alpha = 1$	$\alpha = 0$	$\alpha = 1$
0.00	1.00	1.00	1.00	1.00	1.00	1.00
0.05	0.98	0.97	0.98	0.96	0.84	0.77
0.10	0.95	0.89	0.93	0.86	0.70	0.60
0.20	0.81	0.67	0.77	0.62	0.52	0.38
0.30	0.66	0.47	0.61	0.44	0.40	0.28
0.40	0.50	0.35	0.46	0.32	0.32	0.22
0.50	0.38	0.28	0.36	0.25	0.27	0.18
0.75	0.22	0.17	0.20	0.16	0.17	0.12
1.00	0.16	0.12	0.15	0.11	0.12	0.09

Table 3.2 – Effective width ratio Ψ for fixed-ended beams. (B.S.I., 2004)

$\frac{b}{L}$	Mid-span		Quarter-span		Support	
	$\alpha = 0$	$\alpha = 1$	$\alpha = 0$	$\alpha = 1$	$\alpha = 0$	$\alpha = 1$
0.00	1.00	1.00	1.00	1.00	1.00	1.00
0.05	0.96	0.91	0.85	0.76	0.58	0.50
0.10	0.86	0.72	0.68	0.55	0.41	0.32
0.20	0.58	0.40	0.42	0.31	0.24	0.17
0.30	0.38	0.27	0.30	0.20	0.15	0.11
0.40	0.24	0.18	0.21	0.14	0.12	0.08
0.50	0.20	0.14	0.16	0.11	0.11	0.07
0.75	0.15	0.10	0.10	0.08	0.09	0.06
1.00	0.13	0.09	0.09	0.07	0.07	0.05

With the effective cross-section fully defined, the maximum longitudinal stresses at the top and bottom flange-web intersections can be retrieved taking advantage of the results from standard Euler-Bernoulli beam theory so that:

$$\sigma_{b,SL}^{t,max} = \sigma_b^t \frac{b}{2(b_{e,1} + b_{e,3})}\,, \tag{3.14}$$

$$\sigma_{b,SL}^{b,max} = \sigma_b^b \frac{b_b}{2b_{e,2}}\,. \tag{3.15}$$

Finally, the non-linear stress distribution of the whole cross-section may be approximately calculated through the expressions presented in B.S. 5400 Part 3 (2004), where y is the distance to the web-flange intersection (see Figure 3.6):

Interior top flange:

$$\sigma_{b,SL}^{t} = \sigma_{b,SL}^{t,max}\left[\left(\frac{b_t - 2y}{b_t}\right)^4 + 0.25(5\,\Psi_1 - 1)\left(1 - \left(\frac{b_t - 2y}{b_t}\right)^4\right)\right] \tag{3.16}$$

Projecting top flange:

$$\sigma_{b,SL}^{t} = \sigma_{b,SL}^{t,max}\left[\left(\frac{(b - b_t) - 2y}{(b - b_t)}\right)^4 + 0.25(5k\Psi_3 - 1)\left(1 - \left(\frac{(b - b_t) - 2y}{(b - b_t)}\right)^4\right)\right] \tag{3.17}$$

Bottom flange:

$$\sigma_{b,SL}^{b} = \sigma_{b,SL}^{b,max}\left[\left(\frac{b_b - 2y}{b_b}\right)^4 + 0.25(5\,\Psi_1 - 1)\left(1 - \left(\frac{b_b - 2y}{b_b}\right)^4\right)\right] \tag{3.18}$$

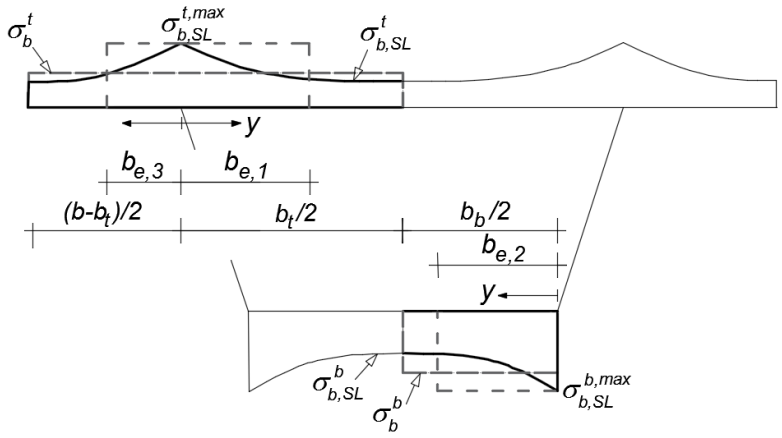

Figure 3.6 – Non-linear distribution of the longitudinal bending stresses in top and bottom flanges

3.2.2.2. Homogenisation rules for elastic bending accounting shear lag in steel-concrete composite box girders

Even though the stress distribution of normal stresses is non-linear, the shear lag phenomenon itself is nonetheless a phenomenon that manifests itself even in linear elastic problems (Lamas, 1982). The shear stiffness of the cross-sections' plates in a plane stress state is directly proportional to the shear modulus G. For this reason, when formulating analytical expressions for bending in steel-concrete composite box girders accounting with shear deformability, Chen & Yen (1980) assumed that the shear behaviour can be translated using an equivalent thickness for the concrete deck such that

$$\left(\frac{t_t}{{t_t}^S}\right)_{b,SL} = \frac{G_s}{G_c} = \frac{E_s}{E_c}\frac{1+\upsilon_c}{1+\upsilon_s} \ . \tag{3.19}$$

If one takes common values for the Poisson's ratio for both steel and concrete – assuming the latter is uncracked – the equivalence coefficient can be approximated by

$$\left(\frac{t_t}{{t_t}^S}\right)_{b,SL} = \frac{E_s}{E_c}\frac{1+\upsilon_c}{1+\upsilon_s} \approx \frac{E_s}{E_c}\frac{1+0.2}{1+0.3} \approx \frac{E_s}{E_c} = n \ . \tag{3.20}$$

Considering the concrete to be uncracked is evidently a limiting hypothesis, namely for regions of negative bending moments, where the concrete slab of a composite deck is under longitudinal tension. Chen & Yen (1980) have proposed to approximately circumvent this limitation by assuming a partial concrete thickness. However, it involves a fair degree of approximation seeing as cracking does not develop solely in the longitudinal or transversal direction, making this a more complex phenomenon which will not be discussed within the present dissertation.

Normal stresses in the top plate can be reported back to the original material as follows:

$${\sigma_{b,SL}}^C = \frac{{\sigma_{b,SL}}^S}{n} \ . \tag{3.21}$$

3.3. TORSION-DISTORTION ANALYSIS OF BOX GIRDERS

Generic moving loads acting on a bridge deck are often asymmetrical with respect to the bridge axis and induce not only bending but also torsion and distortion. Torsional behaviour of closed cross-sectioned elements, such as box girders, can be split into three separate effects (Kollbrunner&Basler, 1969):

- Uniform torsion or Saint-Venant torsion
- Non-uniform or Warping torsion
- Distortion

The first two mechanisms develop as a way to transmit an external torque through cross-section twisting and warping. Saint-Venant torsion is essentially characterized by a constant circulatory shear flow in each cross-section while warping torsion is related with the development of bi-moment and bi-shear stresses (Kollbrunner & Basler, 1969). The sum of uniform, T_{SV}, and non-uniform torsion, T_w equals the total torsional moment T. In generic situations, where these two phenomena coexist and neither of them predominates, it is said that the cross-section is subjected to mixed torsion.

When considering the two previous effects, it is assumed that the cross-sections maintain their in-plane shape. If this is not valid, then the effects of distortion of the cross-section should be accounted for, since the resulting effects can be quite significant.

This chapter aims at revealing how all three effects correlate to the applied asymmetrical loading, arriving in the end to analytical expressions used for the determination of the longitudinal normal stresses. Reference is made to straight, thin-walled, unicellular box girders, which behave elastically and are symmetrical about the vertical axis. Composite action is once again considered through homogenisation of the cross-section.

The following descriptions and reasonings are mostly based on the work done by Maisel & Roll (1974), Chen & Yen (1980), Schlaich & Scheef (1982), Calgaro (1994) and Pedro (1995).

3.3.1. Behaviour of a girder subjected to eccentric loading

Let us start by considering an eccentric loading such as the one in Figure 3.7.

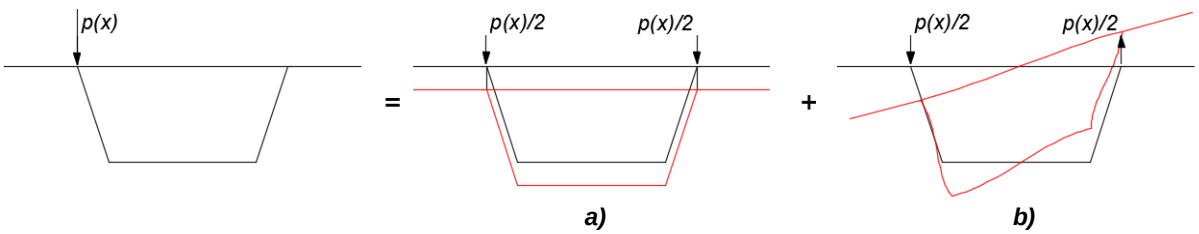

Figure 3.7 – Decomposition of the loading into a) symmetric and b) anti-symmetrical components

The loading can be divided into symmetric and anti-symmetrical components as shown in the figure. The symmetric part is responsible for longitudinal bending of the whole cross-section, which is handled according to the procedures explained in section 3.2. As far as the cross-section goes, it causes an in plane vertical displacement as a rigid body (see Figure 3.7a).

On the other hand, the box girder's response to the anti-symmetrical part (see Figure 3.7b) can be characterized by the coexistence of three force subsystems, which are related to uniform torsion, non-uniform torsion and distortion (see Figure 3.8).

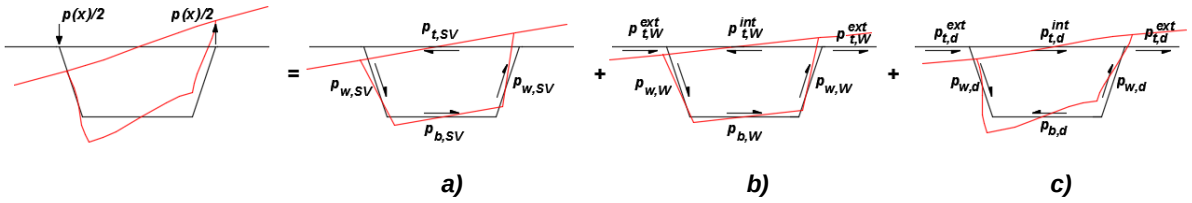

Figure 3.8 – Decomposition of the anti-symmetrical response into a) uniform torsion b) warping torsion and c) distortion

Let us now discuss how to obtain the set of forces of each individual subsystem. The first two may be determined following Benscoter's theory (Benscoter, 1954) for warping torsion, which includes the contribution of bi-shear deformation. This formulation is presented in Sections 3.3.2 and 3.3.3.

Distortional forces on the other hand may only be determined by subtracting the torsional loads to the initial loading. Considering the longitudinal variation of torsional plate forces (which only takes place if the warping torsion is taken into account) of course results in higher complexity. Because the warping torsion shear stresses are usually small, it is fairly common to neglect them whilst determining the distortional forces (Fan & Helwig, 2002). Instead, it is assumed that the torsional forces can be obtained solely from Saint-Venant torsion theory (see Figure *3.9*a).

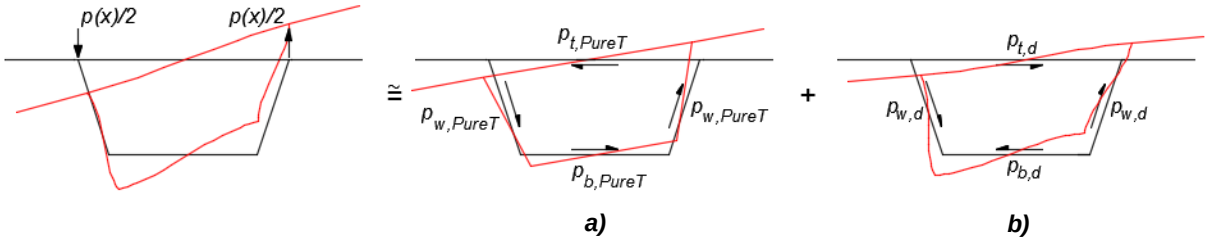

Figure 3.9 – *Approximate decomposition of the anti-symmetrical response into a) pure torsion and b) distortion*

These approximate torsional forces, also designated in literature as pure torsional loads, result from integration of the shear stresses obtained by means of Bredt's formula (see Eq.(3.25)) along plate cross-sectional areas:

$$p_{w,PureT} = \left(\frac{b_t\, b_w}{(b_t + b_b)d}\right)\left(\frac{p(x)}{2}\right), \qquad p_{t,PureT} = \left(\frac{b_t}{b_w}\right)p_{w,PureT} \;,\quad p_{b,PureT} = \left(\frac{b_b}{b_w}\right)p_{w,PureT} \;. \tag{3.22}$$

The components of the distortional system (see Figure *3.9*b) can be obtained knowing that the force system is self-equilibrated and that the sum of the vertical components (in this case of each web torsional and distortional forces) must equal $\frac{p(x)}{2}$, leading to

$$p_{w,d} = \left(\frac{b_b\, b_w}{(b_t + b_b)d}\right)\left(\frac{p(x)}{2}\right) . \tag{3.23}$$

Then, the horizontal forces are calculated by ensuring that resulting moments and forces. By calculating the moments at the top and bottom web-flange junctions, one obtains

$$p_{t,d} = \left(\frac{b_b}{b_w}\right) p_{w,d} \ , \quad p_{b,d} = \left(\frac{b_t}{b_w}\right) p_{w,d} \ . \tag{3.24}$$

Now that the torsional and distortional loads are defined, it is possible to engage in individual considerations regarding uniform torsion, warping torsion and distortion. In what follows, the notation '(x)' is omitted to seek simplicity. Nevertheless, one should be aware that quantities like q, u, T, and others vary along the longitudinal direction.

3.3.2. Uniform torsion

Uniform torsion can be simply described as a twist reacting mechanism involving circulatory shear flows in the cross-section and linear through-thickness shear stresses. For closed-typed cross-sections, such as the case of box-girder bridges, the torsional stiffness is almost entirely given by a uniform shear flow circulating around the closed part, and the linear through-thickness shear can usually be disregarded.

By considering that the cross-section is rigid when rotating around its shear centre, it will only remain plane if for each plate midline point, the strains are proportional to their perpendicular distance to the shear centre Vlasov (1961). For a constant shear flow this would only be possible if the thickness decreases in the same proportion as the perpendicular distance to the shear centre increases. This condition is not valid for the majority of the situations, meaning that the cross-sections will generally warp.

For Saint-Venant torsion theory, warping displacements can be quantified as a function of the rate of twist $\phi_{,x}$, which is assumed constant (the comma indicates a differentiation). Such knowledge will come of particular use further ahead in section 3.3.3 when addressing warping torsion, for it is strictly correlated with out-of-plane behaviour.

3.3.2.1. Hypotheses

When handling Saint-Venant torsional behaviour of a box-girder, four major assumptions are usually considered:

- B1. The in-plane cross-section shape is preserved, i.e., cross-sections remain undeformed within their plane, rotating around the shear centre and warp perpendicularly to their plane;
- B2. Stresses are directly proportional to strains – Hooke's law;
- B3. The box girder is prismatic. The thickness of the composing elements may vary along the cross-section, but not along the length of the girder.
- B4. The cross-section plates are thin-walled. The variation of shear stresses along the thickness and corresponding secondary warping displacements are small and can be neglected.

3.3.2.2. Fundamental equations

Considering only the thin-walled closed cross-section, the torsional system produces a constant shear flow circulating along the closed perimeter. This is given by Bredt's formula:

$$q_{SV} = \frac{T_{SV}}{2\,A_0} = \frac{T_{SV}}{(b_b + b_t)\,d}\ , \qquad (3.25)$$

where A_0 represents the area enclosed by the centre line of the walls composing the cross-section.

The corresponding shear deformation in the mid-surface, is relatable to the tangential and axial displacements, v and u, represented in Figure 3.10 such that:

$$\gamma_{SV} = \frac{q_{SV}}{G\,t} = \frac{\partial u}{\partial s} + \frac{\partial v}{\partial x}\ . \qquad (3.26)$$

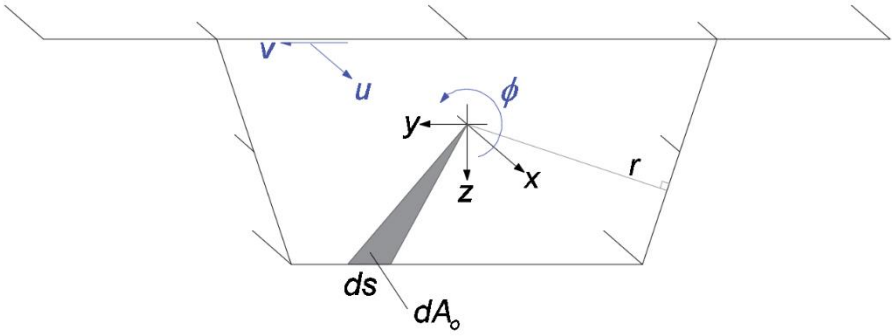

Figure 3.10 – Displacements of the cross-section due to twist

For small angles, rigid body rotation ϕ is correlated with the mid-line tangential displacement by

$$\frac{\partial v}{\partial x} = r\phi_{,x}\ , \qquad (3.27)$$

where r represents the perpendicular distance between the shear centre and the closed wall segment under consideration and $\phi_{,x}$ is constant as already remarked. By replacing (3.27) in (3.26) it comes that

$$du = \left(\frac{q_{SV}}{G\,t} - r\phi_{,x}\right) ds\ . \qquad (3.28)$$

The warping function in any point of the cross section can be determined by integrating du along the mid-line of the entire cross-section, starting at an arbitrary point:

$$u(s) = u_0 + \int_0^{s,cell} \frac{q_{SV}}{G\,t}\,ds - \phi_{,x}\int_0^{s} r\,ds\ . \qquad (3.29)$$

Note that u is not a funtion of x given the hypotheses employed. In this equation, u_0 is the warping displacement at the starting point and the first integral applies only to the cell walls and not to the cantilevers of the top flange. If one integrates u around the closed perimeter and equals this to zero, to ensure continuity of the warping displacements, it comes that

$$\oint \frac{q_{SV}}{G\,t}\,ds = 2\,A_0\,\phi_{,x}\ , \qquad (3.30)$$

where $2\,A_0 = \int_0^s r\,ds$ as a result of geometrical considerations (Calgaro, J. A. Virlogeux, 1988).

Substituting the Saint-Venant shear flow, q_{SV}, according to (3.25), one can obtain

$$\phi_{,x} = \frac{T_{SV}}{G\,J}\ , \tag{3.31}$$

$$J = \frac{4\,{A_0}^2}{\oint \frac{ds}{t}}\ , \tag{3.32}$$

being J the Saint Venant torsional constant for the unicellular box girder. Considering $u_0 = -\ \phi_{,x} C_0$, one can rewrite (3.29) as

$$u(s) = -\phi_{,x}\left(\omega_S(s) - \frac{2\,A_0}{\oint \frac{ds}{t}}\int_0^s \frac{ds}{t} + C_0\right). \tag{3.33}$$

Here $\omega_S(s)$ is a so-called "sectorial coordinate", being calculated by integrating the previously defined tangential radius r around the mid-line, with respect to the shear centre, and starting in an arbitrary point of the closed perimeter:

$$\omega_S(s) = \int_0^s r\,ds\,. \tag{3.34}$$

Since the second term between brackets is also a function of an integration along the mid-line, one can define an equivalent sectorial coordinate $\widetilde{\omega_S}$:

$$\widetilde{\omega_S}(s) = \omega_S(s) - \frac{2\,A_0}{\oint \frac{ds}{t}}\int_0^s \frac{ds}{t}. \tag{3.35}$$

Defining a new quantity $\widetilde{u_S}(s)$, designated as the "normalized unit warping function", it is possible to arrive at a compatibility equation concerning the warping displacement $u(s)$ and the the rate of twist $\phi_{,x}$ for Saint-Venant torsion. The value for the constant C_0 shall be obtained further ahead, in section 3.3.3.3.

$$\widetilde{u_S}(s) = \widetilde{\omega_S}(s) + C_0\ , \tag{3.36}$$

$$u(s) = -\phi_{,x}\,\widetilde{u_S}(s)\ . \tag{3.37}$$

3.3.3. Non-uniform Torsion

If warping is not constant along x, normal strains and stresses arise. The pattern of warping displacements is such that these torsional warping stresses vary both around the cross-sectional perimeter and along the beam, giving way to shear stresses which equilibrate part of the torsional moment.

3.3.3.1. Hypotheses

The development of a formulation accounting for non-uniform torsion is set on the same assumptions mentioned for uniform torsion in 3.3.2.1, along with the following additional premises:

B5. The longitudinal normal stresses can be calculated disregarding Poisson's effect;

B6. Normal displacements due to warping $u(x,s)$ are obtained from

$$u(x,s) = -\tilde{u}_S(s)\frac{d\chi}{dx}\,, \qquad (3.38)$$

where $\chi = \chi(x)$ is a function to be determined, where its derivative is employed as an analogy for the twist angle derivative present in (3.37) and $\tilde{u}_S$ is the normalized unit warping function.

3.3.3.2. Compatibility equation

As seen in section 3.3.2, the uniform torsion formulation sets a correlation between the Saint-Venant torsional shear and the warping displacements of the cross-section. When the warping displacement varies along x, a set of torsional warping stresses σ_w is generated, along with corresponding shear stresses τ_w to be added to those related to uniform torsion, τ_{SV}. Interference between the newly superimposed stresses and those obtained by Saint-Venant theory alter the displacements on a closed cross-section, making (3.37) invalid, since $\phi_{,x}$ is no longer constant. For this reason, it is necessary to consider a new auxiliary function $\chi(x)$, to be dependent on the total shear flow $q = q_{SV} + q_w$. As a result, hypothesis B6 is assumed, advocating that the warping displacements should follow from (3.38).

Having the warping displacements defined, normal strains and stresses can be derived through standard compatibility and constitutive relations for linear elements:

$$\varepsilon_w(x,s) = \frac{du}{dx} = -\tilde{u}(s)\frac{d^2\chi}{dx^2}\,, \qquad (3.39)$$

$$\sigma_w(x,s) = -E\,\tilde{u}(s)\frac{d^2\chi}{dx^2}\,. \qquad (3.40)$$

Before being able to write the equilibrium equation, let us completely define the unit warping function $\widetilde{u_S}(s)$. To do so, it is first necessary to determine the position of the shear centre and the value of the constant C_0, which take place in the following section. Cross-sectional diagrams for both sectorial coordinate $\omega_S(s)$ and unit warping function $\widetilde{u_S}(s)$ are schematically illustrated in Figure 3.11, where *S* is the shear centre, and they are usually obtained starting the integrations in point 0 indicated on the figure.[6].

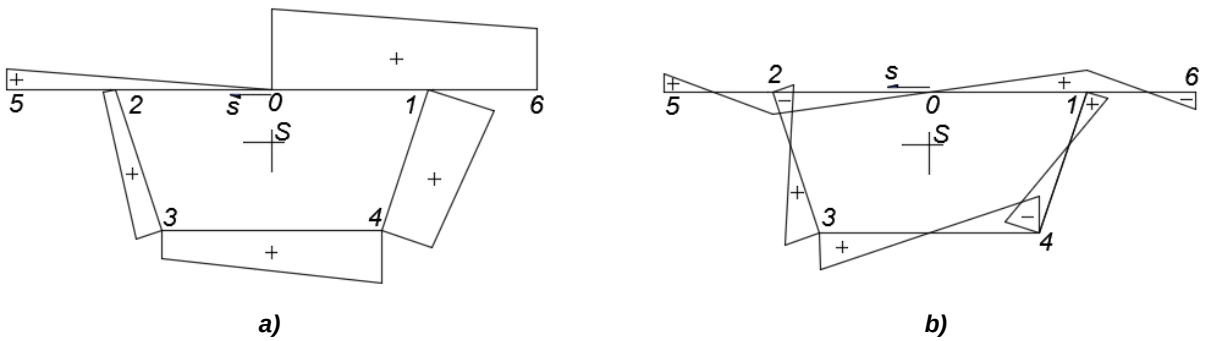

a) ***b)***

Figure 3.11 – a) Sectorial coordinate and b) unit warping function diagrams

[6] The equations of these functions in each of the segments between point *i* and *i*+1 can be obtained by integration using equations (3.35) and (3.36) or consulted in Kollbrunner&Basler (1969) or Pedro (1995).

3.3.3.3. Shear centre

Let us start by considering a segment of a thin-walled cross-section such as the one presented in Figure 3.12, where S is the shear centre, G is the centre of mass, A is a generic point along the mid-line, and P is an initially defined point from which cross-sectional sectorial properties can be calculated.

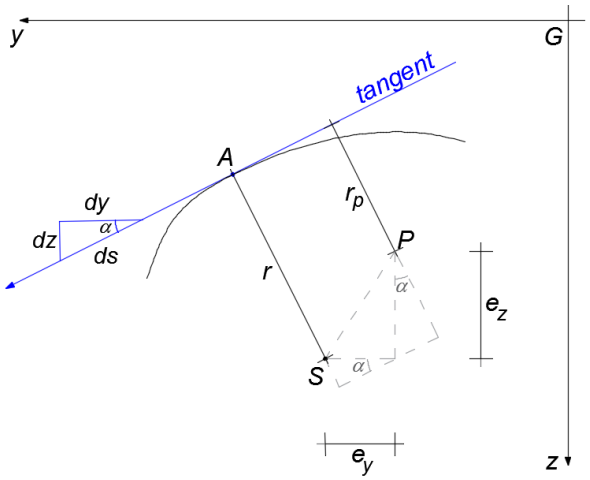

Figure 3.12 – Tangential radii for shifted reference points

The relation between tangential radii r and r_P is given through geometrical considerations and can be expressed by:

$$r = r_P + e_z \frac{dy}{ds} - e_y \frac{dz}{ds} \ . \qquad (3.41)$$

Performing the integration between an arbitrary starting point of the mid-line and point A, and considering (3.34), comes that

$$\int_s (r - r_P) ds = \int_s e_z \, dy - \int_s e_y \, dz \ \leftrightarrow \qquad (3.42)$$

$$\leftrightarrow \omega_S = \omega + (e_z) y - (e_y) z + C_0 \ . \qquad (3.43)$$

Using (3.35), a relation can be established between the equivalent sectorial coordinates calculated with respect to the shear centre ($\widetilde{\omega_S}$) and to the initially defined point P ($\widetilde{\omega_P}$):

$$\widetilde{\omega_S} = \widetilde{\omega_P} + (e_z) y - (e_y) z + C_0 \ . \qquad (3.44)$$

For an element subjected to external torque only, equilibrium dictates that

$$\begin{aligned} &\int_A \sigma_w \, dA = 0 \ , \\ &\int_A \sigma_w y \, dA = 0 \ , \\ &\int_A \sigma_w z \, dA = 0 \ . \end{aligned} \qquad (3.45)$$

Imposing (3.40) and (3.36), one can rewrite the previous system of equations as

$$\begin{aligned} \int_A \widetilde{\omega_P}\, dA + C_0 A = 0 \ , \\ \int_A \widetilde{\omega_P}\, y\, dA \ - e_y\, I_y - e_z\, I_{yz} = 0 \ , \\ \int_A \widetilde{\omega_P}\, z\, dA + e_y\, I_{yz} + e_z\, I_z = 0 \ . \end{aligned} \qquad (3.46)$$

The system of equations can be solved with respect to C_0 and to the location coordinates for the shear centre:

$$\begin{aligned} C_0 = -\frac{1}{A} \int_A \widetilde{\omega_P}\, dA \ , \\ e_y = \frac{I_z S_{\omega z} - I_{yz} S_{\omega y}}{I_y I_z - {I_{yz}}^2} \ , \\ e_z = -\frac{I_y S_{\omega y} - I_{yz} S_{\omega z}}{I_y I_z - {I_{yz}}^2} \ , \end{aligned} \qquad (3.47)$$

where S_{wy} and S_{wz} are sectorial products of inertia defined by

$$\begin{aligned} S_{\omega y} = \int_A \widetilde{\omega_P}\, y\, dA \ , \\ S_{\omega z} = \int_A \widetilde{\omega_P}\, z\, dA \ . \end{aligned} \qquad (3.48)$$

3.3.3.4. Equilibrium equation

Normal stresses due to warping follow from equation (3.40). Establishing equilibrium on an infinitesimal wall element – Figure *3.13* – comes that

$$\frac{d\sigma_w}{dx}\, t + \frac{dq_w}{ds} = 0 \ .$$

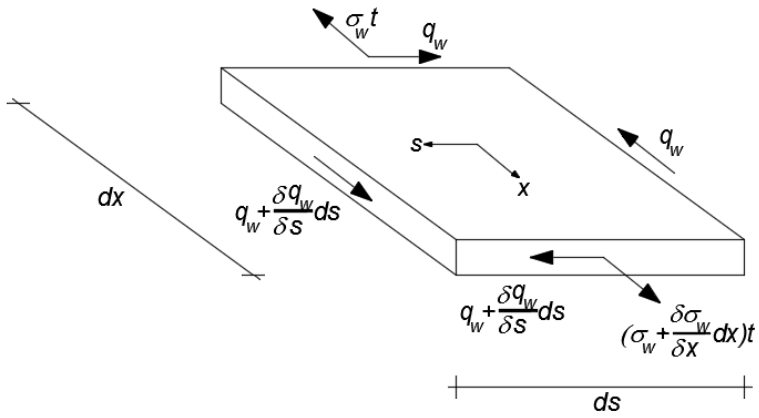

Figure 3.13 *– Equilibrium of an infinitesimal segment of plate subjected to warping torsion*

By replacing (3.40) in (3.49) and subsequently integrating along the mid-line of the cross-section one can deduce the expression for a secondary warping shear flow (q_w) which is in self-equilibrium.

$$E\,\tilde{u}(s)\frac{d^3\chi}{dx^3}t = \frac{dq_w}{ds}\ , \tag{3.49}$$

$$q_w(s) = E\frac{d^3\chi}{dx^3}\int_0^s \tilde{u}(s)t\,ds\ . \tag{3.50}$$

Having defined the warping shear flow, the warping torsion T_w can be determined through integration, as follows

$$T_w = \int_S q_w\, r\, ds = -EI_\omega\frac{d^3\chi}{dx^3}\ , \tag{3.51}$$

where I_ω is the warping constant, defined as

$$I_\omega = \int_S \left(\tilde{u}(s)\right)^2 t\,ds\ . \tag{3.52}$$

The torsion moment is equilibrated through the sum of both uniform and non-uniform contributions, addressed in (3.31) and (3.51) :

$$T = T_{SV} + T_w = GJ\frac{d\phi}{dx} - EI_\omega\frac{d^3\chi}{dx^3}\ . \tag{3.53}$$

On the other hand, the torsional moment can also be written as a function of the total shear flow, which can be determined taking (3.26) and (3.27) into consideration (Calgaro, J. A. Virlogeux, 1988):

$$q = Gt\left(\frac{\partial u}{\partial s} + r\frac{d\phi}{dx}\right)\ , \tag{3.54}$$

$$T = \int_S q\, r\, ds = GI_c\frac{d\phi}{dx} - G\,(I_c - J)\frac{d\chi}{dx}\ , \tag{3.55}$$

where I_c is the shear central second moment of inertia,

$$I_c = \int_S r^2\, t\, ds\ . \tag{3.56}$$

Eliminating $\frac{d\phi}{dx}$ from (3.53) and (3.55) derives the differential equation that relates the warping function χ and the torsional moment:

$$-EI_\omega\frac{d^3\chi}{dx^3} - \mu GJ\frac{d\chi}{dx} = \mu T\ , \tag{3.57}$$

where μ is the warping shear parameter, given by

$$\mu = 1 - \frac{J}{I_c}\ . \tag{3.58}$$

This parameter is a measure of the cross-sectional slenderness with respect to torsion. For very thin walls it approaches unity, meaning that the effect of “warping shear” in torsion has little expression. This effect can also be designated as torsion bi-shear. This has to do with the shape of the unit warping

function $\tilde{u}$ (see Figure 3.11b), in which the two web plates seem to bend with same magnitude but in opposite directions. The same analogy makes it possible to define a new quantity B, designated as bimoment or warping moment, through which the longitudinal stresses can be calculated by a "bending moment" type equation:

$$\sigma_w\,(x,\mathrm{s}) = \tilde{u}(x,s)\frac{B}{I_\omega}\ , \tag{3.59}$$

$$B = -EI_\omega\frac{d^2\chi}{dx^2}\ . \tag{3.60}$$

Solving the differential equation (3.57) with respect to $\frac{d\chi}{dx}$, and applying another derivative, one can obtain the bimoment B as defined in (3.60), and afterwards calculate the torsional warping stresses according to (3.59).

It is possible to write a more generic differential equilibrium equation that relates the warping function χ and a generic torsional load m_T. Such can be achieved by first performing the static equilibrium of an infinitesimal segment of beam (see Figure 3.14):

$$-T + m_T dx + \left(T + \frac{dT}{dx}dx\right) = 0\ , \tag{3.61}$$

which is simplified to

$$-\frac{dT}{dx} = m_T\ . \tag{3.62}$$

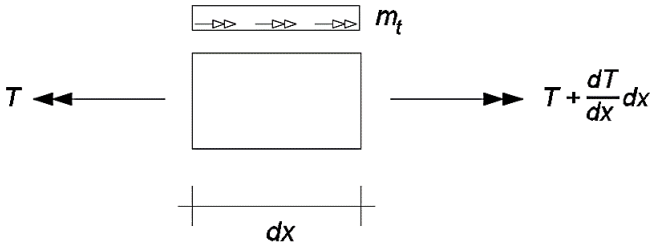

Figure 3.14 – Equilibrium of an infinitesimal segment of a beam subjected to torsional load

Applying a derivative to (3.57) and using the relation obtained in (3.62) comes the general equilibrium equation

$$\frac{EI_\omega}{\mu}\left(\frac{d^4\chi}{dx^4}\right) + GJ\left(\frac{d^2\chi}{dx^2}\right) = m_T(x)\ . \tag{3.63}$$

It is interesting to observe that if the function $\chi(x)$ would have been taken equal to $\phi(x)$, i.e., if bi-shear had been neglected, one would arrive at a similar equilibrium equation, where the warping shear parameter would not take place. This simplified equation corresponds to the so-called von Karman-Christensen theory of torsion (Murray, 1984):

$$EI_\omega\left(\frac{d^4\phi}{dx^4}\right) + GJ\left(\frac{d^2\phi}{dx^2}\right) = m_T(x)\ . \tag{3.64}$$

3.3.3.5. Homogenisation rules for torsion with warping in steel-concrete composite box girders

Torsion with warping accounting for bi-shear in composite box girders has been addressed by Chen & Yen (1980). Similar to that explained in section 3.2.2.2, the definition of shear flows and stresses may be computed using a transformed thickness for the concrete deck so that:

$$\gamma = \frac{q}{G_c\,(t_t{}')_w} = \frac{q}{G_s\,(t_t)_{SV+W}} \leftrightarrow$$
$$\leftrightarrow \left(\frac{t_t{}'}{t_t}\right)_{SV+w} = \frac{G_s}{G_c} \approx \frac{E_s}{E_c} = n \ . \qquad (3.65)$$

Longitudinal stresses in the concrete can be retrieved trough

$$\sigma_w{}^c = \frac{\sigma_w{}^s}{n} = \tilde{u}(x,s)\frac{B}{nI_\omega} \ . \qquad (3.66)$$

3.3.4. Distortion

A box girder subjected to distortional loads responds by deforming its cross-sections in their own plane. Due to compatibility of displacements in the web-flange connections, the walls forming the cross-section undergo displacements in the direction of their mid-lines, which means that, assuming null membrane shear strains, warping is produced (i.e., the walls "bend" longitudinally, see Figure *3.15*). Therefore, each frame's response lies between those of 'a freely deformable' and a 'rigid' cross-section, where the degree of stiffness relies simultaneously on both longitudinal and transverse behaviours. According to Schlaich & Scheef (1982) if the loading changes little in the longitudinal direction and transverse deformation is not prevented, cross-sections behave closer to freely distorting frames. On the contrary, for concentrated loads or for sections in the vicinity of transverse restraints, the limiting case of a fully rigid frame is closer to reality (Schlaich & Scheef, 1982).

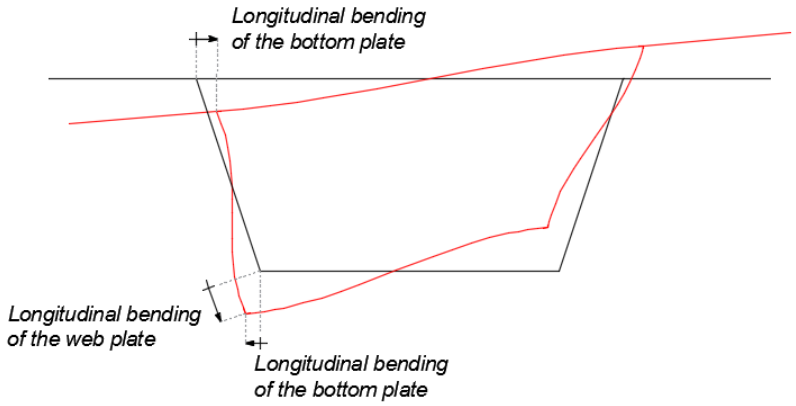

Figure 3.15 – Compatibility of displacements in the distortion of the cross-section

Rephrasing, distortional loads, p_d, acting on a box girder are simultaneously equilibrated by two coupled mechanisms:

1) Longitudinal bending of the plates, related to loads p_d^L
2) Transverse deformation of the cross-section, related to loads p_d^T

The sum of the two contributions in each plate should render the total force, i.e.,

$$p_d = p_d^L + p_d^T \ . \qquad (3.67)$$

In particular, for each of the plates, and knowing that the distortional subsystem is self-equilibrated, it can be concluded that

$$\begin{aligned} p_{w,d}^{L} &= p_{w,d} - p_{w,d}^{T} \ , \\ p_{t,d}^{L} &= p_{t,d} - p_{t,d}^{T} = -\left(\frac{b_b}{b_w}\right)\left(p_{w,d} - p_{w,d}^{T}\right) \ , \\ p_{b,d}^{L} &= p_{b,d} - p_{d,l}^{T} = -\left(\frac{b_t}{b_w}\right)\left(p_{w,d} - p_{w,d}^{T}\right) \ . \end{aligned} \qquad (3.68)$$

3.3.4.1. Hypotheses

The following assumptions are considered when addressing distortion of a box-girder deck (Schlaich & Scheef, 1982; Pedro, 1995):

C1. The length of the plates is large compared to their widths ($\frac{l}{b} > 4$);

C2. The plates are thin-walled;

C3. The cross-section is symmetrical about the vertical axis;

C4. The bridge is prismatic, i.e., the cross-section is constant along the entire width;

C5. The thicknesses of the webs and flanges remain constant in the transverse directions – the effect of haunches are neglected;

C6. End supports are rigid to transverse deformations by means of sufficiently stiff diagrams and also prevent torsional rotations;

C7. The longitudinal connection between plates transmits only shear stresses in the longitudinal direction due to a torsional load;

3.3.4.2. Longitudinal bending of the plates

At first, let us take into consideration a generic segment of the box girder subjected to distortional loads p_d^L, such as those presented in Figure 3.16.

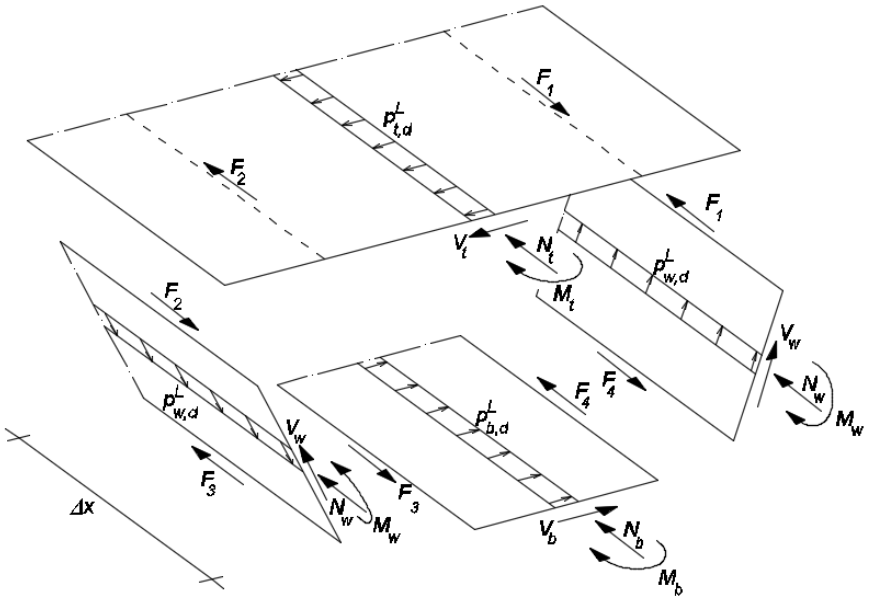

Figure 3.16 – Forces and moments acting on the plates of a segment of box girder bridge subjected to distortion

The loading and cross-section are anti-symmetric and symmetric about the vertical axis, respectively, so the response of the box girder will necessarily be anti-symmetric as well (for example $F_1 = F_2$ and $F_3 = F_4$).

The connection of the plates at the interfaces include equivalent shear flows $f_2(x)$ and $f_3(x)$, whose resultants along the longitudinal direction are $F_2(x)$ and $F_3(x)$:

$$F_2(x) = \int_x f_2(x)\, dx \ , \qquad F_3(x) = \int_x f_3(x)\, dx \ . \tag{3.69}$$

By establishing equilibrium equations for each plate and considering symmetry one can arrive at the internal forces and moments equivalent to the distortional loads and shear forces. Here, $m_{t,d}^L$, $m_{w,d}^L$ and $m_{b,d}^L$ are the bending moments provoked by the distortional loads $p_{t,d}^L$, $p_{w,d}^L$ and $p_{b,d}^L$, respectively. The equations are as follows:

Top flange

$$a)\ N_t = 0$$

$$b)\ M_t = F_2\, b_t - m_{t,d}^L$$

Web

$$c)\ N_w = F_3 - F_2 \tag{3.70}$$

$$d)\ M_w = -(F_2 + F_3)\frac{b_w}{2} + m_{w,d}^L$$

Bottom flange

$$e)\ N_b = 0$$

$$f)\ M_b = F_3\, b_b - m_{b,d}^L$$

The stresses at the intersections can be written for each plate as a function of the internal forces and moments, and of the inertial properties of the cross-section,

Top flange

$$a)\ \sigma_{2,d} = -\frac{M_t b_t}{2I_t}$$

Web

$$b)\ \sigma_{2,d} = -\frac{N_w}{A_w} - \frac{M_w b_w}{2I_w} \tag{3.71}$$

$$c)\ \sigma_{3,d} = -\frac{N_w}{A_w} + \frac{M_w b_w}{2I}$$

Bottom flange

$$d)\ \sigma_{3,d} = \frac{M_b b_b}{2I_b}$$

These expressions make use of the following inertias and area:

$$I_t = \frac{b^3 t_t}{12} \ ; \ I_w = \frac{{b_w}^3 t_w}{12} \ ; \ I_b = \frac{{b_b}^3 t_b}{12} \ ; \ A_w = b_w t_w \tag{3.72}$$

By replacing (3.70) in (3.71) it comes that:

Top flange

$$a)\ \sigma_{2,d} = -\frac{\left[F_2\ b_t - m_{t,d}^L\right] b_t}{2I_t}$$

Web

$$b)\ \sigma_{2,d} = -\frac{[F_3 - F_2]}{A_w} - \frac{\left[-(F_2 + F_3)\frac{b_w}{2} + m_{w,d}^L\right] b_t}{2I_t} \qquad (3.73)$$

$$c)\ \sigma_{3,d} = -\frac{[F_3 - F_2]}{A_w} + \frac{\left[-(F_2 + F_3)\frac{b_w}{2} + m_{w,d}^L\right] b_t}{2I_t}$$

Bottom flange

$$d)\ \sigma_{3,d} = \frac{\left[F_3\ b_b - m_{b,d}^L\right] b_b}{2I_b}$$

Since longitudinal bending of the plates is at hand, taking into account the relation between distortional loads from (3.68), one can write

$$\frac{d^2 m_{t,d}^L}{dx^2} = p_{t,d}^L = -\left(\frac{b_b}{b_w}\right) p_{w,d}^L = \left(\frac{b_b}{b_w}\right) \frac{d^2 m_{w,d}^L}{dx^2}\ ,$$
$$\frac{d^2 m_{b,d}^L}{dx^2} = p_{b,d}^L = -\left(\frac{b_t}{b_w}\right) p_{w,d}^L = \left(\frac{b_t}{b_w}\right) \frac{d^2 m_{w,d}^L}{dx^2}\ . \qquad (3.74)$$

Supposing that the boundary conditions are the same for both web, top and bottom flanges, which is generally the case, the relations between plate distortional loads and plate moments is the same:

$$m_{t,d}^L = -\left(\frac{b_b}{b_w}\right) m_{w,d}^L\ , m_{b,d}^L = -\left(\frac{b_t}{b_w}\right) m_{w,d}^L\ . \qquad (3.75)$$

Therefore, the stresses in (3.73) can be rewritten as a function of F_2, F_3 and $m_{w,d}^L$:

Top flange

$$a)\ \sigma_{2,d} = -\frac{\left[F_2\ b_t + \left(\frac{b_b}{b_w}\right) m_{w,d}^L\right] b_t}{2I_t}$$

Web

$$b)\ \sigma_{2,d} = -\frac{[F_3 - F_2]}{A_w} - \frac{\left[-(F_2 + F_3)\frac{b_w}{2} + m_{w,d}^L\right] b_w}{2I_w} \qquad (3.76)$$

$$c)\ \sigma_{3,d} = -\frac{[F_3 - F_2]}{A_w} + \frac{\left[-(F_2 + F_3)\frac{b_w}{2} + m_{w,d}^L\right] b_w}{2I_w}$$

Bottom flange

$$d)\ \sigma_{3,d} = \frac{\left[F_3\ b_b + \left(\frac{b_t}{b_w}\right) m_{w,d}^L\right] b_b}{2I_b}$$

Equalling the stresses obtained for the different plates in (3.76) and defining a set of geometrical quantities, one can derive the following equations

$$F_2\left(\frac{3}{\alpha_t}+2\right)+\ F_3=3\left(1-\frac{\beta}{\alpha_t}\right)\frac{m_{w,d}^L}{b_w}\ ,$$
$$F_2+\ F_3\left(\frac{3}{\alpha_b}+2\right)=3\left(1-\frac{1}{\beta\ \alpha_t}\right)\frac{m_{w,d}^L}{b_w}\ , \qquad (3.77)$$

where

$$\alpha_t=\frac{12\ I_t}{{b_t}^2 A_w}\ ;\ \alpha_b=\frac{12\ I_b}{{b_b}^2 A_w}\ ;\ \beta=\frac{b_b}{b_t}\ . \qquad (3.78)$$

The system of equations can be solved with respect to F_2 and F_3:

$$F_2=\frac{\alpha_t(\alpha_b\beta+3\beta+1)-(2\ \alpha_b+3)\beta^2}{\beta[(\alpha_t+2)(\alpha_b+2)-1]}\frac{m_{w,d}^L}{b_w}\ ,$$
$$F_3=\frac{\alpha_b(\alpha_b\beta+3\beta+\beta^2)-(2\ \alpha_t+3)}{\beta[(\alpha_t+2)(\alpha_b+2)-1]}\frac{m_{w,d}^L}{b_w}\ . \qquad (3.79)$$

Substituting the shear resultants in (3.76), the stresses in the top and bottom edges of the web become related to the web moment $m_{w,d}^L$ as follows

$$\sigma_{2,d}=-\frac{(1+\beta)(1+\alpha_b\beta+2\beta)}{\beta[(\alpha_t+2)(\alpha_b+2)-1]}\frac{m_{w,d}^L\ b_w}{2\ I_w}\ ,$$
$$\sigma_{3,d}=\frac{(1+\beta)(2+\alpha_t+\beta)}{\beta[(\alpha_t+2)(\alpha_b+2)-1]}\frac{m_{w,d}^L\ b_w}{2\ I_w}\ . \qquad (3.80)$$

The position of the neutral axis can now be obtained considering a linear stress diagram in the web, which is congruent with the hypothesis taken for the longitudinal bending of the plates. One may then define y_t ad y_b as the distances measured along the web to the top and bottom edges, respectively:

$$y_t=\frac{|\sigma_2|}{|\sigma_2|+|\sigma_3|}=\frac{(1+\beta)(1+\alpha_b\beta+2\beta)}{\alpha_t+\alpha_b\beta+3(1+\beta)}b_w\ , \qquad (3.81)$$

$$y_b=b_w-y_t\ . \qquad (3.82)$$

One can equally write an equivalent second moment of inertia for the web, $I_{w,e}$, so that the stresses originated from bending of all plates in the cross-section match those obtained from the individual analysis of the web plate subjected to $p_{w,d}^L$. Considering a local web referential:

$$\sigma_{2,d}=-\frac{m_{w,d}^L\ y_t}{2\ I_{w,e}}\ ,\quad \sigma_{3,d}=\frac{m_{w,d}^L\ y_b}{2\ I_{w,e}}\ , \qquad (3.83)$$

where

$$I_{w,e}=\frac{2\beta\ [(\alpha_t+2)(\alpha_b+2)-1]}{(1+\beta)[\alpha_t+\alpha_b\beta+3(1+\beta)]}\ I_w\ . \qquad (3.84)$$

The stress diagram for the cross-section is completely defined, since it is anti-symmetrical and linear (see Figure 3.17). The web subjected to $p_{w,d}^{L}$ can be analysed as a beam, for which web in-plane displacements Δ_w are retrievable through an equation similar to that derived in 3.2.1.2:

$$p_{w,d}^{L} = \frac{d^4 \Delta_w}{dx^4} \, EI_{w,e} \ . \tag{3.85}$$

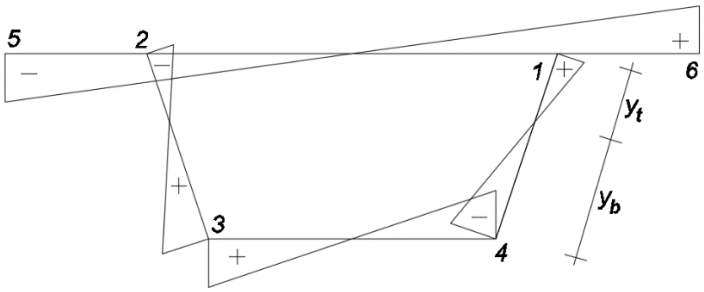

Figure 3.17 – Generic distortional warping stresses

3.3.4.3. Transverse deformation of the cross-section

In this section, the cross-section is analysed as an individual frame subjected to the distortional subsystem p_d^T. This is equivalent to a set of anti-symmetrical diagonal loads applied at the intersections (see Figure 3.18a). These can be defined considering the length of the diagonal g so that

$$S_d = = \frac{g}{b_w} \, p_{w,d}^{T} \ . \tag{3.86}$$

$$g = \sqrt{\left(\frac{b_t + b_b}{2}\right)^2 + d^2} \tag{3.87}$$

Solving the statically indeterminate structure, an anti-symmetrical transverse moment distribution is obtained (see Figure 3.18b):

$$\begin{aligned} \overline{m_2} &= -\overline{m_1} = \frac{1 + \beta(2 + r_b)}{2 + 2\beta + 2\beta^2 + r_t + r_b\beta^2} \frac{b_b d}{g} \left(\frac{S_d}{2}\right), \\ \overline{m_4} &= -\overline{m_3} = \frac{2 + \beta + r_t}{2 + 2\beta + 2\beta^2 + r_t + r_b\beta^2} \frac{b_b d}{g} \left(\frac{S_d}{2}\right), \end{aligned} \tag{3.88}$$

where

$$r_t = \frac{b_t}{b_w} \frac{\bar{I}_w}{\bar{I}_t} \ ; \ r_b = \frac{b_b}{b_w} \frac{\bar{I}_w}{\bar{I}_b} \ , \tag{3.89}$$

which makes reference to the transverse moments of inertia per unit length

$$\bar{I}_t = \frac{{t_t}^3}{12\,(1-\nu^2)} ; \ \bar{I}_w = \frac{{t_w}^3}{12(1-\nu^2)} \ ; \ \bar{I}_b = \frac{{t_b}^3}{12(1-\nu^2)} \ . \tag{3.90}$$

Figure 3.18 – a) Equivalent diagonal loads and b) corresponding transverse bending moments

Applying the unit dummy load method, considering only transverse bending contributions and substituting (3.86) in (3.88), the diagonal displacement δ is related to $p_{w,d}^{T}$ by

$$p_{w,d}^{T} = \frac{12\ g\ E\bar{I}_w}{b_t b_b d^2} k_2 \delta\ , \qquad (3.91)$$

$$k_2 = \frac{2 + 2\beta + 2\beta^2 + r_t + r_b\beta^2}{\beta[(r_t + 2)(r_b + 2) - 1]}\ . \qquad (3.92)$$

At this point, the relations between diagonal deformation of the cross-section and the transverse displacement of the plates are still unknown. To calculate them, displacements Δ_t, Δ_w, Δ_b, m_i and n_i are defined (see Figure 3.19). The first three are measured along the respective top, web and bottom plate planes. Displacements m_i and n_i are perpendicular to the top/bottom and web plates, respectively, and can be expressed in terms of the latter my means of geometric considerations:

$$\begin{aligned} m_1 &= \left[|\Delta_w| - |\Delta_t|\frac{b_t - b_b}{2b_w}\right]\frac{d}{b_w}\ , \\ n_1 &= \left[|\Delta_t| - |\Delta_w|\frac{b_t - b_b}{2b_w}\right]\frac{d}{b_w}\ , \\ m_3 &= \left[|\Delta_w| + |\Delta_b|\frac{b_t - b_b}{2b_w}\right]\frac{d}{b_w}\ , \\ n_3 &= \left[|\Delta_b| + |\Delta_w|\frac{b_t - b_b}{2b_w}\right]\frac{d}{b_w}\ . \end{aligned} \qquad (3.93)$$

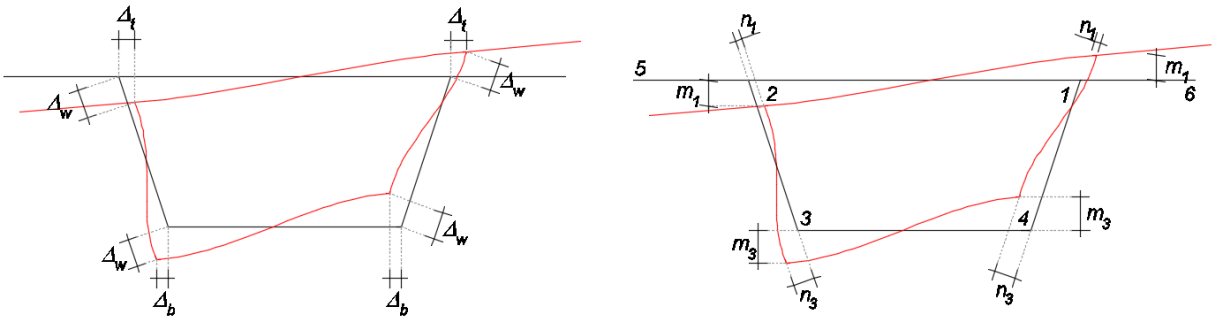

Figure 3.19 – Auxiliary displacements of the distorted frame

According to Figure 3.17, equality of longitudinal stresses at the plate ends dictates that curvatures in the web and remaining plates follow a proportionality rule. Assuming the support conditions are the same for each plate, the curvatures and displacements between different plates are bound by the same absolute ratio. Taking into account (3.81), the following ratios are deducted:

$$\begin{aligned} \frac{\sigma_{2,d}}{E} = \left(\frac{1}{R_t}\right)\frac{b_t}{2} = \left(\frac{1}{R_w}\right)y_t \quad &\leftrightarrow \quad \frac{|\Delta_t|}{|\Delta_w|} = \frac{\left(\frac{1}{R_t}\right)}{\left(\frac{1}{R_w}\right)} = \frac{2y_t}{b_t} \\ \frac{\sigma_{3,d}}{E} = \left(\frac{1}{R_b}\right)\frac{b_b}{2} = \left(\frac{1}{R_w}\right)y_b \quad &\leftrightarrow \quad \frac{|\Delta_b|}{|\Delta_w|} = \frac{\left(\frac{1}{R_b}\right)}{\left(\frac{1}{R_w}\right)} = \frac{2y_b}{b_b} \end{aligned} \qquad (3.94)$$

Using the previous results in (3.93) comes:

$$\begin{aligned} m_1 &= |\Delta_w| \left[1 - \frac{2\,y_t}{b_t}\frac{b_t - b_b}{2b_w}\right]\frac{d}{b_w}\ , \\ n_1 &= |\Delta_w| \left[\frac{2\,y_t}{b_t} - \frac{b_t - b_b}{2b_w}\right]\frac{d}{b_w}\ , \\ m_3 &= |\Delta_w| \left[1 + \frac{2\,y_b}{b_b}\frac{b_t - b_b}{2b_w}\right]\frac{d}{b_w}\ , \\ n_3 &= |\Delta_w| \left[\frac{2\,y_b}{b_b} + \frac{b_t - b_b}{2b_w}\right]\frac{d}{b_w}\ . \end{aligned} \qquad (3.95)$$

Following geometrical correlations, the diagonal displacements can be expressed as a function of the auxiliary normal displacements:

$$\begin{aligned} \delta_1 &= \frac{n_1}{cos\varphi}cos\theta + \frac{m_1}{cos\varphi}\ [sin\theta cos\varphi + cos\theta sin\varphi]\ , \\ \delta_3 &= \frac{n_3}{cos\varphi}cos\theta + \frac{m_3}{cos\varphi}[sin\theta cos\varphi - cos\theta sin\varphi]\ . \end{aligned} \qquad (3.96)$$

Here, θ, and φ respectively represent the angle the diagonal makes with the horizontal and the angle the web makes with the vertical. Some helpful trigonometrical relations can be written:

$$sin\theta = \frac{d}{g}\ ;\ cos\theta = \frac{b_t + b_b}{2g}\ ;\ sin\varphi = \frac{b_t - b_b}{2b_w}\ ;\ cos\theta = \frac{d}{b_w} \qquad (3.97)$$

The diagonal deformation is a result of the combined diagonal displacements δ_1 and δ_3. Combining the expressions presented in (3.96) and (3.95), one can determine it through:

$$\delta = \delta_1 + \delta_3 = \frac{2b_w}{\beta\ g}k_1\ \Delta_w\ , \qquad (3.98)$$

$$k_1 = \frac{[\alpha_t + \beta^2(\alpha_b + 2) + 2(\beta + 1)]\ (1 + \beta)}{\alpha_t + \alpha_b\beta + 3(\beta + 1)}\ . \qquad (3.99)$$

Finally, it is possible to write an equation that relates the distortional load and the in-plane displacement of a web plate, accounting for the global transverse effect of the frame:

$$\begin{aligned} p_{w,d}^T &= k\ \Delta_w\ , \\ k &= \frac{24\ b_w}{{b_b}^2 d^2}k_1 k_2 E\bar{I}_w\ . \end{aligned} \qquad (3.100)$$

3.3.4.4. Equilibrium equation

In the previous sections, it was shown how the effect of distortion on a box girder can be determined by calculating the displacement of the web, Δ_w, and afterwards applying relations to obtain displacements, stresses and internal forces and moments throughout the whole cross-section. Therefore, it is possible to undertake an individual in-plane bending analysis only of the web plate, subjected to $p_{w,d} = p_{w,d}^L + p_{w,d}^T$ and elastically restrained along its span, i.e., considering the web plate as a beam on an elastic foundation. Substituting (3.85) and (3.100) into (3.67) comes

$$p_{w,d} = \frac{d^4\Delta_w}{dx^4}\ EI_{w,e} + k\ \Delta_w \qquad (3.101)$$

This bending equation is equal to that derived in 3.2.1.2 but with an additional term which represents the elastic foundation. This simulates the stiffness of the cross-section to transverse deformation. Once the displacement field in the web along its axis is determined, the corresponding longitudinal bending moments can be found through:

$$m_{w,d}^{L} = -EI_{w,e}\frac{d^2\Delta_w}{dx^2} \qquad (3.102)$$

The distortional warping stresses can then finally be assessed through (3.83).

3.3.4.5. Homogenisation rules for distortion in steel-concrete composite box girders

The previous subsections have handled the effect of distortion on a box girder composed of a single material. This can be extended to steel-concrete composite cross-sections by transforming them into homogenous cross-sections of equivalent thicknesses, with reference usually being made to steel. However, as shown above, distortion involves simultaneous response of the plates to longitudinal and transverse bending. For this reason, when accounting for distortion, one needs to take into account two separate equivalent thicknesses (Calgaro, J. A. Virlogeux, 1988):

- Longitudinal bending of the plate

$$\left(\frac{{t_t}^S}{t_t}\right)_d^L = n = \frac{E_s}{E_c} \qquad (3.103a)$$

- Transverse bending

$$\left(\frac{{t_t}^S}{t_t}\right)_d^T = \sqrt[3]{n} \qquad (3.104b)$$

The longitudinal stresses due to distortion in the steel plates can be determined according to the previous reasoning. Stresses in the concrete deck, however, should be reported back to the composite cross-section by means of

$${\sigma_d}^C = \frac{{\sigma_d}^S}{n} \qquad (3.104)$$

3.3.5. Loads eccentric with respect to the webs

Up until this point, all discussions were based upon the principle that the box girder was subjected to loadings equivalent to vertical loads applied at the web-deck connecting joints. Unfortunately, this is hardly a common case, as eccentricities usually take place.

Let us now consider a set of generic vertical loads located anywhere along the top flange (see Figure 3.21). The equivalent nodal forces and moments m_A, m_B, p_A, p_B can be calculated by considering statically equivalent loads as shown in the figure[7].

[7] For the interior span, use can be made of the results presented in Table 3.4 concerning the solution of the equilibrium equations for elastic bending. Nodal forces and moments for loads applied at the projecting top flange segments can be obtained directly through rigid-body diagram.

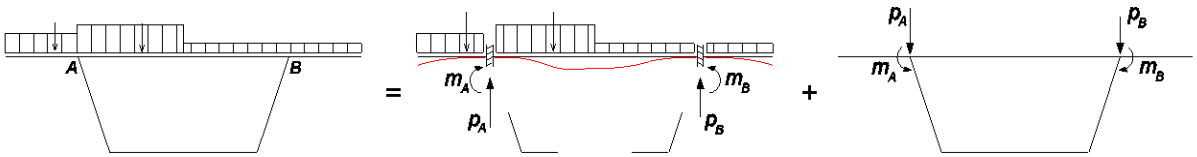

Figure 3.21 – Equivalent nodal loads for vertical loading applied at the top flange

The nodal forces and moments can once again be split into their symmetric and anti-symmetric components, as shown in Figure 3.20.

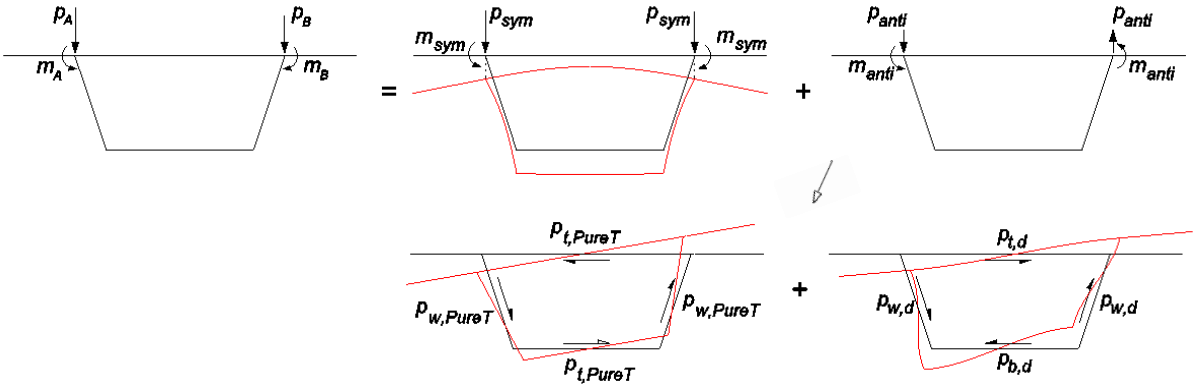

Figure 3.20 – Decomposition of the nodal loads into the pure torsional and distortional subsystems

The subdivision of the anti-symmetric parcel leads to pure torsional

$$p_{t,PureT} = \left(\frac{b_t}{b_w}\right) p_{w,PureT} \ , \quad p_{b,PureT} = \left(\frac{b_b}{b_w}\right) p_{w,PureT} \ , \tag{3.105a}$$

where

$$p_{w,PureT} = \left(\frac{b_w}{(b_t + b_b)d}\right)\left(\frac{(p_A - p_B)b_t}{2} + m_A - m_B\right), \tag{3.106b}$$

and distortional subsystem loads (Schlaich & Scheef, 1982),

$$p_{t,d} = \left(\frac{b_b}{b_w}\right) p_{w,d} \ , \quad p_{b,d} = \left(\frac{b_t}{b_w}\right) p_{w,d} \ , \tag{3.106a}$$

where

$$p_{w,d} = \left(\frac{b_b\, b_w}{(b_t + b_b)d}\right)\left(\frac{(p_A - p_B)b_t}{2}\right) - \left(\frac{b_w}{b_b d}\right)\left(\frac{\beta}{1+\beta} + \frac{r_t - 3\beta - 2\beta r_b}{(r_t + 2)(r_b + 2) - 1}\right)(m_A - m_B)\,. \tag{3.107b}$$

The distortional response can be calculated by conducting the analysis of one of the web plates as a beam on elastic foundation subjected to the distortional load presented in (3.106a). For the torsion analysis, the external toque may be computed as

$$m_T = \left(\frac{(p_A - p_B)b_t}{2} + m_A - m_B\right). \tag{3.107}$$

3.4. SOLUTION OF THE EQUILIBRIUM EQUATIONS

The solutions of the equilibrium equations for elastic bending, mixed torsion and distortion (see Table 3.3) are those that satisfy equilibrium and compatibility for a given loading and boundary conditions. This chapter unveils the solutions considering the cases of concentrated loads (Q) and distributed loads (q). Regarding support conditions for each span, reference will be made to two boundary situations: a simply supported beam (see Figure 3.22a) and a beam fixed on both ends (see Figure 3.22b).

Table 3.3 – Equilibrium equations for bending, torsion with warping and distortion

Loading	Equation[8]	Reference
Elastic bending	$\frac{d^4w}{dx^4} EI_y = q(x)$	(3.9)
Torsion with warping	$\frac{EI_\omega}{\mu}\left(\frac{d^4\chi}{dx^4}\right) + GJ\left(\frac{d^2\chi}{dx^2}\right) = m_T(x)$	(3.63)
Distortion	$\frac{d^4\Delta_w}{dx^4} I_{w,e} + k\,\Delta_w = q_{w,d}(x)$	(3.101)

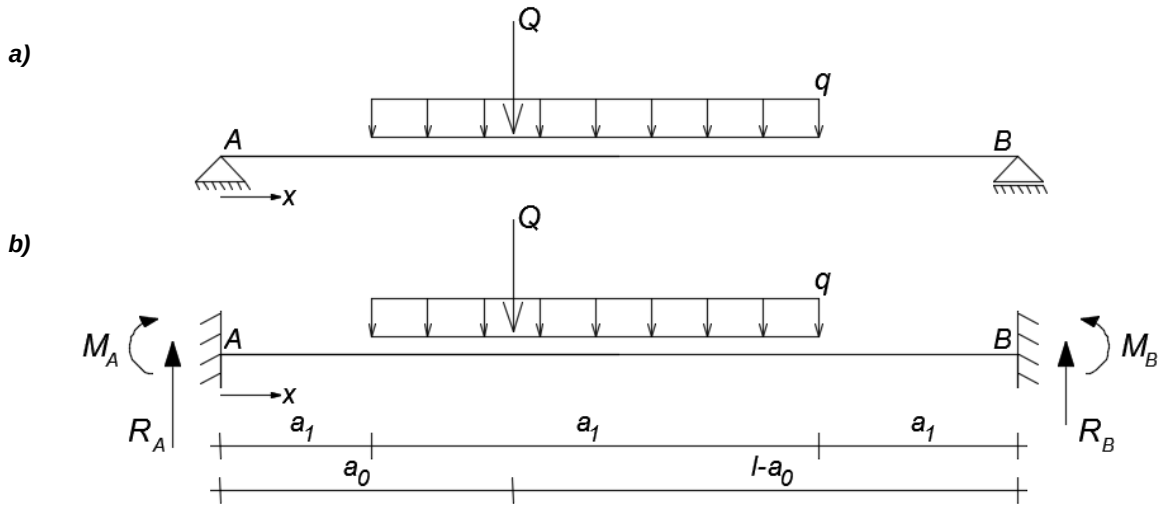

Figure 3.22 – Loading and support conditions

3.4.1. Elastic bending

The solution to the Euler-Bernoulli beam equation (3.9) is of general access within the study field (see for example Brazão Farinha & Correia dos Reis (1992)). Table 3.3 presents the results for support reactions R_A, R_B, M_A and M_B, as well as for the bending moment $M(x)$ in the two case scenarios of support conditions illustrated in Figure 3.22.

[8] For the uniformly distributed load, the notation $q(x)$ = "q" is used hereafter.

Table 3.4 – Solution of the equilibrium equations for bending

Support conditions	**Simply Supported**		**Fixed at both ends**	
Type of loading	**Concentrated** $(\boldsymbol{Q})$	**Distributed** $(\boldsymbol{q})$	**Concentrated** $(\boldsymbol{Q})$	**Distributed** $(\boldsymbol{q})$[9]
R_A	$Q\dfrac{(l-a_0)}{l}$	$q\dfrac{a_2(2a_3+a_2)}{2l}$	$Q\dfrac{(l-a_0)^2}{l^3}(l+2a_0)$	$q\dfrac{a_2}{4l^3}[4a_3l^2+2a_2l^2+4a_4{a_5}^2-4{a_4}^2a_5+{a_2}^2(a_4-a_5)]$
R_B	$Q-R_A$	qa_2-R_A	$Q-R_A$	qa_2-R_A
M_A	0	0	$-Qa_0\dfrac{(l-a_0)^3}{l^2}$	$-q\dfrac{a_2}{12l^2}[12a_4{a_5}^2+{a_2}^2(l-3a_5)]$
M_B	0	0	$-Q{a_0}^2\dfrac{(l-a_0)}{l^2}$	$-q\dfrac{a_2}{12l^2}[12{a_4}^2a_5+{a_2}^2(l-3a_4)]$
$M(x)$	**Concentrated loading** $(\boldsymbol{Q})$**:** $M_A+R_Ax \quad 0\le x\le a_0$; $M_B+R_B(l-x) \quad a_0\le x\le l$		**Distributed loading** $(\boldsymbol{q})$**:** $M_A+R_Ax \quad 0\le x\le a_1$; $M_A+R_Aa_1+[2R_A-q(x-a_1)]\dfrac{x-a_1}{2} \quad a_1\le x\le a_1+a_2$; $M_B+R_B(l-x) \quad a_1+a_2\le x\le l$	

[9] $a_4=a_1+a_2/2$, $a_5=l-a_4$

3.4.2. Torsion with warping

The solution for the problem of torsion with warping takes the general form

$$\frac{d\chi}{dx} = c_1 \cosh\left(\frac{x}{\zeta}\right) + c_2 \operatorname{senh}\left(\frac{x}{\zeta}\right) + c_3 \frac{x}{\zeta} + c_4 \ , \qquad (3.108)$$

where χ is the function present in (3.38) that allows for the warping variation along x; c_1, c_2, c_3 and c_4 are constants of integration, and ζ is a characteristic length defined by

$$\zeta = \sqrt{\frac{EI_\omega}{\mu GJ}} \ . \qquad (3.109)$$

It should be noticed that the solution includes the contribution of warping shear deformability, taken into account through the parameter μ. If this effect is not to be considered, the results may be obtained by simply deleting this parameter in equation (3.109).

Maisel & Roll (1974) summarizes the solutions for torsional moment produced by the eccentric loadings shown in Figure 3.22, in which the distributed load is uniformly extended throughout the whole span and the supports A and B do not allow for any rotation of the cross-section.

The boundary conditions for mixed torsion in the two considered scenarios are:

Simply supported span with no warping restriction at the ends

$$B_A = B_B = 0$$

Span fixed at both ends with warping restrained (3.110)

$$B_A = B_B = 0$$

$$\left(\frac{d\chi}{dx}\right)_A = \left(\frac{d\chi}{dx}\right)_B = 0$$

The corresponding torsional moment diagrams can be determined through:

Concentrated load

$$T(x) = -\frac{l - a_0}{l} M_T \qquad 0 \le x \le a_0$$

$$T(x) = \frac{a_0}{l} M_T \qquad a_0 < x \le l \qquad (3.111)$$

Uniformly distributed load

$$T(x) = \left(x - \frac{l}{2}\right) m_T \qquad 0 \le x \le l$$

Based on the work done by Kollbrunner, Hajdin and Heilig, Maisel & Roll (1974) have compiled a set of expressions which contain the analytical solutions presented in Table 3.5.

Table 3.5 – Solutions of the equilibrium equation for warping with torsion (adapted from Maisel & Roll (1974)*)*

Support conditions	**Simply Supported**	**Fixed at the ends**
Type of loading	**Concentrated** (M_T)	
Bimoment B	$M_T \mu\zeta \dfrac{sinh\frac{l-a_0}{\zeta}}{sinh\frac{l}{\zeta}} sinh\frac{x}{\zeta}$ $\quad 0 \le x \le a_0$ $M_T \mu\zeta \dfrac{sinh\frac{a_0}{\zeta}}{sinh\frac{l}{\zeta}} sinh\frac{l-x}{\zeta}$ $\quad a_0 \le x \le l$	$\mu\,\zeta M_T\left(C_1\cosh\frac{x}{\zeta}+C_2\sinh\frac{x}{\zeta}\right)$ $\quad 0 \le x \le a_0$ $\mu\,\zeta M_T\left(C_1\cosh\frac{x}{\zeta}+C_2\sinh\frac{x}{\zeta}-\sinh\frac{x-a_0}{\zeta}\right)$ $\quad a_0 \le x \le l$ $C_1 = \dfrac{\left(\frac{l-a_0}{\mu\zeta}-\sinh\frac{l-a_0}{\zeta}\right)\left(1-cosh\frac{l}{\zeta}\right)-\left(\frac{l}{\mu\zeta}-\sinh\frac{l}{\zeta}\right)\left(1-cosh\frac{l-a_0}{\zeta}\right)}{2-2cosh\frac{l}{\zeta}+\frac{l}{\mu\zeta}\sinh\frac{l}{\zeta}}$ $C_2 = \dfrac{\left(\frac{l-a_0}{\mu\zeta}-\sinh\frac{l-a_0}{\zeta}\right)\sinh\frac{l}{\zeta}+\left(1-cosh\frac{l}{\zeta}\right)\left(1-cosh\frac{l-a_0}{\zeta}\right)}{2-2cosh\frac{l}{\zeta}+\frac{l}{\mu\zeta}\sinh\frac{l}{\zeta}}$
Type of loading	**Uniformly distributed** $(\boldsymbol{m_T})$	
Bimoment B	$m_T\mu\zeta^2\left(1-\dfrac{sinh\frac{l-x}{\zeta}}{sinh\frac{l}{\zeta}}-\dfrac{sinh\frac{x}{\zeta}}{sinh\frac{l}{\zeta}}\right)$	$m_T\mu\zeta^2\left(1-\dfrac{\frac{l}{2\zeta}}{tanh\frac{l}{2\zeta}}\dfrac{sinh\frac{x}{\zeta}+sinh\frac{l-x}{\zeta}}{sinh\frac{l}{\zeta}}\right)$

3.4.3. Distortion

As mentioned in the previous sections, the box girders' distortional response can be analysed through the beam on elastic foundation analogy. A solution for this equivalent problem has been studied to some extent by Hetenyi (1946), whose findings serve as the basis for the following deductions and results.

Let us consider an elastically supported finite beam subjected to standard concentrated and distributed loads – Figure 3.23a – and a similar beam, subjected to the same loading, but with infinite length – Figure 3.23b.

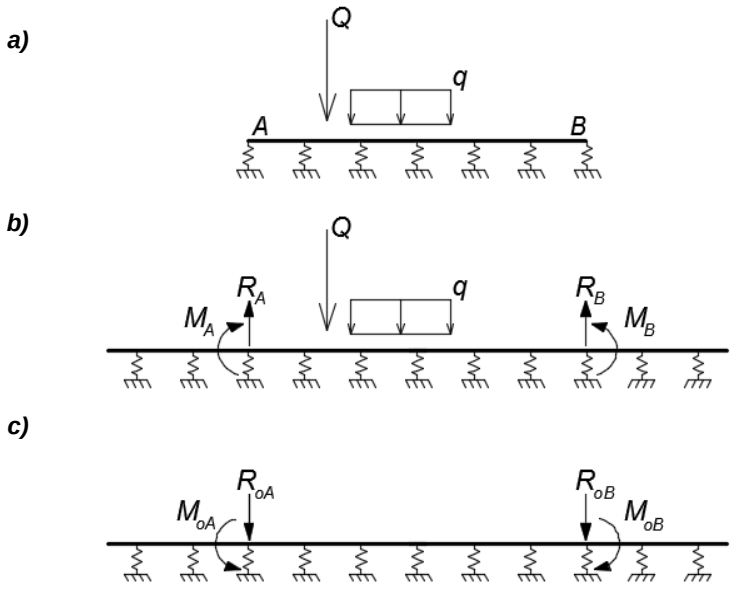

Figure 3.23 – Procedure of analysis for a beam on an elastic foundation

The first step of the procedure involves the analysis of the beam of infinite length. As a result of this analysis, bending moments, shear forces, rotations and displacements are developed at points A and B, which correspond to the ends of the beam of finite length. For the two systems to be equivalent, it is necessary to introduce in points A and B of the infinite beam a set of additional forces and bending moments so that the boundary conditions are fulfilled. For the particular case displayed in Figure 3.23a, such conditions take the following form

$$\begin{aligned} \sum F_A &= \sum F_B = 0 \\ \sum M_A &= \sum M_B = 0 \end{aligned} \qquad (3.112)$$

The solution of the finite-length beam will therefore come as a superposition of the solutions for the beam of infinite length subjected to the initial loading – Figure 3.23b – and to the additional "end" loads – Figure 3.23c which were calculated by solving the system of equations (3.112). The generic expressions are presented in equations (3.113) and (3.114).

$$\begin{aligned}\Delta_{w,A}=\frac{\lambda}{2k}[&R_{oA}\bar{A}(x)+R_{oB}\bar{A}(l-x)+Q\bar{A}(|x-a_0|)\,]\\&+\frac{\lambda^2}{k}[M_{oA}\bar{B}(x)+M_{oB}\bar{B}(l-x)]\\&+\frac{q}{2k}\{c_1[\bar{D}(a_1-x)-\bar{D}(a_1+a_2-x)]\\&+c_2[2-\bar{D}(x-a_1)-\bar{D}(a_1+a_2-x)]\\&+c_3[\bar{D}(x-a_1-a_2)-\bar{D}(x-a_1)]\}\ ,\end{aligned}\qquad (3.113)$$

$$\begin{aligned}M_{w,A}=\frac{1}{4\lambda}[&R_{oA}\bar{C}(x)+R_{oB}\bar{C}(l-x)+Q\bar{C}(|x-a_0|)\,]\\&+\frac{1}{2}[M_{oA}\bar{D}(x)+M_{oB}\bar{D}(l-x)]\\&+\frac{q}{4\lambda^2}\{-c_1[\bar{B}(a_1-x)-\bar{B}(a_1+a_2-x)]\\&+c_2[\bar{B}(x-a_1)+\bar{B}(a_1+a_2-x)]\\&-c_3[\bar{B}(x-a_1-a_2)-\bar{B}(x-a_1)]\}\ ,\end{aligned}\qquad (3.114)$$

where

$$\begin{array}{lll}c_1=1 & c_2=c_3=0 & 0\le x\le a_1\\ c_2=1 & c_1=c_3=0 & a_1\le x\le a_1+a_2\\ c_3=1 & c_1=c_2=0 & a_1+a_2\le x\le l\end{array}\qquad (3.115)$$

The functions $\bar{A}(x)$, $\bar{B}(x)$, $\bar{C}(x)$ and $\bar{D}(x)$ are defined according to:

$$\begin{aligned}\bar{A}(x)&=e^{-\lambda x}(cos\lambda x+sin\lambda x)\,,\\ \bar{B}(x)&=e^{-\lambda x}sin\lambda x\ ,\\ \bar{C}(x)&=e^{-\lambda x}(cos\lambda x-sin\lambda x)\,,\\ \bar{D}(x)&=e^{-\lambda x}cos\lambda x\end{aligned}\qquad (3.116)$$

and

$$\lambda=\frac{1}{L_d}=\sqrt[4]{\frac{k}{4EI_{w,e}}}\qquad (3.117)$$

The parameter L_d is the characteristic length for distortion (Schlaich & Scheef, 1982). It relates the longitudinal bending stiffness of the beam ($EI_{w,e}$) with the transverse stiffness of the cross-section (k).

The solutions for the system of equations presented in (3.112) are more easily obtained when considering the initial loading divided up into its symmetric and anti-symmetrical components:

$$\begin{array}{ll}M_A^{sym}=\frac{1}{2}(M_A+M_B) & R_A^{sym}=\frac{1}{2}(R_A+R_B)\\ M_A^{anti}=\frac{1}{2}(M_A-M_B) & R_A^{anti}=\frac{1}{2}(R_A-R_B)\end{array}\qquad (3.118)$$

The corresponding symmetric and anti-symmetrical sets of end moments and forces can be retrieved by

$$\begin{aligned} M_{oA} &= M_{oA}^{sym} + M_{oA}^{anti} & \qquad R_{oA} &= R_{oA}^{sym} + R_{oA}^{anti} \\ M_{oB} &= M_{oB}^{sym} + M_{oB}^{anti} & \qquad R_{oB} &= R_{oB}^{sym} + R_{oB}^{anti} \end{aligned} \tag{3.119}$$

The previous clarifications were directed at the specific case of a beam elastically supported along the span and without end supports. For the situations presented in Figure 3.22, the boundary conditions can be described as follows, where Δ_w are the web displacements and θ the corresponding rotations:

- Simply supported beam

$$a)\ \Delta_{w,A} = \Delta_{w,B} = 0$$
$$b)\ \sum M_A = \sum M_B = 0 \tag{3.120}$$

- End-fixed beam

$$c)\ \Delta_{w,A} = \Delta_{w,B} = 0$$
$$d)\ \theta_A = \theta_B = 0$$

Following the same procedures, expressions were obtained by Hetenyi (1946) for the values of M_{oA}, M_{oB}, R_{oA} and R_{oB} in these circumstances. Based on this work, Pedro (1995) compiled and synthesized the results for the specific loading and support conditions at hand, which are presented in Table 3.6.

Table 3.6 – Particular solutions for the distortion equilibrium equation (adapted from Pedro (1995)*)*

Support conditions	**Simply Supported**		**Fixed at both ends**	
Type of loading	**Concentrated (Q)**	**Distributed (q)**	**Concentrated (Q)**	**Distributed (q)**
R_A	$y_A = \frac{Q\lambda}{2k}\bar{A}(a_0)$	$y_A = \frac{q}{2k}[\bar{D}(a_1) - \bar{D}(a_1 + a_2)]$	$y_A = \frac{Q\lambda}{2k}\bar{A}(a_0)$	$y_A = \frac{q}{2k}[\bar{D}(a_1) - \bar{D}(a_1 + a_2)]$
R_B	$y_B = \frac{Q\lambda}{2k}\bar{A}(l - a_0)$	$y_B = \frac{q}{2k}[\bar{D}(a_3) - \bar{D}(a_2 + a_3)]$	$y_B = \frac{Q\lambda}{2k}\bar{A}(l - a_0)$	$y_B = \frac{q}{2k}[\bar{D}(a_3) - \bar{D}(a_2 + a_3)]$
M_A	$M_A = \frac{Q}{4\lambda}\bar{C}(a_0)$	$M_A = -\frac{q}{4\lambda^2}[B(a_1) - \bar{B}(a_1 + a_2)]$	$\theta_A = \frac{Q\lambda^2}{k}\bar{B}(a_0)$	$\theta_A = \frac{q}{2k}[\bar{A}(a_1) - \bar{A}(a_1 + a_2)]$
M_B	$M_B = \frac{Q}{4\lambda}\bar{C}(l - a_0)$	$M_B = -\frac{q}{4\lambda^2}[B(a_3) - \bar{B}(a_2 + a_3)]$	$\theta_B = \frac{Q\lambda^2}{k}\bar{B}(l - a_0)$	$\theta_B = \frac{q}{2k}[\bar{A}(a_3) - \bar{A}(a_2 + a_3)]$
	$y_A^{sym} = \frac{1}{2}(y_A + y_B)$ $M_A^{sym} = \frac{1}{2}(M_A + M_B)$ $y_A^{anti} = \frac{1}{2}(y_A - y_B)$ $M_A^{anti} = \frac{1}{2}(M_A - M_B)$		$y_A^{sym} = \frac{1}{2}(y_A + y_B)$ $\theta_A^{sym} = \frac{1}{2}(\theta_A + \theta_B)$ $y_A^{anti} = \frac{1}{2}(y_A - y_B)$ $\theta_A^{anti} = \frac{1}{2}(\theta_A - \theta_B)$	
	$R_{oA}^{sym} = 4\lambda\xi_I\left[M_A^{sym}\bar{B}(l) - 2\lambda^2 EI_{w,e}y_A^{sym}[1 + \bar{D}(l)]\right]$ $M_{oA}^{sym} = -2\xi_I\left[M_A^{sym}[1 + \bar{A}(l)] - 2\lambda^2 EI_{w,e}y_A^{sym}[1 + \bar{C}(l)]\right]$ $R_{oA}^{anti} = -4\lambda\xi_{II}\left[M_A^{anti}\bar{B}(l) + 2\lambda^2 EI_{w,e}y_A^{anti}[1 - \bar{D}(l)]\right]$ $M_{oA}^{anti} = -2\xi_{II}\left[M_A^{anti}[1 - \bar{A}(l)] - 2\lambda^2 EI_{w,e}y_A^{anti}[1 - \bar{C}(l)]\right]$		$R_{oA}^{sym} = 8\lambda^2 EI_{w,e}\xi_I\left[\theta_A^{sym}\bar{B}(l) - \lambda^2 y_A^{sym}[1 - \bar{C}(l)]\right]$ $M_{oA}^{sym} = -4\lambda EI_{w,e}\xi_I\left[\theta_A^{sym}[1 + \bar{A}(l)] - 2\lambda y_A^{sym}B(l)\right]$ $R_{oA}^{anti} = -8\lambda^2 EI_{w,e}\xi_I\left[\theta_A^{anti}\bar{B}(l) + \lambda^2 y_A^{anti}[1 + \bar{C}(l)]\right]$ $M_{oA}^{anti} = -4\lambda EI_{w,e}\xi_I\left[\theta_A^{anti}[1 - \bar{A}(l)] + 2\lambda y_A^{sym}B(l)\right]$	
	$\xi_I = \frac{1}{2}\frac{e^{\lambda l}}{\cosh\lambda l + \cos\lambda l}$	$\xi_{II} = \frac{1}{2}\frac{e^{\lambda l}}{\cosh\lambda l - \cos\lambda l}$	$\xi_I = \frac{1}{2}\frac{e^{\lambda l}}{\sinh\lambda l + \sin\lambda l}$	$\xi_{II} = \frac{1}{2}\frac{e^{\lambda l}}{\sinh\lambda l - \sin\lambda l}$
	$R_{oA} = R_{oA}^{sym} + R_{oA}^{anti}$ $R_{oB} = R_{oB}^{sym} + R_{oB}^{anti}$		$M_{oA} = M_{oA}^{sym} + M_{oA}^{anti}$ $M_{oB} = M_{oB}^{sym} + M_{oB}^{anti}$	

4. GENERALIZED BEAM THEORY (GBT)

4.1. GENERAL CONSIDERATIONS

The analysis of a box girder bridge, either composite or non-composite, can be executed by making use of GBT, i.e., Generalized Beam Theory. This theory has been proven to be an elegant and insightful approach for the structural analysis of thin-walled prismatic members such as the ones considered here (Gonçalves & Camotim, 2010; Gonçalves, R., Ritto-Corrêa, M., & Camotim, D., 2010).

GBT analysis makes possible to allow for global load-carrying mechanisms, such as longitudinal bending, torsion and distortion, as well as other global/local structural responses. Any of these can be considered within the analyses as an individual cross-section deformation mode, whose amplitude function is the unknown and generally varies along the longitudinal direction. The amplitude functions are determined by solving the resulting equilibrium equations.

This chapter introduces the fundamental principles of this theory, first developed by Schardt (1989) as a continuation of the pioneering work done by Vlasov (1961), and subject of further intensive research by Camotim and co-workers, as well as the procedure followed for the implementation of a GBT displacement-based finite element. At the same time and whenever possible, comparison is made between this approach and that presented in Chapter 3, concerning the Classical Formulations.

It should be noted that unlike in the Classical Formulations, in GBT there is no need to homogenise the cross-section, as long as the elastic properties of each wall are properly defined. Although explicit consideration of the effects of steel reinforcement and of shear connection slip have been considered in other GBT formulations (Gonçalves & Camotim, 2010; Henriques, Gonçalves, & Camotim, 2015), they are not included in the present work.

4.2. FUNDAMENTAL FORMULATIONS

The definition of the fundamental equations in GBT begins by setting up reasonable simplifying hypotheses. This will allow for the development of a thin-walled beam theory which is efficient and, at the same time, sufficiently accurate.

4.2.1. Hypotheses

D1. Small displacements;
D2. Fibres normal to the mid-plane of the walls remain undeformed and perpendicular to the mid-plane in the deformed configuration – Kirchhoff's thin-plate hypothesis;
D3. Homogenous and isotropic elastic materials in accordance with Hooke's law;
D4. The walls are subjected to a plane stress state;
D5. The loads are applied at the mid-plane of the walls only.

4.2.2. Equilibrium equations

Let us first consider the reference configuration presented in Figure 4.1, in which *x*, *y* and *z* are the local axes of each wall segment along the longitudinal, cross-section mid-line and thickness directions, respectively.

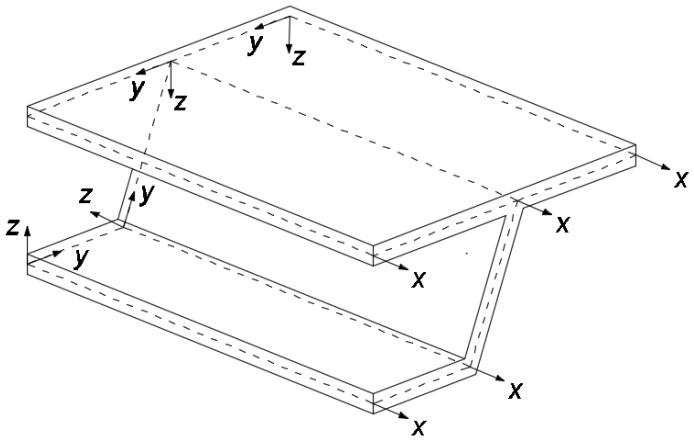

Figure 4.1 – Arbitrary thin-walled member geometry and local coordinate systems

The displacement field of each wall can be taken generically as

$$\boldsymbol{U}(x,y,z) = \begin{bmatrix} U_x \\ U_y \\ U_z \end{bmatrix} . \tag{4.1}$$

According to the small displacements hypothesis, the strain tensor components result directly as

$$\begin{aligned} \varepsilon_{xx} &= U_{x,x} \ , \\ \varepsilon_{yy} &= U_{y,y} \ , \\ \varepsilon_{zz} &= U_{z,z} \ , \\ \gamma_{xy} = \gamma_{yx} &= U_{x,y} + U_{y,x} \ , \\ \gamma_{xz} = \gamma_{zx} &= U_{x,z} + U_{z,x} \ , \\ \gamma_{yz} = \gamma_{zy} &= U_{y,z} + U_{y,x} \ , \end{aligned} \tag{4.2}$$

which can be put together in matrix form as:

$$\boldsymbol{\varepsilon}(x,y,z) = \begin{bmatrix} \varepsilon_{xx} & \frac{\gamma_{xy}}{2} & \frac{\gamma_{xz}}{2} \\ \gamma_{yx} & \varepsilon_{yy} & \frac{\gamma_{yz}}{2} \\ \frac{\gamma_{zx}}{2} & \frac{\gamma_{zy}}{2} & \varepsilon_{zz} \end{bmatrix} . \tag{4.3}$$

According to Kirchhoff's hypothesis, one has

$$\varepsilon_{zz} = \gamma_{xz} = \gamma_{yz} = 0 \ , \tag{4.4}$$

meaning that the strain tensor can be reduced to a column vector:

$$\boldsymbol{\varepsilon}(x,y,z) = \begin{Bmatrix} \varepsilon_{xx} \\ \varepsilon_{yy} \\ \gamma_{xy} \end{Bmatrix} . \tag{4.5}$$

At the same time, Kirchhoff's assumption allows for the displacement field of each wall to be written as a function of the local mid-surface displacements u, v and w, which are measured respectively along x, y and z directions:

$$\boldsymbol{U}(x,y,z) = \begin{bmatrix} u(x,y) - zw_{,x}(x,y) \\ v(x,y) - zw_{,y}(x,y) \\ w(x,y) \end{bmatrix} . \qquad (4.6)$$

In turn, these displacements can also be expressed as a sum of two uncoupled components, one regarding the membrane component and another regarding the flexural component (see Figure 4.2).

$$\boldsymbol{U}(x,y,z) = \overbrace{\begin{bmatrix} u(x,y) \\ v(x,y)) \\ w(x,y) \end{bmatrix}}^{membrane} + \overbrace{\begin{bmatrix} -z\, w_{,x}(x,y) \\ -z\, w_{,y}(x,y) \\ 0 \end{bmatrix}}^{flexural} . \qquad (4.7)$$

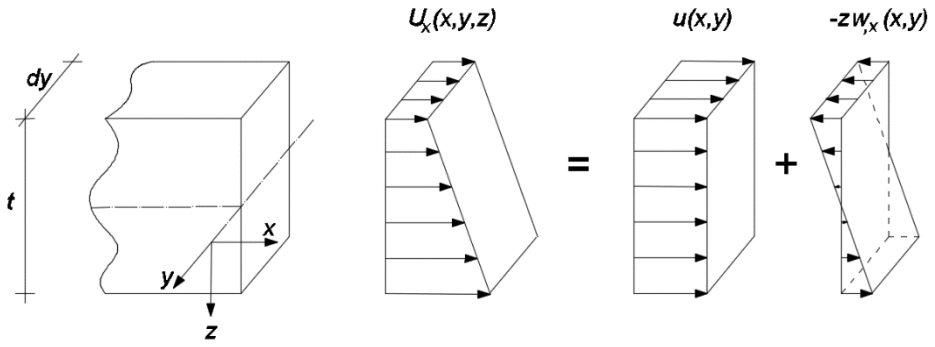

Figure 4.2 – Membrane and flexural components for displacement U_x

Consequently, the strain tensor can be equally written as the sum of membrane $[\,]^M$ and flexural $[\,]^F$ deformations,

$$\begin{aligned} {\varepsilon_{xx}}^M &= u_{,x} \;;\; {\varepsilon_{xx}}^F = -zw_{,xx} \;, \\ {\varepsilon_{yy}}^M &= v_{,y} \;;\; {\varepsilon_{yy}}^F = -zw_{,yy} \;, \\ {\gamma_{xy}}^M &= u_{,y} + v_{,x} \;;\; {\gamma_{xy}}^F = -2zw_{,xy} \;. \end{aligned} \qquad (4.8)$$

Let us now take special attention to the mid-surface displacements. According to GBT, the deformed configuration is expressed as a linear combination of the cross-section deformation modes, whose amplitude functions vary along the longitudinal direction. Therefore, one can define

$$\begin{aligned} u(x,y) &= \sum \bar{u}_k(y)\Phi_{k,x}(x) \;, \\ v(x,y) &= \sum \bar{v}_k(y)\Phi_k(x) \,, \\ w(x,y) &= \sum \bar{w}_k(y)\Phi_k(x) \;, \end{aligned} \qquad (4.9)$$

where k = 1, …, D, D is the number of deformation modes, $\bar{u}_k$, $\bar{v}_k$ and $\bar{w}_k$ are the deformation mode displacement components and Φ_k are their amplitude functions along the axis of the beam.

The definition of the deformation modes, i.e., $\bar{u}_k$, $\bar{v}_k$ and $\bar{w}_k$, is itself a very specific and somewhat complex problem, which has been the subject of several works, as previously mentioned. Ideally, the procedure to be used should determine a hierarchic set of cross-section deformation modes, where the

"participation factor" of each mode decreases with the order of the mode within the set. At the same time, the procedure should ensure that only the first few modes are suitable for arriving at a sufficiently accurate deformed configuration (Gonçalves et al., 2010). As a result of this line of investigation, a *freeware* program entitled GBTUL was developed and made available at http://www.civil.ist.utl.pt/gbt/, allowing for a rapid calculation of the deformation modes for arbitrary cross-sections.

It should be noted that in (4.9) the expression for the displacement u contains a first order derivative $\Phi_{k,x}$. This is adopted to make it possible to accommodate Vlasov's assumption (null membrane shear strains ${\gamma_{xy}}^M = 0 \leftrightarrow \bar{u}_{,y} + v_{,x} = 0$), which is common in GBT analysis since it leads to significant computational savings without sacrificing accuracy. However, it should be noted that adopting $\Phi_{k,x}$ can be done without any loss of generality (Gonçalves et al., 2010).

Incorporating (4.9) in (4.7) leads to

$$\boldsymbol{U}(x,y,z) = \begin{bmatrix} \sum \bar{u}_k(y)\Phi_{k,x}(x) \\ \sum \bar{v}_k(y)\Phi_k(x) \\ \sum \bar{w}_k(y)\Phi_k(x) \end{bmatrix} + \begin{bmatrix} -z\sum \bar{w}_k(y)\Phi_{k,x}(x) \\ -z\sum \bar{w}_{k,y}(y)\Phi_k(x) \\ 0 \end{bmatrix}, \qquad (4.10)$$

which can be rewritten in matrix grouping modal displacements and amplitudes $\bar{u}_k$, $\bar{v}_k$, $\bar{w}_k$, Φ_k and $\Phi_{k,x}$ into vectors $\bar{\boldsymbol{u}}$, $\bar{\boldsymbol{v}}$, $\bar{\boldsymbol{w}}$, $\boldsymbol{\Phi}$ and $\boldsymbol{\Phi}_{,x}$, respectively:

$$\boldsymbol{U}(x,y,z) = \begin{bmatrix} 0 & \bar{\boldsymbol{u}}^t \\ \bar{\boldsymbol{v}}^t & 0 \\ \bar{\boldsymbol{w}}^t & 0 \end{bmatrix} \begin{bmatrix} \boldsymbol{\Phi} \\ \boldsymbol{\Phi}_{,x} \end{bmatrix} - z \begin{bmatrix} 0 & \bar{\boldsymbol{w}}^t \\ {\bar{\boldsymbol{w}}_{,y}}^t & 0 \\ 0 & 0 \end{bmatrix} \begin{bmatrix} \boldsymbol{\Phi} \\ \boldsymbol{\Phi}_{,x} \end{bmatrix} = \boldsymbol{\Xi}_U \begin{bmatrix} \boldsymbol{\Phi} \\ \boldsymbol{\Phi}_{,x} \end{bmatrix}. \qquad (4.11)$$

By taking (4.8) into account, the strain tensor can be defined as a function of an auxiliary matrix $\boldsymbol{\Xi}_{\boldsymbol{\varepsilon}}$ such that

$$\boldsymbol{\varepsilon}(x,y,z) = \begin{bmatrix} 0 & 0 & \bar{\boldsymbol{u}}^t \\ {\bar{\boldsymbol{v}}_{,y}}^t & 0 & 0 \\ 0 & (\bar{\boldsymbol{u}}_{,y} + \boldsymbol{\nu})^t & 0 \end{bmatrix} \begin{bmatrix} \boldsymbol{\Phi} \\ \boldsymbol{\Phi}_{,x} \\ \boldsymbol{\Phi}_{,xx} \end{bmatrix} - z \begin{bmatrix} 0 & 0 & \bar{\boldsymbol{w}}^t \\ {\bar{\boldsymbol{w}}_{,yy}}^t & 0 & 0 \\ 0 & 2{\bar{\boldsymbol{w}}_{,y}}^t & 0 \end{bmatrix} \begin{bmatrix} \boldsymbol{\Phi} \\ \boldsymbol{\Phi}_{,x} \\ \boldsymbol{\Phi}_{,xx} \end{bmatrix} = \boldsymbol{\Xi}_{\varepsilon} \begin{bmatrix} \boldsymbol{\Phi} \\ \boldsymbol{\Phi}_{,x} \\ \boldsymbol{\Phi}_{,xx} \end{bmatrix}. \qquad (4.12)$$

Stresses can be easily obtained through a constitutive relation operator $\boldsymbol{C_e}$, which in this case refers to isotropic linear elastic materials:

$$\begin{Bmatrix} \sigma_{xx} \\ \sigma_{yy} \\ \tau_{xy} \end{Bmatrix} = \boldsymbol{C_e} \begin{Bmatrix} \varepsilon_{xx} \\ \varepsilon_{yy} \\ \gamma_{xy} \end{Bmatrix} = \begin{bmatrix} \frac{\alpha E}{1-\nu^2} & \frac{\nu E}{1-\nu^2} & 0 \\ \frac{\nu E}{1-\nu^2} & \frac{\alpha E}{1-\nu^2} & 0 \\ 0 & 0 & G \end{bmatrix} \begin{Bmatrix} \varepsilon_{xx} \\ \varepsilon_{yy} \\ \gamma_{xy} \end{Bmatrix}. \qquad (4.13)$$

Here, α is a factor that equals 1 unless wall membrane transverse extensions are assumed null ($\varepsilon_{yy}^M = 0$), in which case $\alpha = (1-\nu^2)$ is adopted for the membrane terms to avoid over-stiff solutions.

One should be aware that a plane stress state is assumed, which is mildly inconsistent with the plane strain state of (4.5) for materials with non-null Poisson ratio.

The equilibrium equations are then derived applying the Principle of Virtual Work which, assuming that loads f are applied at the walls mid-surface, results in the following equation system:

$$\delta W_{int} + \delta W_{ext} = -\int_V \delta \boldsymbol{\varepsilon}^t \boldsymbol{\sigma}\, dV + \int_\Omega \delta \boldsymbol{U}^t \boldsymbol{f}\, d\Omega = 0 \ , \tag{4.14}$$

where V is the initial volume of the bar and Ω is its mid-surface. Taking into account the strain and stresses from (4.12) and (4.13), the virtual work equation becomes

$$-\int_V \begin{bmatrix} \delta\boldsymbol{\Phi} \\ \delta\boldsymbol{\Phi}_{,x} \\ \delta\boldsymbol{\Phi}_{,xx} \end{bmatrix}^T {\boldsymbol{\Xi}_\varepsilon}^t \boldsymbol{C_e}\, \boldsymbol{\Xi}_\varepsilon \begin{bmatrix} \boldsymbol{\Phi} \\ \boldsymbol{\Phi}_{,x} \\ \boldsymbol{\Phi}_{,xx} \end{bmatrix} dV + \int_\Omega \delta \boldsymbol{U}^t \boldsymbol{f}\, d\Omega = 0 \ . \tag{4.15}$$

Knowing that the amplitude functions are by definition variable only along the longitudinal axis, the previous expression can be further developed into

$$-\int_L \begin{bmatrix} \delta\boldsymbol{\Phi} \\ \delta\boldsymbol{\Phi}_{,x} \\ \delta\boldsymbol{\Phi}_{,xx} \end{bmatrix}^T \boldsymbol{M} \begin{bmatrix} \boldsymbol{\Phi} \\ \boldsymbol{\Phi}_{,x} \\ \boldsymbol{\Phi}_{,xx} \end{bmatrix} dx + \int_\Omega \delta \boldsymbol{U}^t \boldsymbol{f}\, d\Omega = 0 \ , \tag{4.16}$$

where L is the member length and $\boldsymbol{M}$ is an auxiliary matrix defined as

$$\boldsymbol{M} = \int_A \int_{-t/2}^{t/2} {\boldsymbol{\Xi}_\varepsilon}^t \boldsymbol{C_e}\, \boldsymbol{\Xi}_\varepsilon\, dz\, dy \ . \tag{4.17}$$

in which A refers to the cross-section area

Through consideration of (4.12), this matrix can be reformulated as an agglutination of the GBT linear stiffness matrices $\boldsymbol{B}$, $\boldsymbol{C}$, $\boldsymbol{D_1}$, $\boldsymbol{D_2}$ and ${\boldsymbol{D_2}}^t$, each of them associated with distinct strain components, namely transverse extension/bending, primary/secondary warping, membrane/flexural shear and membrane/flexural Poisson effects, respectively.

$$\boldsymbol{M} = \begin{bmatrix} \boldsymbol{B} & [\boldsymbol{0}] & \boldsymbol{D_2} \\ [\boldsymbol{0}] & \boldsymbol{D_1} & [\boldsymbol{0}] \\ {\boldsymbol{D_2}}^t & [\boldsymbol{0}] & \boldsymbol{C} \end{bmatrix} \tag{4.18}$$

$$\begin{aligned} B_{ij} &= {B_{ij}}^M + {B_{ij}}^F = \int_S \frac{Et}{1-\nu^2} v_{i,y} v_{j,y}\, dy + \int_S \frac{Et^3}{12(1-\nu^2)} w_{i,yy} w_{j,yy}\, dy \\ C_{ij} &= {C_{ij}}^M + {C_{ij}}^F = \int_S \frac{\alpha Et}{1-\nu^2} u_i u_j\, dy + \int_S \frac{Et^3}{12(1-\nu^2)} w_i w_j\, dy \\ {D_1}_{ij} &= {D_1}_{ij}^{\ M} + {D_1}_{ij}^{\ F} = \int_S Gt\,(u_{i,y} + v_i)(u_{j,y} + v_j)\, dy + \int_S \frac{Gt^3}{3} w_i w_j\, dy \\ {D_2}_{ij} &= {D_2}_{ij}^{\ M} + {D_2}_{ij}^{\ F} = \int_S \frac{\nu Et}{1-\nu^2} u_i v_{j,y}\, dy + \int_S \frac{\nu Et^3}{12(1-\nu^2)} w_i w_{j,yy}\, dy \end{aligned} \tag{4.19}$$

At the same time, the second term of (4.16), which concerns the external work, may also be developed according to (4.11), leading to

$$\delta W_{ext} = \int_\Omega \begin{bmatrix} \delta\boldsymbol{\Phi} \\ \delta\boldsymbol{\Phi}_{,x} \end{bmatrix}^t {\boldsymbol{\Xi}_U}^t \boldsymbol{f}\, d\Omega. \tag{4.20}$$

4.2.3. Deformation modes and additional simplifying hypothesis

For some beam type-problems, two additional assumptions may be employed. These introduce further kinematic constraints that are intended to reduce the number of admissible deformation modes (and hence DOFs) without jeopardizing the accuracy of the results:

E1. Transverse membrane strains are discarded ($\varepsilon_{yy}^{M} = 0$)

E2. Membrane shear strains are null ($\gamma_{xy}^{M} = 0$) - Vlasov's assumption[10].

The first hypothesis immediately leads to discarding transverse extension modes and is acceptable in most beam-type problems, such as those of box-girder bridge decks acted by standard vertical loads. As a result of this hypothesis,

$$v_{,y} = 0 \leftrightarrow \boldsymbol{B^M} = 0 \,, \tag{4.21}$$

and for the membrane terms $\alpha = (1 - \nu^2)$, (4.22)

meaning that (4.19) should be rewritten as

$$\begin{aligned} B_{ij} = {B_{ij}}^{F} &= \int_S \frac{Et^3}{12(1-\nu^2)} w_{i,yy} w_{j,yy}\, dy \\ C_{ij} = {C_{ij}}^{M} + {C_{ij}}^{F} &= \int_S Et u_i u_j\, dy + \int_S \frac{Et^3}{12(1-\nu^2)} w_i w_j\, dy \\ {D_1}_{ij} = {D_1}_{ij}^{M} + {D_1}_{ij}^{F} &= \int_S Gt\big(u_{i,y} + v_i\big)\big(u_{j,y} + v_j\big)\, dy + \int_S \frac{Gt^3}{3} w_i w_j\, dy \\ {D_2}_{ij} = {D_2}_{ij}^{F} &= \int_S \frac{\nu Et^3}{12(1-\nu^2)} w_i w_{j,yy}\, dy \end{aligned} \tag{4.23}$$

Assumption E2 on the other hand is not admissible when dealing with closed-type cross-section members, because of the significant role played by membrane shear deformation in the torsional response. It is also not satisfactory if vertical shear is important or when shear lag effects are relevant.

Despite the fact that assumption E2 cannot be enforced in all deformation modes, it is still advantageous to employ it in order to subdivide the deformation modes into distinct sets (or families).

The first set to be considered here consists of the modes where assumption E2 is valid, i.e., the so-called "Vlasov's modes". It should be noted that, due to the kinematic restraints given by putting together assumptions E1 and E2, the warping mid-plane displacements u_k are necessarily linear. These modes are depicted in Figure 4.3 and correspond to:

Mode 1. Axial extension

Mode 2. Major axis bending

Mode 3. Minor axis bending

Mode 4. Distortion

[10] Similarities can be constructed between Vlasov's hypothesis for the cross-section walls and Bernoulli's hypothesis for bending in beams.

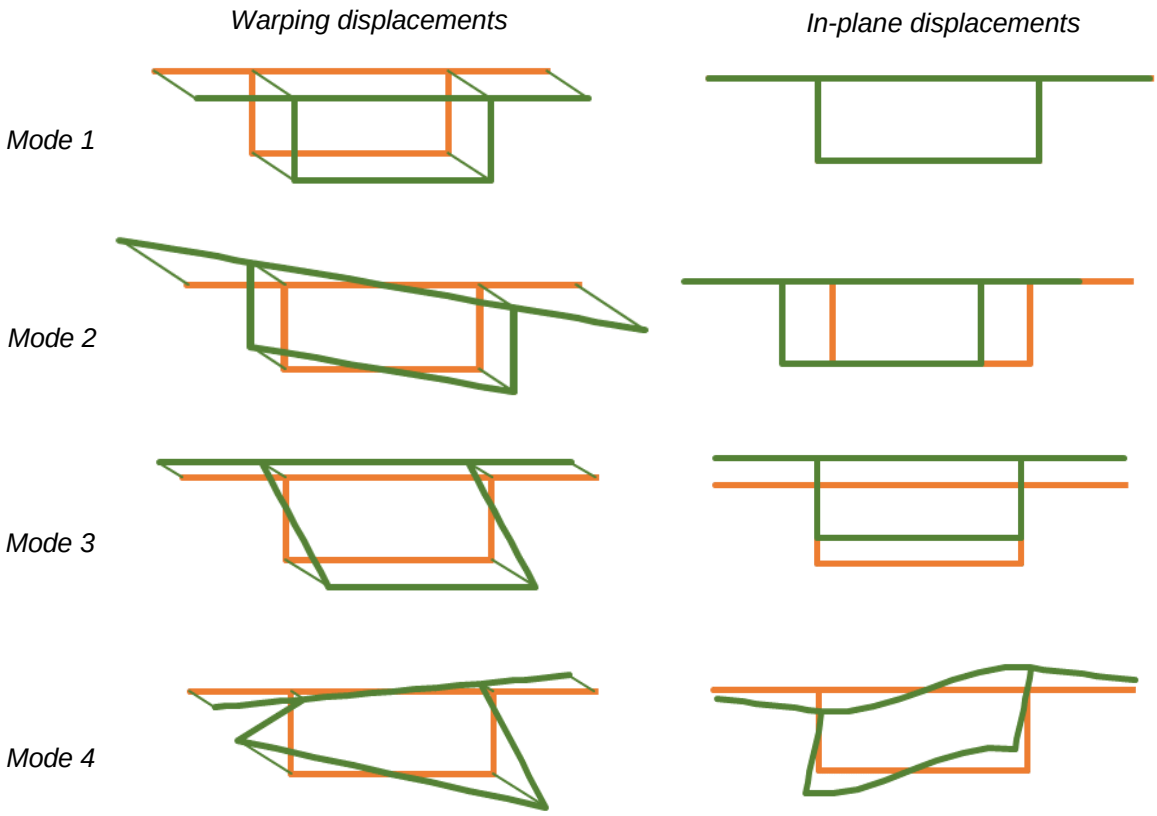

Figure 4.3 – Set of Vlasov's deformation modes

For comparison with Classical Formulations, it should be pointed out that all these modes are orthogonal with respect to matrix C. This means that the axial extension mode does not cause any bending moment nor the "bimoment" associated with distortion and vice-versa. Furthermore, their respective in-plane displacements v and w are determined performing a frame type-analysis, in which u and v are linked through Vlasov's hypothesis.

A second set comprehends the deformation modes related with the shear deformation of the cross-section to torsion and distortion. As mentioned previously, these modes do not comply with Vlasov's assumption. Mode 5 (see Figure 4.4) consists of the deformed shape of the cross-section when considering a constant shear flow circulating around the closed perimeter and is orthogonalized with respect to C against modes 1 through 3 (hence it does not produce axial force nor bending, but it is not orthogonal with respect to distortion).

As seen in section 3.3.3, if bi-shear is to be considered, the warping displacements are no longer strictly correlated to the in-plane twist. This effect can be replicated by taking into account an additional mode (mode 6), which has the same warping shape function as that associated with torsion. Although not addressed in the Classical Formulations approach, the same can be said for the influence of distortion "bi-shear", which is related to mode 7.

Mode 5. Torsion (cell shear flow)

Mode 6. Torsion warping (allows for torsion bi-shear)

Mode 7. Distortion warping (allows for distortion "bi-shear")

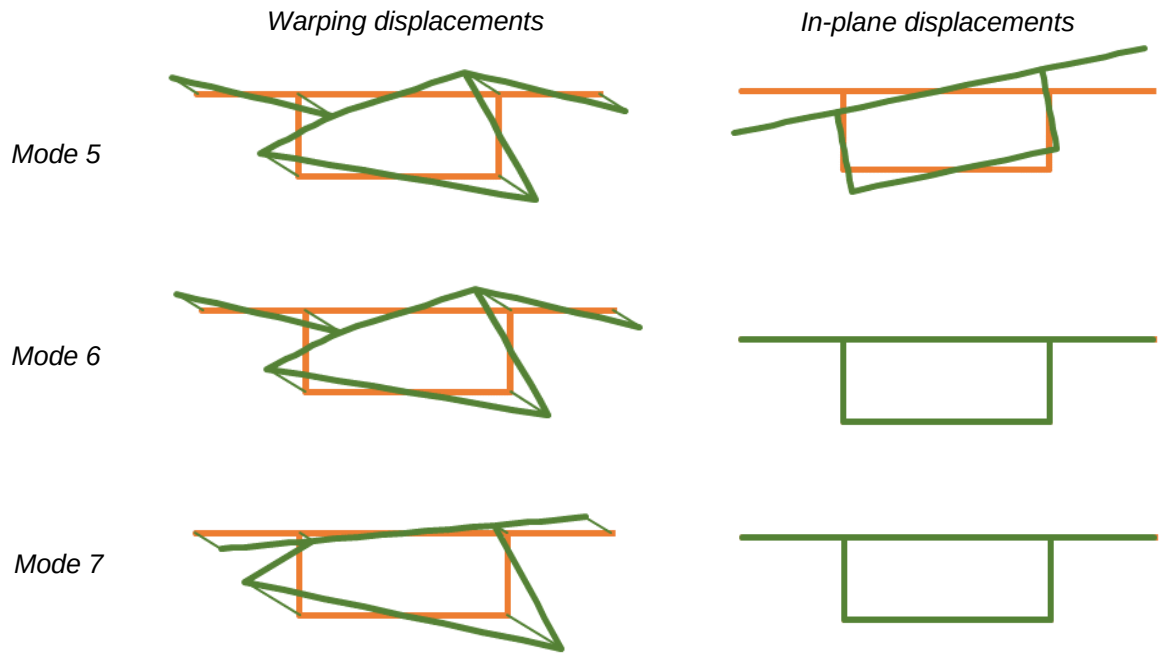

Figure 4.4 – Set of torsion/distortion shear deformation modes

The last set of deformation modes consists on further shear modes that seek to allow for shear lag deformation (see Figure 4.5). It contains both symmetric and anti-symmetric warping modes ($u_k \neq 0, v_k = w_k = 0$) in both top and bottom flanges, allowing to capture more accurately the effect of shear lag deformation in each plate. Although more modes could be considered, these were found sufficient in the analysis of numerical examples, to be discussed in Chapter 6.

Mode 8. Quadratic in projecting top flange (symmetric)
Mode 9. Quartic in projecting top flange (symmetric)
Mode 10. Quartic in interior top flange (symmetric)
Mode 11. Quartic in bottom flange (symmetric)
Mode 12. Quadratic in projecting top flange (anti-symmetrical)
Mode 13. Quartic in projecting top flange (anti-symmetrical)
Mode 14. Cubic in interior top flange (anti-symmetrical)
Mode 15. Cubic in bottom flange (anti-symmetrical)

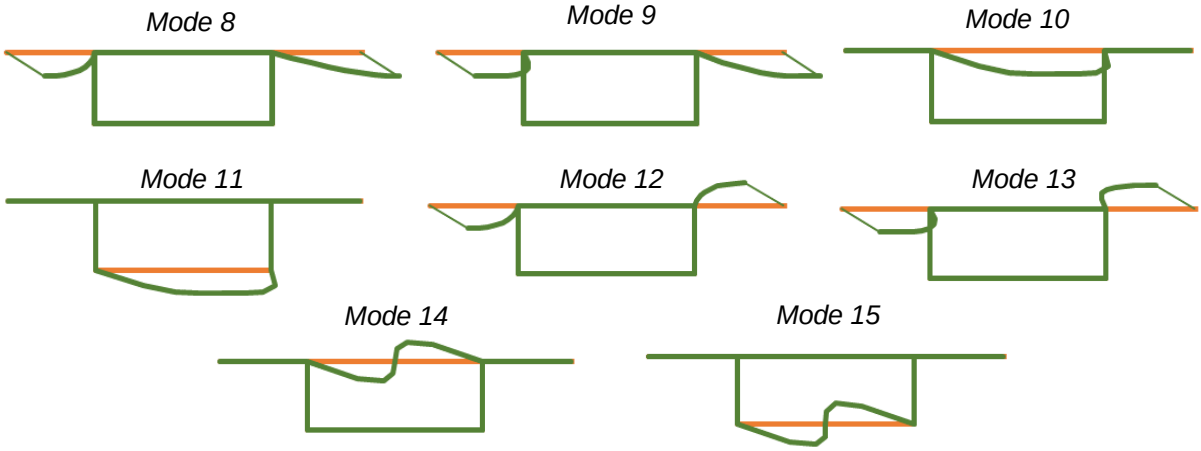

Figure 4.5 – Warping displacements of shear lag warping modes (in-plane displacements are null)

4.3. DEFINITION OF A FINITE ELEMENT

The solution for the structural problems here presented may be approximated by means of a finite element based on GBT. Just as in other finite element models, discretization and interpolation procedures play a major role in both efficiency and accuracy. Two types of discretization are performed:

i. Transverse discretization, which influences the definition of the deformation modes. For the purposes of this dissertation, it suffices to consider a subdivision of the cross-section in six walls, connected at their intersections[11] (see Figure 4.6). Such discretization makes it possible to obtain directly from GBTUL modes 1 through 5 presented in the previous section. Modes 6 and 7 are defined by the warping displacements of modes 5 and 4, respectively. The additional shear lag modes can be defined analytically.

Figure 4.6 – Discretization of the cross-section into natural nodes and wall segments (extracted from GBTUL).

ii. Longitudinal discretization, where the total length of the member, L, is divided into n smaller elements of given lengths l_i. In GBT analyses it is customary to consider equal length elements ($l_i = l = L/n$), even though *h-refinement* can also be performed. In the direct application of this method to the analysis of box girder bridges, it is mandatory to discretize in such a way that the element nodes coincide with sections of discontinuity, as is the case of intermediate supports or diaphragms.

In the context of the longitudinal discretization, for each element, the modal amplitude functions contained in the vector $\boldsymbol{\Phi}$ can be approximated as

$$\boldsymbol{\Phi}(x) = \boldsymbol{\Psi}(x)\, \boldsymbol{d_e} \qquad (4.24)$$

where $\boldsymbol{\Psi}$ is the matrix containing the longitudinal shape functions, and $\boldsymbol{d_e}$ is the vector containing the degrees of freedom of the element, which are nodal values for the amplitude functions and their derivatives.

As can be seen in (4.11), the displacements $\boldsymbol{U}(x,y,z)$ are a function of a first derivative with respect to the x axis, thus requiring C^1 class functions. This also holds in the y direction, but the deformation modes are directly calculated ensuring this compatibility. In this situation, it is possible to make use of Hermite's cubic interpolation functions (see Figure 4.7a), defined as

$$H_1 = 2\left(\frac{x}{l_i}\right)^3 - 3\left(\frac{x}{l_i}\right)^2 + 1 \quad , \; H_2 = l_i\left(\left(\frac{x}{l_i}\right)^3 - 2\left(\frac{x}{l_i}\right)^2 + \frac{x}{l_i}\right) ,$$
$$H_3 = -2\left(\frac{x}{l_i}\right)^3 + 3\left(\frac{x}{l_i}\right)^2 , \qquad H_4 = L_i\left(\left(\frac{x}{l_i}\right)^3 - \left(\frac{x}{l_i}\right)^2\right) . \qquad (4.25)$$

[11] According to GBTUL notation, the discretized nodes can be designated as i) natural nodes, if they are placed at the wall connections or outstands, or as ii) intermediate nodes, if they are located within the walls.

The amplitude function for mode k can then be approximated through

$$\Phi_k(x) = H_1(x)\Phi_k(0) + H_2(x)\Phi_{k,x}(0) + H_3(x)\Phi_k(l_i) + H_4(x)\Phi_{k,x}(l_i) \quad (4.26)$$

For pure warping modes ($\bar{u}_k \neq 0, \bar{v}_k = \bar{w}_k = 0$), these interpolation functions cannot be utilized, because the amplitude is given not as a function of Φ_k but only of $\Phi_{k,x}$ (see (4.11)) and that would lead to a linear dependence of H_1 and H_3. To circumvent this issue, in such situations Lagrange's linear and quadratic hierarchic polynomials are frequently employed (see Figure 4.7b),

$$F_1 = 1 - \left(\frac{x}{l_i}\right),\ F_2 = \left(\frac{x}{l_i}\right),\ F_3 = 4\left(\left(\frac{x}{l_i}\right) - \left(\frac{x}{l_i}\right)^2\right), \quad (4.27)$$

So, that the amplitude of warping modes results from

$$\Phi_{k,x}(x) = F_1(x)\Phi_{k,x}(0) + F_2(x)\Phi_{k,x}(l_i) + F_3(x)\Phi_{k,x}\left(\frac{l_i}{2}\right). \quad (4.28)$$

The analytical expression for the function Φ_k related with warping modes can then be defined through the operator for primitivation $P(\,)$:

$$\Phi_k(x) = P\big(F_1(x)\big)\Phi_k(0) + P\big(F_2(x)\big)\Phi_k(l_i) + P\big(F_3(x)\big)\Phi_k\left(\frac{l_i}{2}\right), \quad (4.29)$$

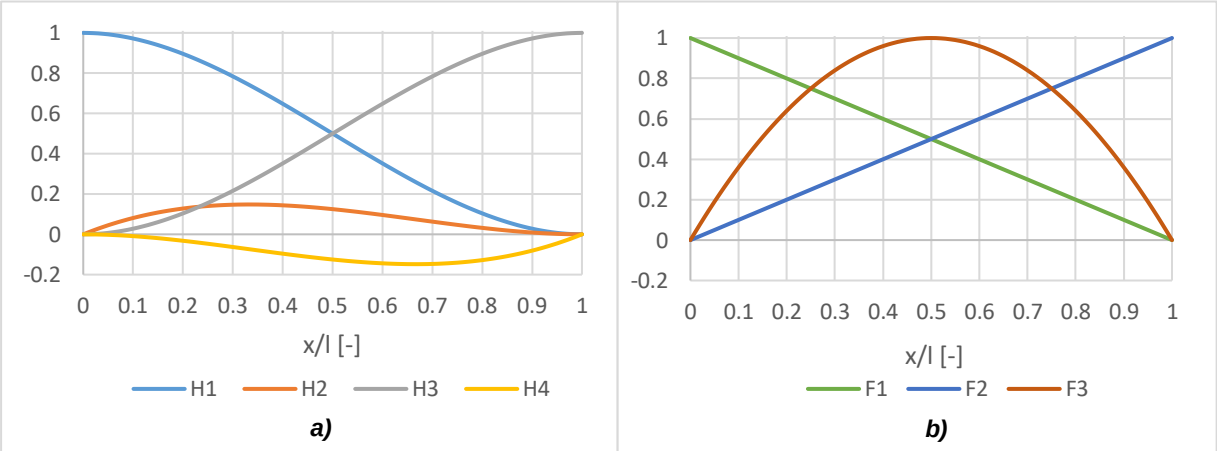

Figure 4.7 – a) Hermite's cubic interpolation polynomials and b) Lagrange's linear and quadratic hierarchic interpolation polynomials

The combination of the set of these shape functions leads to a finite element with three nodes, where the first node ($x = 0$) is associated with H_1, H_2 and F_1, the second node ($x = {}^{l_i}/_2$) refers strictly to function F_3 and the third and final node ($x = l_i$) is related to H_3, H_4 and F_2. For a set of N deformation modes subdivided into warping (N_w) and non-warping modes, shape function matrix Ψ of dimensions $N \times (4N - N_w)$ can be organized as

$$\boldsymbol{\Psi} = \left[\begin{array}{c|c|c|c|c|c} \widetilde{\boldsymbol{H_1}} & \begin{matrix}0\\ P(\widetilde{\boldsymbol{F_1}})\end{matrix} & \widetilde{\boldsymbol{H_2}} & \begin{matrix}0\\ P(\widetilde{\boldsymbol{F_3}})\end{matrix} & \widetilde{\boldsymbol{H_3}} & \begin{matrix}0\\ P(\widetilde{\boldsymbol{F_2}})\end{matrix} \\ 0 & & 0 & & 0 & \widetilde{\boldsymbol{H_4}} \end{array}\right], \quad (4.30)$$

where $\widetilde{\boldsymbol{X}}$ designates a diagonal matrix sized after the number of associated deformation modes in which each diagonal term is equal to function X. The vector $\boldsymbol{d_e}$ is defined in accordance with $\boldsymbol{\Psi}$ as

$$\boldsymbol{d_e} = \begin{bmatrix} \Phi_1(0) \\ \vdots \\ \Phi_{N-N_w}(0) \\ \hline \Phi_{N-N_w+1}(0) \\ \vdots \\ \Phi_N(0) \\ \hline \Phi_{N+1,x}(0) \\ \vdots \\ \Phi_{2N-N_w,x}(0) \\ \hline \Phi_{2N-N_w+1}\left(\frac{l_i}{2}\right) \\ \vdots \\ \Phi_{2N}\left(\frac{l_i}{2}\right) \\ \hline \Phi_{2N+1}(l_i) \\ \vdots \\ \Phi_{3N-N_w}(l_i) \\ \hline \Phi_{3N-N_w+1}(l_i) \\ \vdots \\ \Phi_{4N}(l_i) \\ \hline \Phi_{4N+1,x}(l_i) \\ \vdots \\ \Phi_{4N-N_w,x}(l_i) \end{bmatrix} , \tag{4.31}$$

Using (4.24) and setting up one equation per each virtual variation in equation (4.20), one obtains, for each element

$$\left(\int_{l_i} \begin{bmatrix} \boldsymbol{\Psi} \\ \boldsymbol{\Psi}_{,x} \\ \boldsymbol{\Psi}_{,xx} \end{bmatrix}^T \boldsymbol{M} \begin{bmatrix} \boldsymbol{\Psi} \\ \boldsymbol{\Psi}_{,x} \\ \boldsymbol{\Psi}_{,xx} \end{bmatrix} dx \right) \boldsymbol{d_e} = \int_{\Omega_e} \begin{bmatrix} \boldsymbol{\Psi} \\ \boldsymbol{\Psi}_{,x} \end{bmatrix}^t \boldsymbol{\Xi}_U{}^t \boldsymbol{f}\, d\Omega \tag{4.32}$$

In this expression it is possible to identify both the element stiffness matrix $\boldsymbol{K_e}$ and the equivalent nodal force vector $\boldsymbol{F_e}$

$$\boldsymbol{K_e} = \int_{l_i} \begin{bmatrix} \boldsymbol{\Psi} \\ \boldsymbol{\Psi}_{,x} \\ \boldsymbol{\Psi}_{,xx} \end{bmatrix}^T \boldsymbol{M} \begin{bmatrix} \boldsymbol{\Psi} \\ \boldsymbol{\Psi}_{,x} \\ \boldsymbol{\Psi}_{,xx} \end{bmatrix} dx \ , \tag{4.33}$$

$$\boldsymbol{F_e} = \int_{\Omega_e} \begin{bmatrix} \boldsymbol{\Psi} \\ \boldsymbol{\Psi}_{,x} \end{bmatrix}^t \boldsymbol{\Xi}_U{}^t \boldsymbol{f}\, d\Omega \ , \tag{4.34}$$

which must be assembled, as usual, to obtain the global equilibrium system of equations, expressed in its most general form:

$$\boldsymbol{K}\boldsymbol{d} = \boldsymbol{F} \ . \tag{4.35}$$

Finally, having obtained the vector $\boldsymbol{d_e}$ for each element, the longitudinal normal stresses can be computed from (4.12) and (4.13), leading to

$$\sigma_{xx} = \sigma_{xx}^M + \sigma_{xx}^F = E(\overline{\boldsymbol{u}}^t \boldsymbol{\Psi}_{,xx})\boldsymbol{d_e} - \frac{E}{1-\nu^2}\left(z\overline{\boldsymbol{w}}^t \boldsymbol{\Psi}_{,xx}\right)\boldsymbol{d_e} \ . \tag{4.36}$$

4.4. IMPLEMENTATION IN MATLAB

The beam finite element introduced was implemented in *MATLAB* (The MathWorks Inc., 2014). A main routine was developed which can be subdivided into the following sections:

Section 1) Initial parameters:

Input data is established concerning geometry, constitutive parameters, loading (concentrated loads, line loads, area loads and self-weight specifications), support conditions and internal diaphragm locations. It is assumed that the box-girder bridge cross-section is divided into six walls as presented previously in Figure 4.6, of constant thickness, elastic properties and density. The loads are all assumed to be vertical and applied at the mid-surfaces and are defined by their magnitude and their relevant coordinates in a global XYZ referential (see Figure 4.8).

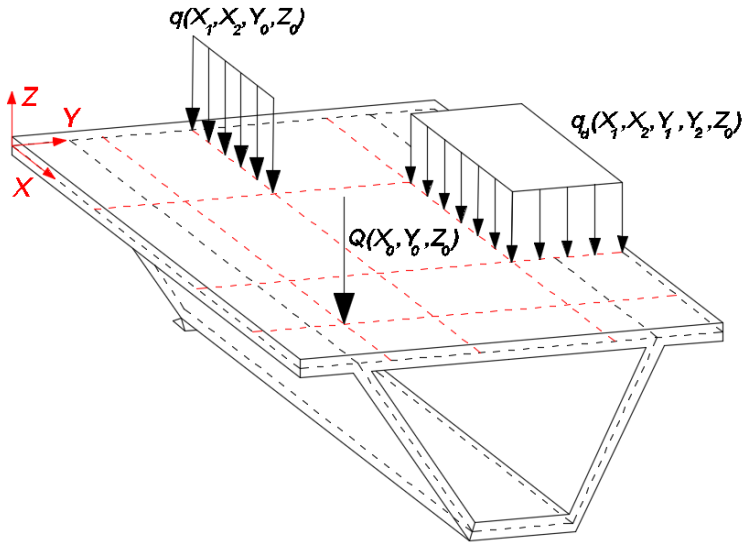

Figure 4.8 – Global referential and general load specific coordinates

Section 2) Model definitions:

Involves aspects related to longitudinal discretization and selection of deformation modes. Each element's walls are defined by their end-nodes' (X, Y, Z) coordinates. The loads are then subdivided according to their location in terms of finite element and wall (see Figure 4.9) and new coordinates are calculated, this time with respect to the local axes already illustrated in Figure 4.1. In this section it is also possible to define which deformation modes are to be considered in the analysis.[12]

Section 3) Definition of deformation modes and GBT matrices:

First, global deformation modes 1 through 5 are extracted from the output files of the GBTUL program ($\bar{u}_1,\ldots,\bar{u}_5$,$\bar{v}_1,\ldots,\bar{v}_5$ and $\bar{w}_1,\ldots,\bar{w}_5$). Afterwards, the warping displacements of modes 8 through 15 in each wall are defined analytically.

[12] As discussed before, GBT formulation allows for a user-defined consideration of the deformation modes to be included in the analysis. For example, it is possible to analyse the box-girder bridge as a beam with in-plane rigid cross-section simply by withdrawing from the set of active deformation modes all those containing transverse flexure ($B_k \neq 0$).

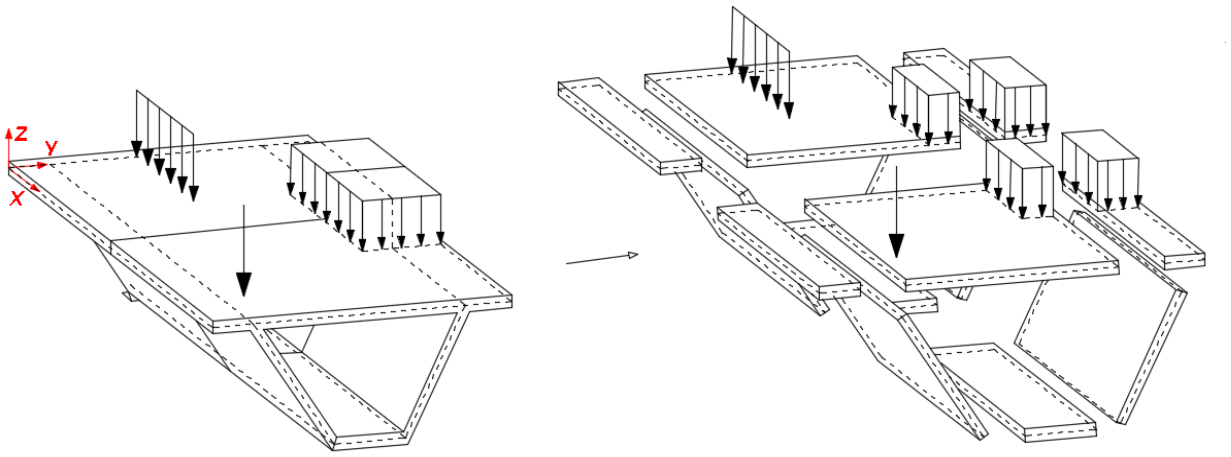

Figure 4.9 – Subdivision of the loads into each element and wall

The individual participation of these modes that intend to allow for shear lag may only be clearly analysed if they are uncoupled with each other and with global modes 1 through 5. This can be done by following the Gram-Schmidt orthogonalization process with respect to matrix C (see Figure 4.10, mode 8 is initially coupled with axial extension and minor axis bending). It should be noted that by the end of this process, modes 1 through 4 should remain unaltered for they are orthogonal with respect to matrix C (recall section 0). Mode 5 however has necessarily changed (torsion is coupled with distortion) and therefore should be re-extracted from GBTUL. Warping shear modes for accounting bi-shear in torsion and distortion (modes 6 and 7) are added subsequently, so that they do not take part in the orthogonalization process.

In order to ensure that the analysis of modal participations is not biased by the scale of each modal shape functions $\bar{u}_k$, $\bar{v}_k$ and $\bar{w}_k$, a normalization procedure is followed. Seeing as the goal is to study the longitudinal normal stresses, each mode is normalized so that the maximum warping displacement equals one.

Having the deformation modes fully defined, the GBT linear stiffness matrices $\boldsymbol{B}$, $\boldsymbol{C}$, $\boldsymbol{D_1}$ and $\boldsymbol{D_2}$ are obtained using *MATLAB*'s symbolic calculation commands.

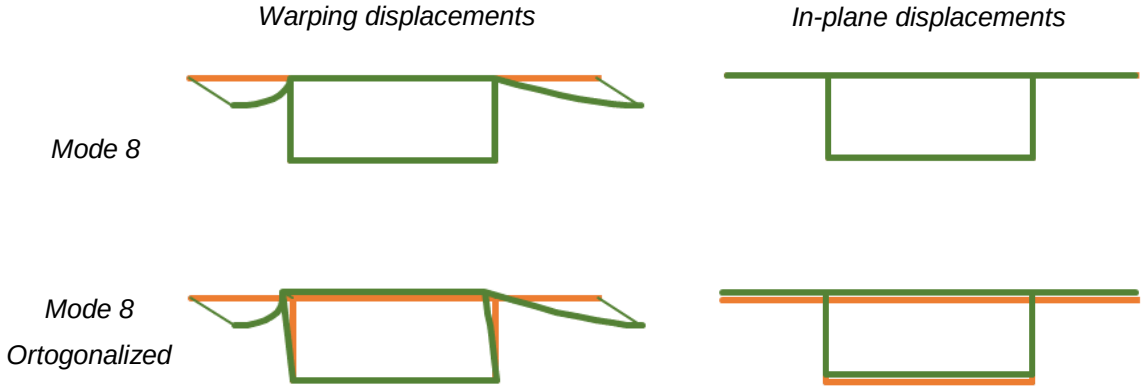

Figure 4.10 – Comparison of mode 6 before and after orthogonalization procedure

Section 4) Building of the global force vector and stiffness matrix

Calculates the element stiffness matrix and equivalent nodal forces as defined in (4.33) and (4.34) using once again MATLAB's symbolic tools. Special notice should be given to the decomposition of the vertical self-weight load on the webs into the respective local axes.

The global stiffness matrix and force vector are then assembled following the superposition rule illustrated in Figure 4.11. In this routine, allowance was given to the definition of load cases to be solved separately.

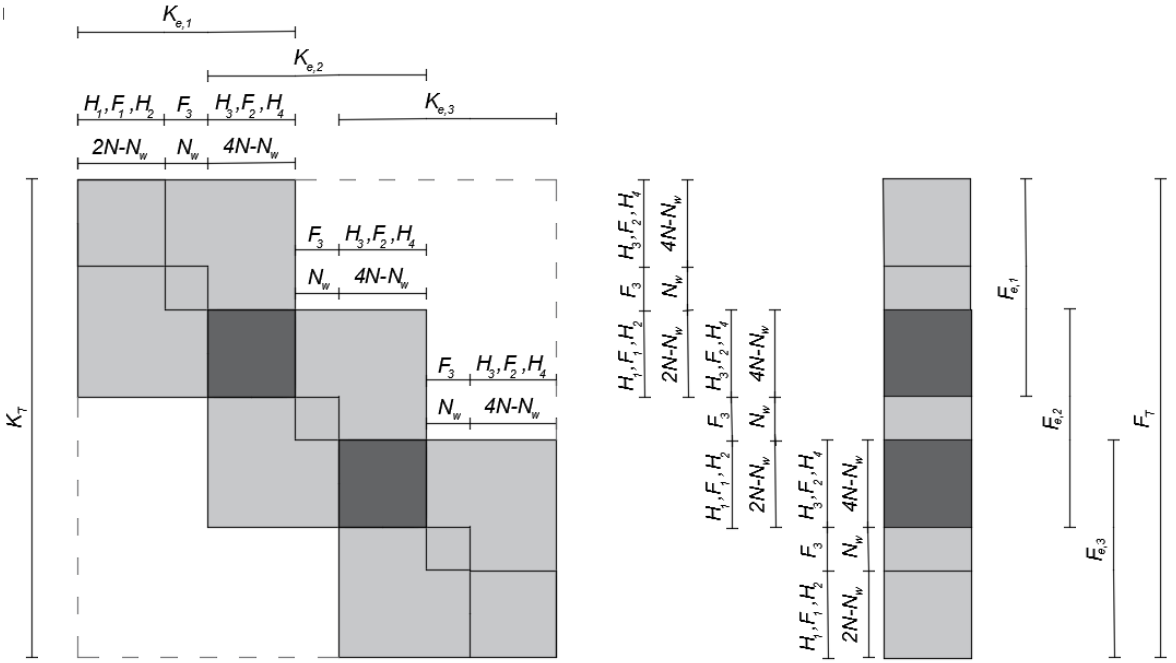

Figure 4.11 – Assembly of global stiffness matrix and force vector for a member discretized in three elements

Section 5) Selection of active DOF's:

Each DOF is first attributed to the respective deformation mode. Then, a subset of these DOF's is restrained according to user input (as mentioned in Section 3) and/or boundary conditions (e.g. rigid body movements at the supports or distortion in sections where diaphragms exist). This can be achieved simply by eliminating the corresponding DOF columns and lines from the global stiffness matrix and force vector.

Section 6) Solving of the equilibrium equations:

Solves the system of linear equilibrium equations and obtains the approximated longitudinal nodal amplitudes for each deformation mode.

Section 7) Calculation of longitudinal stresses:

Computes and stores the stresses obtained in start and end nodes of every element with respect to every single deformation mode and load case. It also makes possible a procedure for averaged stress smoothing. For visualization purposes, the stresses in each wall are assessed for nine different locations equidistant along the y axis and exported to a *Microsoft Excel* spreadsheet.

5. THEORETICAL COMPARISON BETWEEN CLASSICAL FORMULATIONS AND GBT

Along the previous chapters, two distinct methods of analysis were presented. The first relates to the employment of classical solutions for bending, torsion with warping and distortion, as well as a simplified methodology for the consideration of shear lag effect in bending. The second entails the use of GBT, an emergent theory dedicated to the study of thin-walled structures, as basis for definition of a finite element model.

This chapter seeks to put into evidence some of the theoretical differences between both of these approaches, discussing the effects they may have on the results for longitudinal stresses in steel-concrete composite box-girder bridges.

At first, it should be noted that both approaches consider a variety of cross-section deformed configurations, previously referred to in GBT formulations as “deformation modes”, which are variable along the longitudinal axis of the member. For each approach, the modes’ amplitude functions can be determined by means of equilibrium equations. Thus, the comparison between the two methods becomes more clear when analysing separately each method’s (i) pre-defined deformation modes and (ii) established longitudinal equilibrium equations.

Of course, this comparison can only be made for the deformation modes that are simultaneously contemplated in both approaches, namely bending (GBT modes 2 and 3), distortion (GBT mode 4) and torsion with warping accounting for bi-shear (GBT modes 5 and 6).

The effect of shear lag in Classical Formulations is considered through semi-empirical adjustment of the bending results and not through additional equilibrium equations. This implicates that the same comparison cannot be performed. Even so, some considerations can be woven concerning the cross-sectional shape of the classical shear lag mode and GBT modes 8 through 11.

The remaining GBT modes (7 and 12-15) are not present in the classical approach, but allow for the analysis to grow in precision with the enrichment of the deformation mode field, since they allow for the effects of bi-shear in distortion and also anti-symmetrical shear lag in the top and bottom flanges.

5.1. COMPARISON OF CROSS-SECTION DEFORMATION MODES

Each cross-section deformation mode is simultaneously characterized according to its in-plane (v_k and w_k) and out-of-plane displacements (u_k). For the case of minor-axis bending, both Classical Formulations and GBT assume a rigid body translation of the cross-section in its own plane, which remains normal to the longitudinal axis (following Vlasov’s hypothesis as a generalization of the Euler-Bernoulli hypothesis).

When dealing with torsion with warping accounting for the effect of bi-shear, Classical Formulations consider that the warping displacements do not depend only on the in-plane rigid body behaviour. That is to say, two distinct deformation modes are considered, one concerning only the rigid body rotation (governed by function $\phi(x)$) and another related solely to the warping displacements of the cross-sections walls, whose amplitude function is equal to $\chi(x)$. The deformation field is obtained by the linear

combination of these two modes. Since the "shape" of the warping displacements predicted in GBT matches the one in Classical Formulations (given by $\widetilde{u_s}(s)$ and illustrated in Figure 3.11), the deformation field obtained by linear combination is necessarily the same mode space (see Figure 5.1).

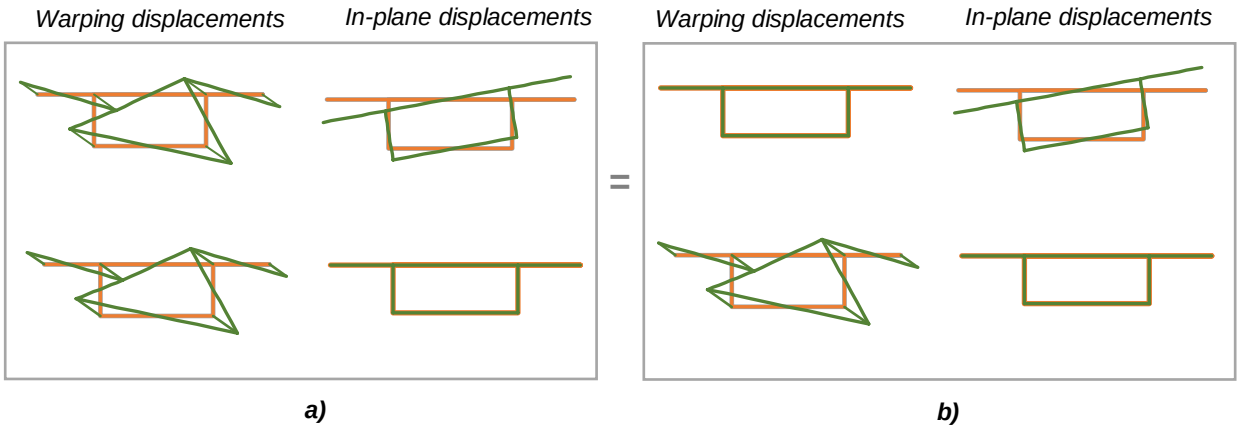

Figure 5.1 – Representation of the equality of torsional displacement fields in a) GBT formulation b) Classical Formulations

The definition of the distortional deformation mode in the Classical Formulations was based on the combination of the longitudinal bending behaviour of the plates with a transverse frame type of response. In the longitudinal analysis, Vlasov's hypothesis was assumed implicitly when stating that each plate would behave as an Euler-Bernoulli beam subjected to in-plane loads. In the frame analysis, transverse extension of the walls was neglected, meaning once again that the classical definition of the distortional deformed configuration coincides with the one presented for the GBT-based approach.

As far as shear lag effect in bending is concerned, the Classical Formulations make use of a single global shear lag mode, whereas GBT analyses allow for the consideration of a broader set of modes. Evidently, this should result in higher accuracy when performing the GBT-based approach, because the effect of shear lag deformability may vary along the plates. Even so, it should be pointed out that the most of the GBT shear lag modes were defined as quartic based on the classical expressions for shear lag in bending (see equations (3.16) to (3.18)).

It should be noted that for composite cross-sections, the homogenisation procedure may lead to slight differences in the cross-section deformation modes due to some of the adopted simplifications.

5.2. COMPARISON OF THE EQUILBRIUM EQUATIONS

Establishing the comparison between differential equilibrium equations, the GBT equilibrium equations from (4.20) can be rewritten in the differential form as

$$\boldsymbol{C\Phi}_{,xxxx} - \boldsymbol{D\Phi}_{,xx} + \boldsymbol{B\Phi} = \boldsymbol{f}_{x,x} + \boldsymbol{f}_y + \boldsymbol{f}_z \qquad (5.1)$$

with

$$\boldsymbol{D} = \boldsymbol{D_1} - \boldsymbol{D_2} - \boldsymbol{D_2}^t \qquad (5.2)$$

As for the Classical Formulations, the equivalent expressions for bending, torsion with warping and distortion can be obtained from those in (3.9), (3.53), (3.55) and (3.101)[13], and expressed in matrix form so that:

$$\begin{bmatrix} EI_y & 0 & 0 & 0 \\ 0 & EI_\omega & 0 & 0 \\ 0 & 0 & 0 & 0 \\ 0 & 0 & 0 & -EI_{w,e}\dfrac{p\cos\varphi}{p_{w,d}} \end{bmatrix} \begin{bmatrix} v_{,xxxx} \\ \chi_{,xxxx} \\ \phi_{,xxxx} \\ \Delta_{w,xxxx} \end{bmatrix} + \begin{bmatrix} 0 & 0 & 0 & 0 \\ 0 & -G(J-I_c) & G(J-I_c) & 0 \\ 0 & G(J-I_c) & GI_c & 0 \\ 0 & 0 & 0 & 0 \end{bmatrix} \begin{bmatrix} v_{,xx} \\ \chi_{,xx} \\ \phi_{,xx} \\ \Delta_{w,xx} \end{bmatrix} + \begin{bmatrix} 0 & 0 & 0 & 0 \\ 0 & 0 & 0 & 0 \\ 0 & 0 & 0 & 0 \\ 0 & 0 & 0 & k\dfrac{p\cos\varphi}{p_{w,d}} \end{bmatrix} \begin{bmatrix} v \\ \chi \\ \phi \\ \Delta_x \end{bmatrix} = \begin{bmatrix} p \\ 0 \\ m \\ p \end{bmatrix} \quad (5.3)$$

Through careful inspection, it is possible to notice correspondence with the system of equations presented in (5.1), where the amplitude functions Φ_k are respectively given in terms of the vertical displacement of the cross-section v, of the warping function χ, of the angle of twist ϕ and of the in-plane displacement of the web Δ_w.

An equivalent system, obtained with the GBT approach, can then be sought:

$$\begin{bmatrix} C_{vv} & 0 & 0 & 0 \\ 0 & {C_{\chi\chi}}^M & 0 & {C_{\Delta_w\chi}}^M \\ 0 & 0 & {C_{\phi\phi}}^F & {C_{\Delta_w\phi}}^F \\ 0 & {C_{\chi\Delta_w}}^M & {C_{\phi\Delta_w}}^F & {C_{\Delta_w\Delta_w}}^F \end{bmatrix} \begin{bmatrix} v_{,xxxx} \\ \chi_{,xxxx} \\ \phi_{,xxxx} \\ \Delta_{w,xxxx} \end{bmatrix} + \begin{bmatrix} 0 & 0 & 0 & 0 \\ 0 & {D_{\chi\chi}}^M & {D_{\phi\chi}}^M & 0 \\ 0 & {D_{\chi\phi}}^M & D_{\phi\phi} & {D_{\Delta_w\phi}}^F \\ 0 & 0 & {D_{\phi\Delta_w}}^F & {D_{\Delta_w\Delta_w}}^F \end{bmatrix} \begin{bmatrix} v_{,xx} \\ \chi_{,xx} \\ \phi_{,xx} \\ \Delta_{w,xx} \end{bmatrix} + \begin{bmatrix} 0 & 0 & 0 & 0 \\ 0 & 0 & 0 & 0 \\ 0 & 0 & 0 & 0 \\ 0 & 0 & 0 & {B_{\Delta_w\Delta_w}}^F \end{bmatrix} \begin{bmatrix} v \\ \chi \\ \phi \\ \Delta_x \end{bmatrix} = \begin{bmatrix} p \\ 0 \\ m \\ p \end{bmatrix} \quad (5.4)$$

At this point, several conclusions can be withdrawn. The first is that in both approaches, if only these four modes are considered, the effect of bending is independent from torsion and distortion.

Secondly, the GBT torsion and distortion equations are coupled, as seen by the existence of non-diagonal terms in the last three lines of the system of equations (${C_{\Delta_w\chi}}^M$, ${C_{\chi\Delta_w}}^M$, ${C_{\Delta_w\phi}}^F$, ${C_{\phi\Delta_w}}^F$, ${D_{\phi\chi}}^M$, ${D_{\chi\phi}}^M$, ${D_{\Delta_w\phi}}^F$ and ${D_{\phi\Delta_w}}^F$). In the Classical Formulations these terms are null, because i) several of these coefficients relate to wall flexural behaviour, which is often disregarded in more classical approaches and ii) in the determination of $p_{w,d}$ it was assumed that χ coincided with ϕ for uncoupling purposes, which corresponds to neglecting torsion bi-shear deformation.

Finally, since Kirchhoff's hypothesis was adopted, in GBT formulation the longitudinal amplitude functions are always at least of class C^1. The same is not always true in Classical Formulations, where in some cases, such as in the torsional response case, it suffices to consider that the displacements are C^0 continuous. This will lead to some additional discrepancies in the results for sections near concentrated loads, diaphragms and supports.

[13] φ is the angle of inclination of the web with respect to the vertical axis.

In conclusion, even though the cross-section deformation modes generally coincide, the Classical Formulations present differences with respect to the GBT approach in terms of the equilibrium equations for torsion with warping accounting for bi-shear and distortion. These might lead to differences in the longitudinal stress distributions, as will be discussed in the following chapter.

6. ANALYSIS OF NUMERICAL EXAMPLES

6.1. GENERAL CONSIDERATIONS

This chapter presents analyses made on two different case studies of box-girder bridges. The first relates to a concrete box-girder bridge, whose classical results for bending, torsion and distortion are published in Maisel & Roll (1974) and can be confronted with those obtained in this work**.**

As it will be shown, for the case of a concentrated mid-span load, this box girder's wide flanges and low cross-section height-to-width ratio (d/b) make the shear lag and torsion/distortion effects very relevant for the determination of the longitudinal stresses. For this reason, this example was also found suitable for calibrating the GBT shear lag modes (symmetric and anti-symmetric) by comparing the stress distribution in the GBT finite element analyses with those obtained through a shell finite element model developed in the *software* ADINA (Bathe, 2016).

Having calibrated the GBT shear lag modes, analyses were then conducted on a second example. This refers to a 36-meter span composite steel-concrete box-girder bridge deck, loaded with standard road traffic, as defined in NP EN 1991-2. Three distinct situations were considered with respect to cross-section diaphragms: spaced every 7.2 meters (four intermediate diaphragms), spaced every 12 meters (two intermediate diaphragms) and spaced at 36 meters (i.e. diaphragms only at the end support sections).

According with standards, the uniform variable load representative of road traffic should be placed in the most unfavourable configurations in both longitudinal and transverse configurations (which, as it will be shown, depends on the distribution of diaphragms along the span). Consequently, the most unfavourable load cases are placed to obtain the maximum longitudinal stresses for the joint action of bending, torsion and distortion. At the same time, design notes are obtained regarding the evaluation of distortion effects for box girders with intermediate diaphragms.

Finally, the longitudinal stresses for the design scenario are obtained through both Classical Formulations and GBT method.

6.2. NUMERICAL EXAMPLE 1

This first example deals with a simply supported 30 m span concrete box-girder bridge of constant cross-section (see Figure 6.1), acted by a concentrated load Q = 1000 kN placed at mid-span, and a uniform longitudinal line load of 50 kN/m, both applied in one of the web-top slab joints. Diaphragms are only at the end support sections.

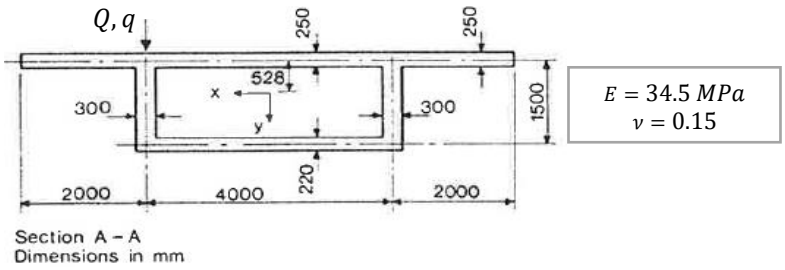

Figure 6.1 – Loading, geometry and material properties (adapted from Maisel & Roll (1974)*)*

The mid-surface longitudinal stresses which are here subject of comparison were obtained through i) the Classical Formulations ii) a GBT displacement-based finite element model using 30 elements of equal length and iii) a shell finite element model using 1800 4-node shell elements in the commercial program ADINA. Figure 6.2 presents the cross-section diagrams for the mid-span section as well as the longitudinal diagram for σ_{xx}^{M} in the intersection line of the top flange with the loaded web.

The GBT results show very good agreement with those obtained with the shell finite element model. The stresses obtained following the Classical Formulations appear to be a good estimate but deviate more with respect to the FEM stress curves, especially for mid-span concentrated load case.

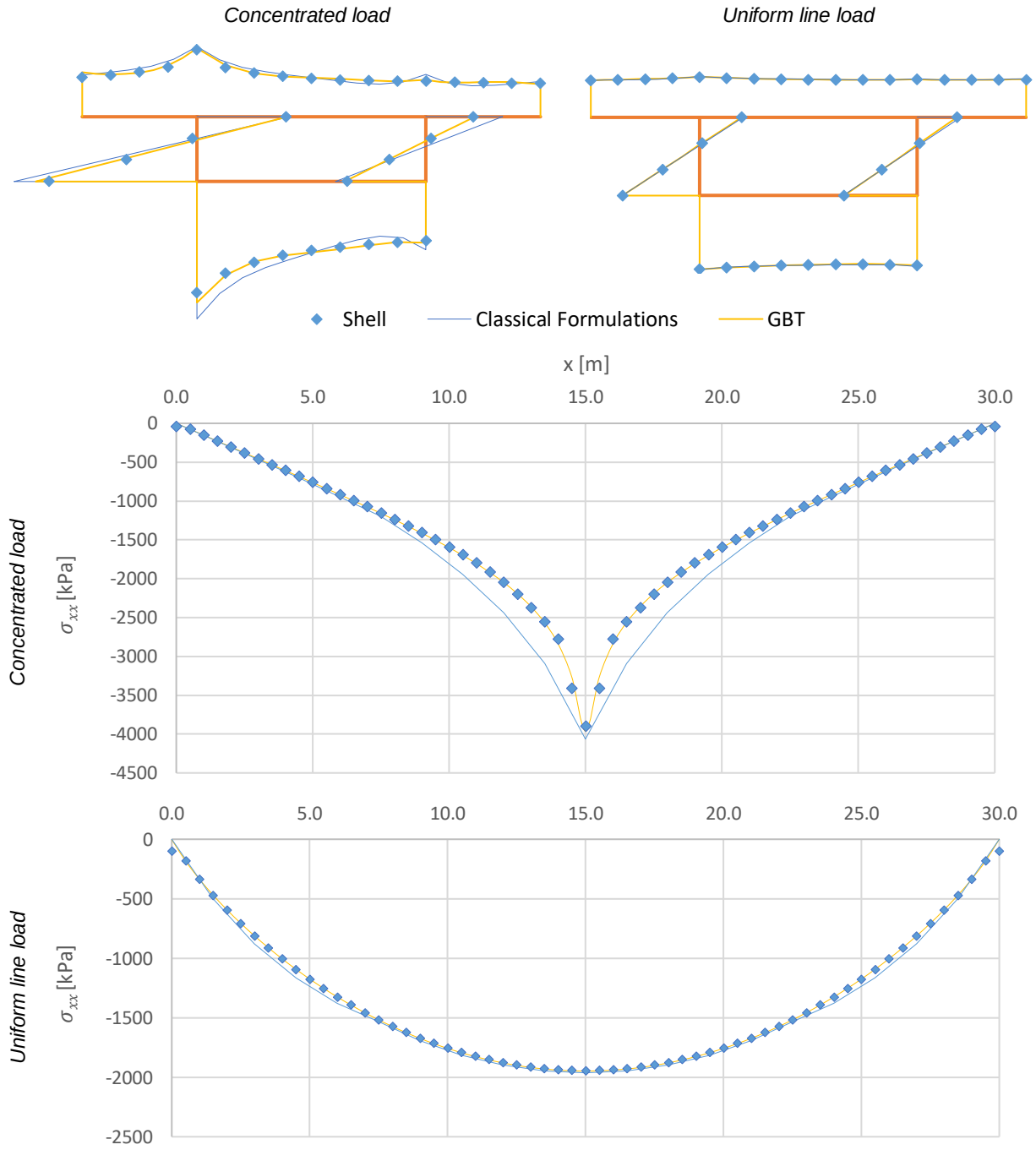

Figure 6.2 – Stresses at mid span and longitudinal stress diagram obtained by Classical Formulations, GBT and Shell FEM (ADINA)

As explained previously, it is possible to evaluate the participation of each mode in the global response. Figures 6.3 and 6.4 show the relevant modal contributions for both the Classical Formulations and GBT along the span. To make them more readable, the participations of bi-shear in torsion and distortion were added to the torsion and distortion modes, respectively. For the same reason, the stresses resulting from shear lag modes were combined into symmetric and anti-symmetric shear lag components.

The individual participations for all modes (in the case of GBT) can also be consulted in Annex 1, and all equivalent diagrams for the case of the uniform load can be found in Annexes 2, 3 and 4.

It should be pointed out that the classical formulations results for bending, torsion and distortion for the case of the concentrated load coincide with the ones published in Maisel & Roll (1974) and are included in Annex 5.

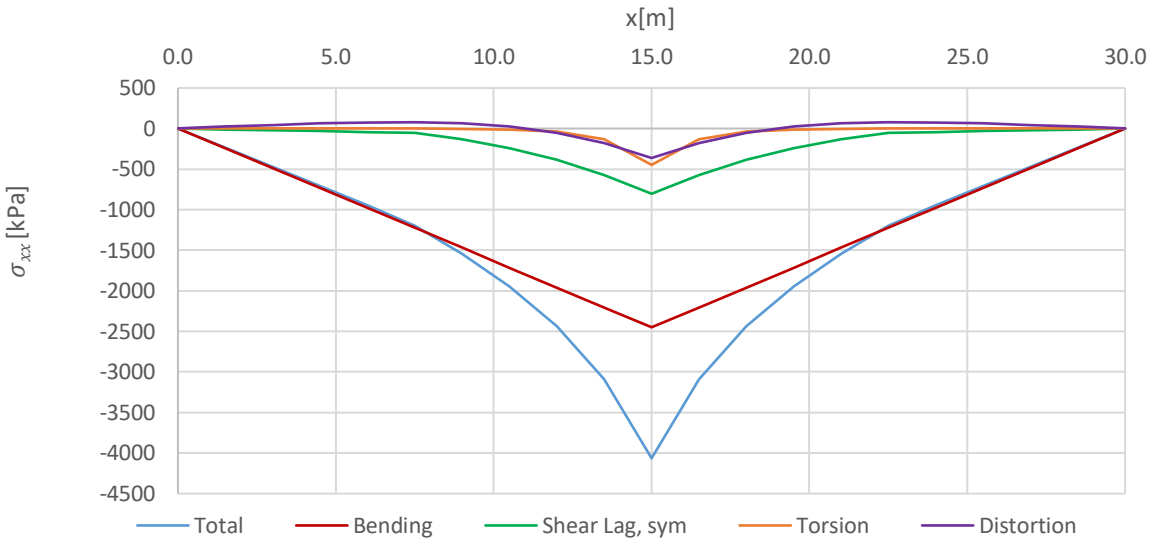

Figure 6.3 – Modal stress participations for the concentrated load according to Classical Formulations

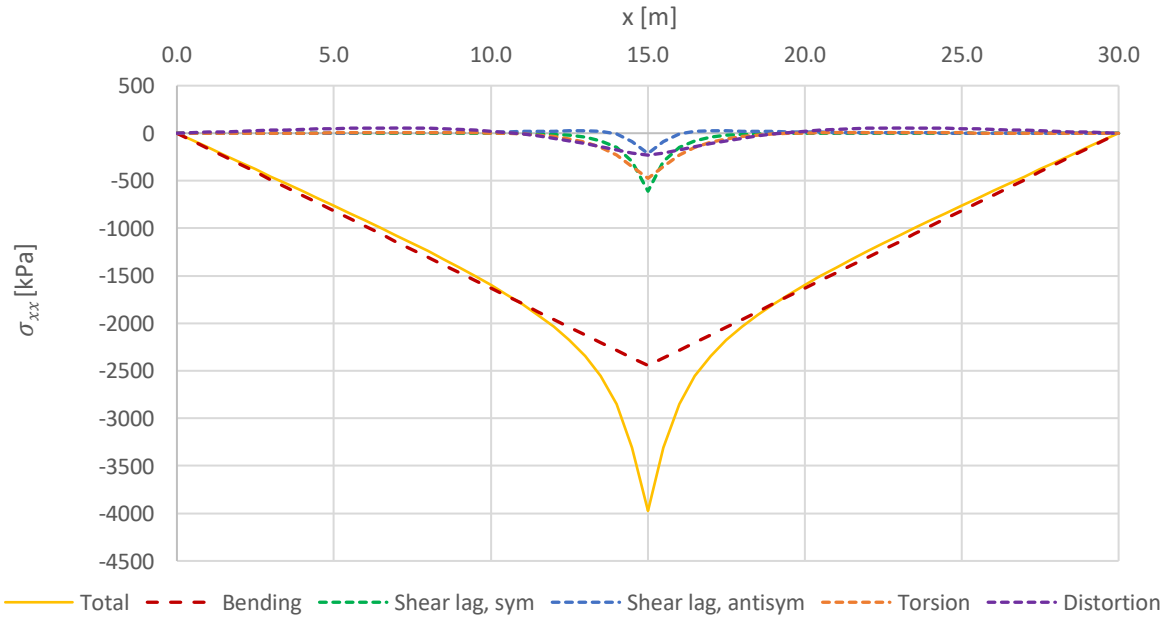

Figure 6.4 – Modal stress participations for the concentrated load according to GBT

The differences in the modal participations obtained with the two methods are further illustrated in Figures 6.5 to 6.7.

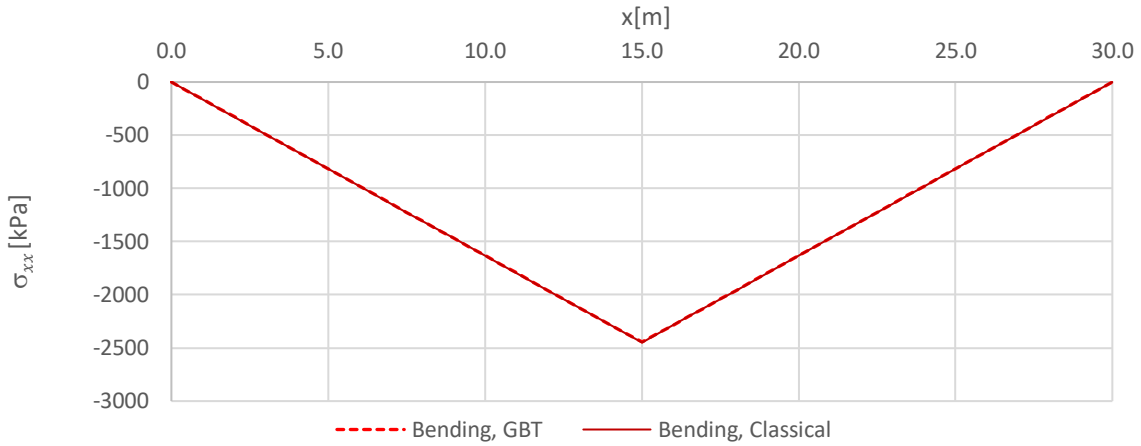

Figure 6.5 – Bending stresses at the web-top flange intersection obtained by the Classical Formulations and GBT

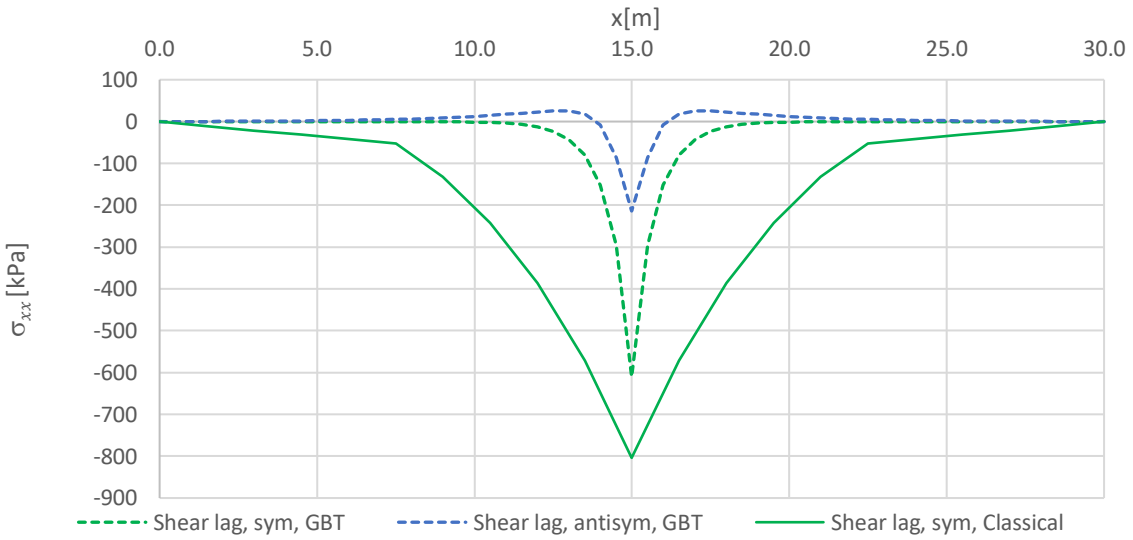

Figure 6.6 – Shear lag stresses at the web-top flange intersection obtained by Classical Formulations and GBT

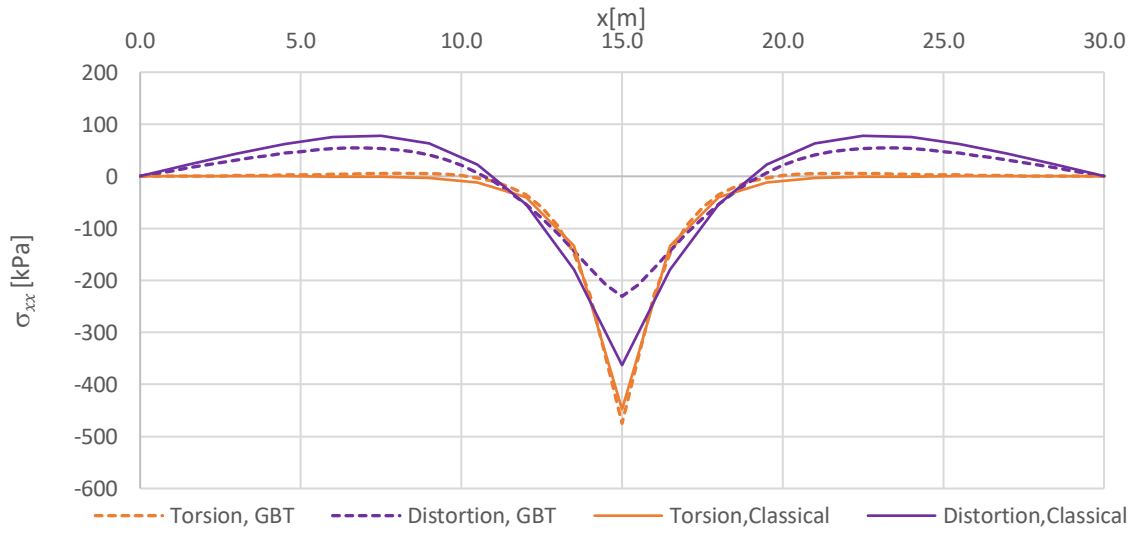

Figure 6.7 – Torsion and distortion stresses at the web-top flange intersection by Classical Formulations and GBT

It is possible to observe that, in general, the Classical Formulations have similar longitudinal profiles to those obtained in the GBT analysis. Higher discrepancies are noticed in terms of the shear lag effects, which is understandable due to the fact that the first approach is fairly simplified in order to provide a more practical approach to designers. The results for bending coincide and those for torsion with warping including bi-shear are very similar. The same does not happen however for the distortional mode, in which the GBT formulation results in smaller stresses throughout the span. The explanations for these differences have been discussed in Chapter 5. Another source of divergence comes from the inclusion of distortion bi-shear in the GBT approach.

6.3. NUMERICAL EXAMPLE 2

The second case study is a simply supported composite steel-concrete box-girder bridge. The thickness of both steel and concrete walls is constant along a 36-meter span (see Figure 6.8). Three different situations will be considered in what regards diaphragms: spaced every 7.2 meters, spaced every 12 meters and spaced every 36 meters (corresponds to having only diaphragms at the end supports).

The existence of internal diaphragms poses a serious issue in the application of Classical Formulations, due to the uncertainty in the specification of the boundary conditions for the problem of distortion and even to identify the spans for torsion and distortion. Hence, the box-girder bridge subjected to eccentric loads shall be analysed first through GBT and afterwards reference shall be given on how to apply the Classical Formulations.

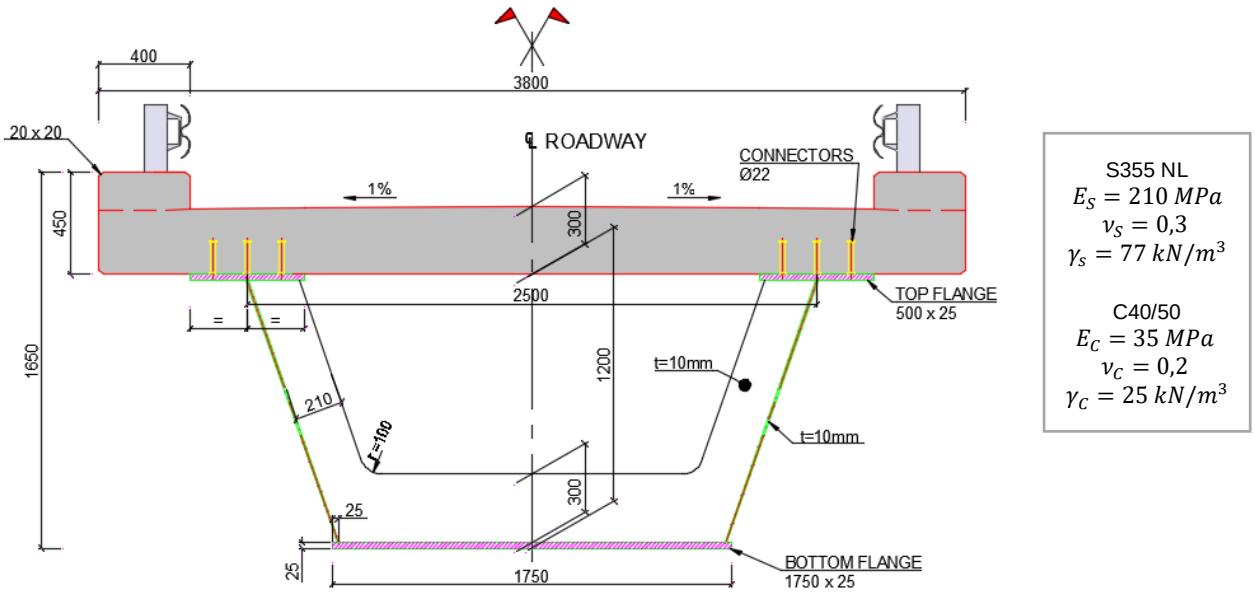

Figure 6.8 – Cross-section of the composite steel-concrete box girder bridge

Some simplifications were considered to obtain the cross-section of the structural system (see Figure 6.9)

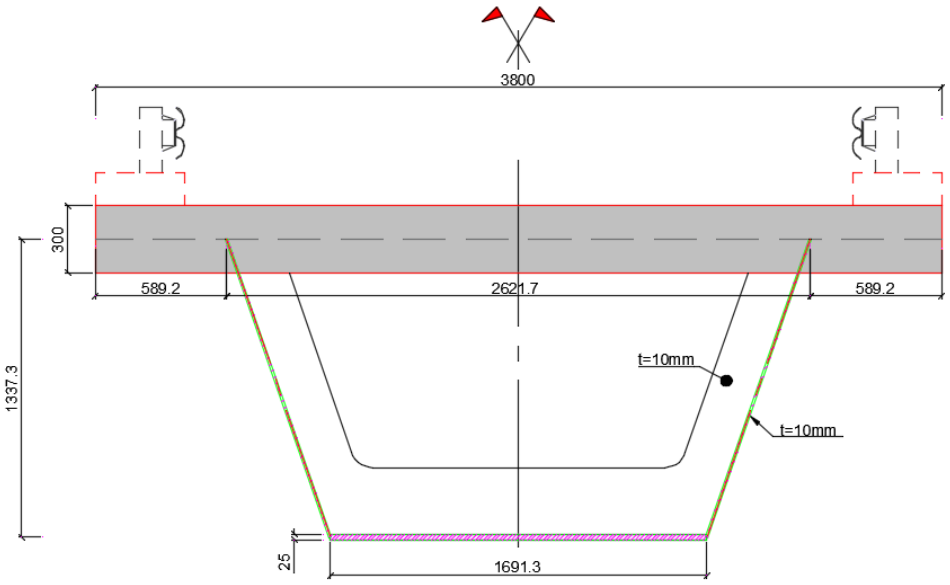

Figure 6.9 – Simplified composite cross-section

The box-girder bridge was considered to be loaded with:

1. Permanent actions:
   - Self-weight of the structural system – as a simplification, the contribution of the internal diaphragms was considered by considering an increment of the steel weight of the box girder of 15% ($\gamma_s = 77 \times 1{,}15 = 88{,}55\ kN/m^3$; $\gamma_c = 25\ kN/m^3$);
   - Self-weight of safety barriers (total of $1\ kN/m$) and kerbs ($\gamma_c \times 0.15 = 3{,}75 kN/m^2$);
2. Traffic actions:
   - Load Model 1 NP EN 1991-2 – one-axle with two concentrated loads ($Q_k = 300kN$)[14] and uniformly distributed load ($q_k = 9kN/m^2$) in notional lane 1 (Figure 6.10).

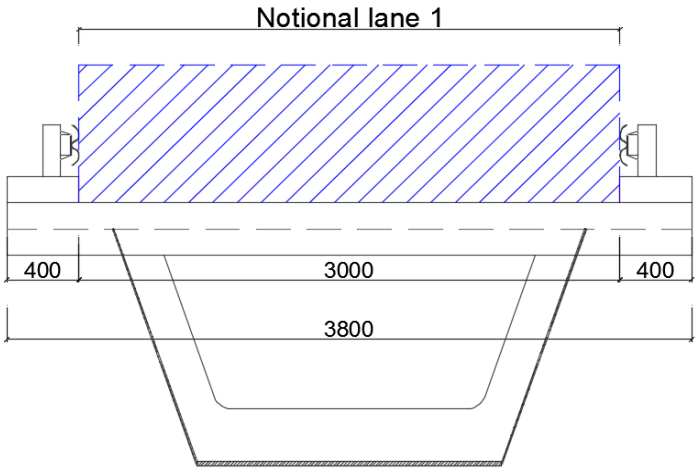

Figure 6.10 – Division of the carriageway into notional lanes

[14] For spans greater than 10 meters and dealing with global longitudinal verifications, NP EN 1991-2 (2005) allows the replacement of the standard two-axle concentrated loads (tandem system) by an equivalent one-axle with only two concentrated loads.

In what regards global verifications, NP EN 1991-2 also states that the uniformly distributed loads should be applied only in the unfavourable part of the influence surface, both longitudinally and transversally. Naturally, considering that the entire area of the notional lane is loaded will lead to the maximum longitudinal bending stresses. However, such would also produce null longitudinal stresses from torsion and distortion, seen as the notional lane is centred with the box girders axis of symmetry. It may happen that when considering only an eccentric part of the vertical load, the increase in torsional and/or distortional stresses outweighs the decrease in bending stresses. Therefore, two distinct load case arrangements were initially considered (see Figure 6.11).

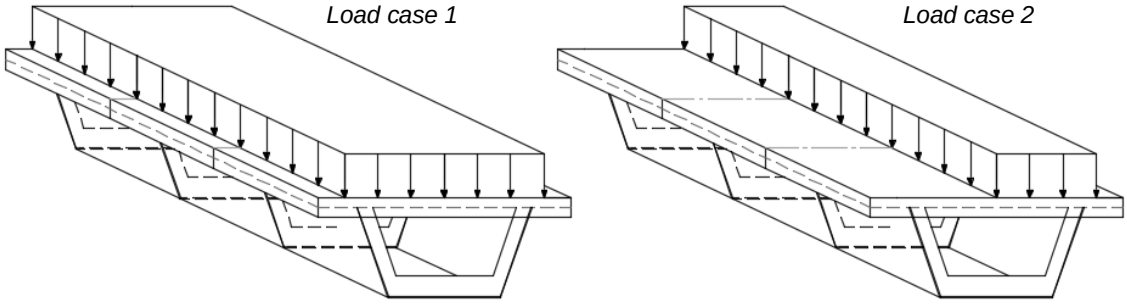

Figure 6.11 – Variable uniform load arrangements considering two internal diaphragms

The maximum longitudinal stresses along the span, obtained by analysing both load cases for each diaphragm spacing configuration can be observed in Figure 6.12. As expected, for the load case 2, the increase in diaphragm spacing gives rise to higher maximum distortional stresses. However, the increase in stresses due to torsion and distortion does not compensate the decrease in bending stresses caused by considering only half of the total load, meaning that load case 1 is governing for obtaining the maximum longitudinal stresses. It should be pointed out that this conclusion only holds for the current box-girder example; and may not hold for other cases.

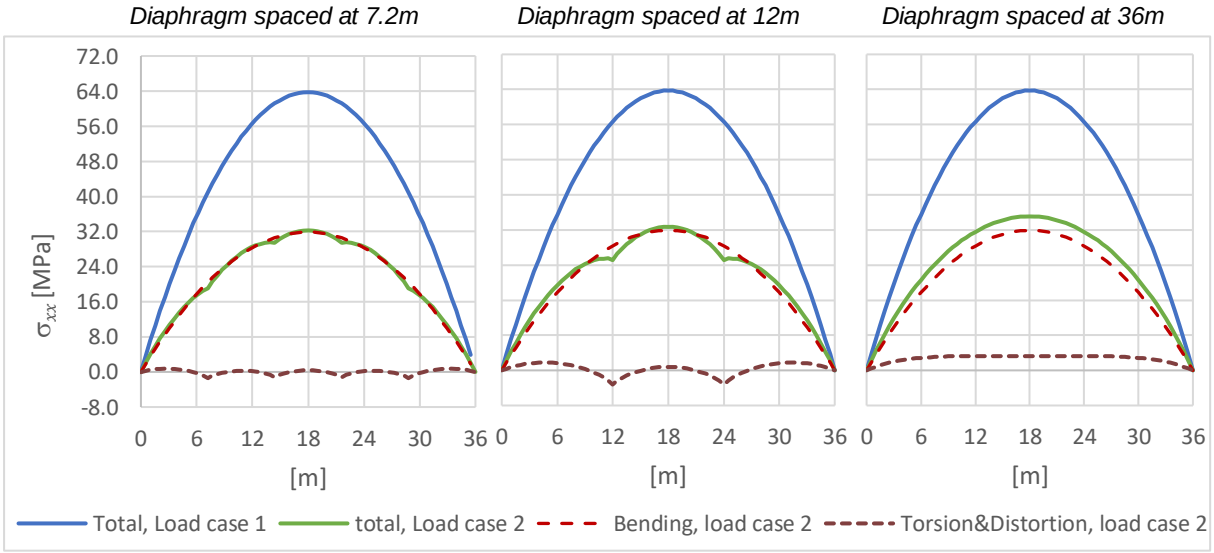

Figure 6.12 – Comparison between maximum longitudinal stresses of load cases 1 and 2

Another important conclusion can be drawn from a closer look at the combined effects from torsion and distortion for the load case 2 (Figure 6.13). In fact, the longitudinal evolution of stresses due to

torsion and distortion, for the configurations with intermediate diaphragms, suggest the existence of behaviour similar to that of a continuous beam over several “supports” (in this case diaphragms). Analogous results have been presented by Pedro (1995) while analysing the longitudinal stresses obtained in a similar roadway bridge by means of a shell finite element model. And, comparing the values of these stresses with the number of span diaphragms, it is clear the important effect in reducing the longitudinal stresses due to torsion presented by this transversal restrain of the box-girder deformation.

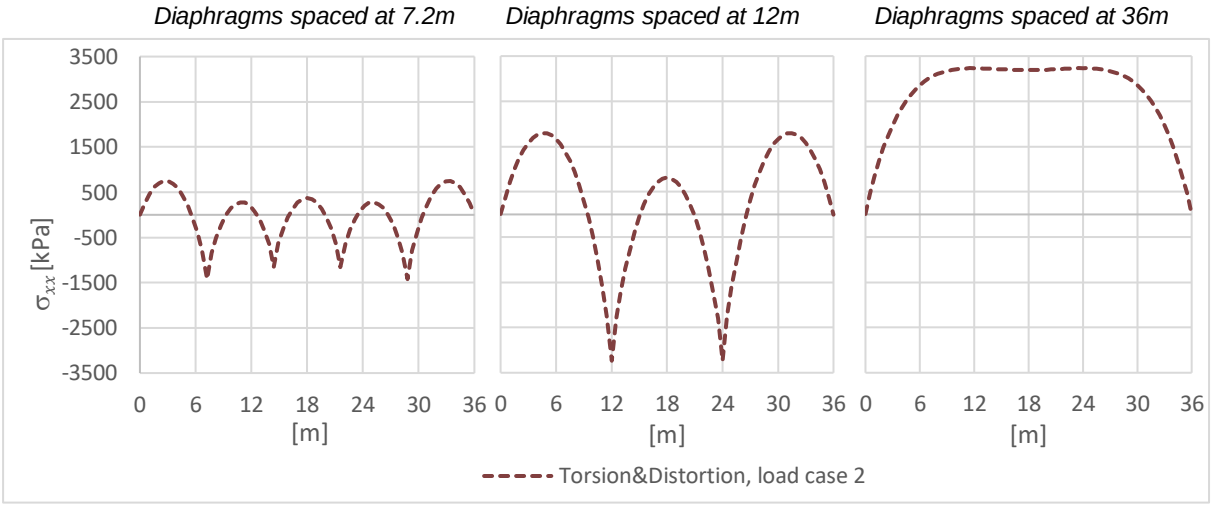

Figure 6.13 – Maximum positive stresses due to combined torsion and distortion participations

Finally, separating the effects of torsion and distortion (see Figure 6.14), it becomes clear that the combined behaviour is overall ruled by distortion, except for sections in the vicinities of the intermediate diaphragms, where the torsional warping stresses peak.

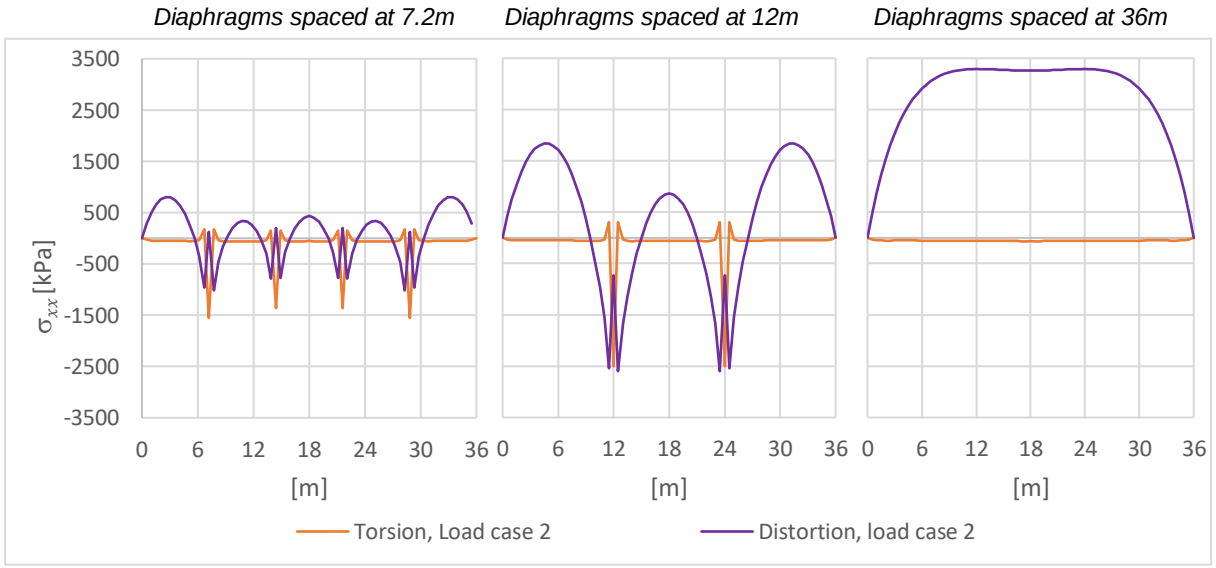

Figure 6.14 – Maximum stresses due to torsion and distortion effects

Given these results, two additional notes can be discussed. The first is that since the distortional warping stresses predominate over the torsional ones, the theoretical model that might be better suitable to describe the results of Figure 6.13 is that of a continuous beam on an elastic foundation, where the supports are placed at the locations of the intermediate diaphragms.

The second interesting result is that, if the distortional response is close to that of a continuous beam, then a third load case considering alternating load eccentricities may reveal itself to be even more unfavourable (see Figure 6.15).

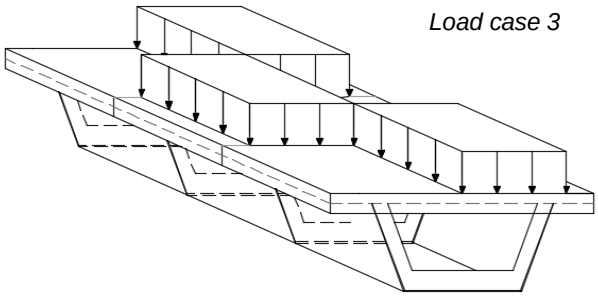

Figure 6.15 – Additional loading arrangement considering two internal diaphragms

Through simple analogy with the continuous beam, one might predict that, for load case 2, the stresses in the central span between diaphragms come closer to the situation of a beam with fixed ends, with a span length equal to the distance between diaphragms. Similarly, for load case 3, a simply supported span would be more adequate.

These are in line with the conclusions of the results presented in Figure 6.16, in which the stresses in the box-girder are compared with the ones from equivalent spans, obtained also through the GBT finite element model. For load case 3, due to symmetry conditions, the simply supported scenario matches perfectly, while, for load case 2, slight differences exist, especially when considering a higher distance between intermediate diaphragms.

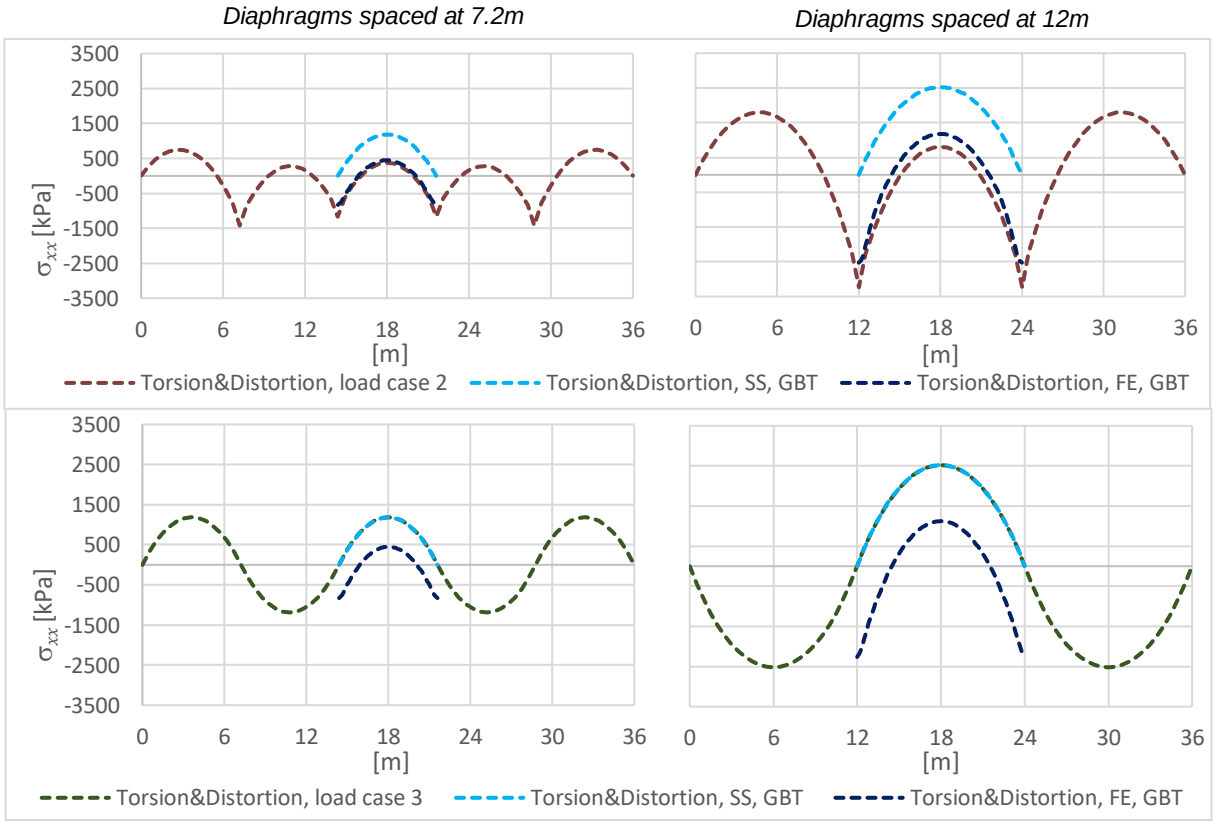

Figure 6.16 – Comparison of the combined torsional and distortional stresses with equivalent simply supported (SS) and fixed-ended models (FE) (GBT)

These results provide some guidance concerning the application of the Classical Formulations for box girders with intermediate spans. Considering the same spans and boundary conditions does not lead to equally satisfactory results (see Figure 6.17), but seems to offer an upper limit to the longitudinal stresses at mid-span.

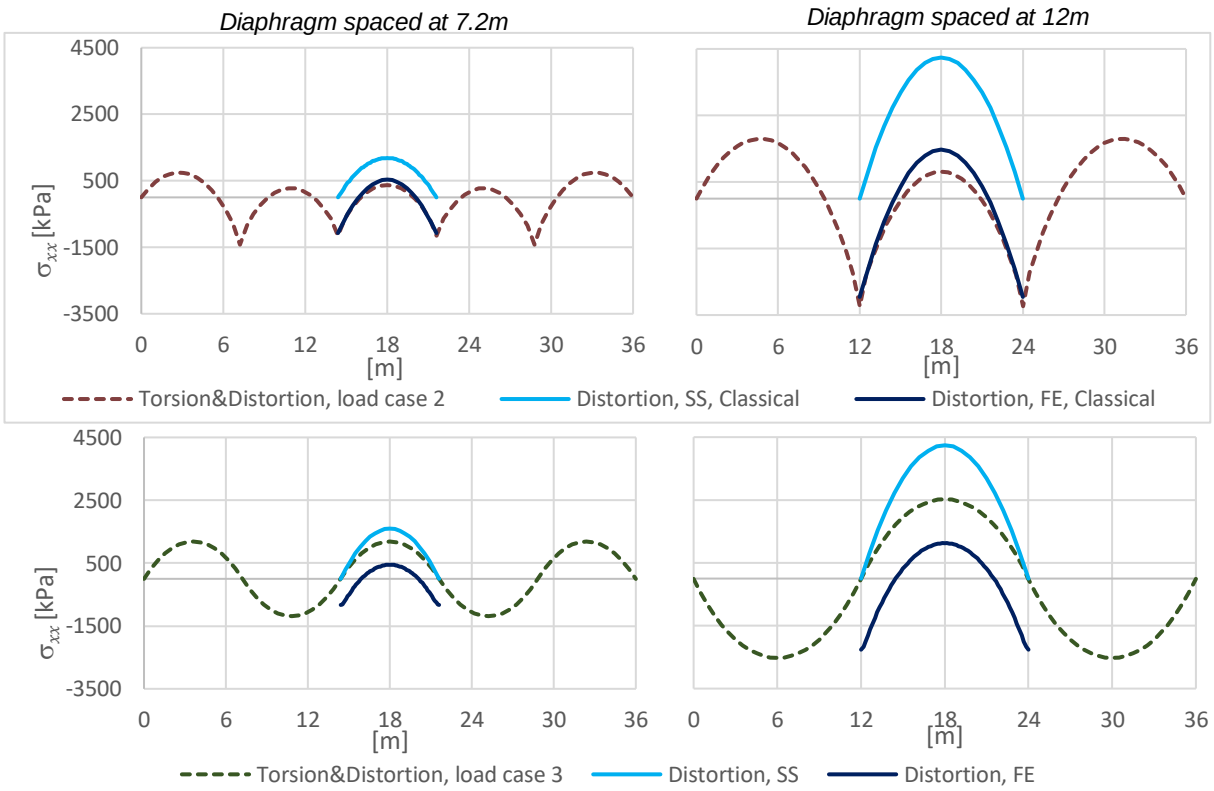

Figure 6.17 – Comparison of the combined torsional and distortional stresses with equivalent simply supported (SS) and fixed-ended models (FE) (Classical Formulations)

Readdressing the subject of global analysis of the box-girder bridge subjected to uniform loads, it can be observed that load case 3 provides mid-span longitudinal stress which are substantially higher than the ones obtained for load case 2. There is an increase in around 216% and 212% for the configurations with 4 and 2 intermediate diaphragms, respectively. Even so, load case 1 continues to be the most unfavourable for all diaphragm spacing configurations (see Figure 6.18).

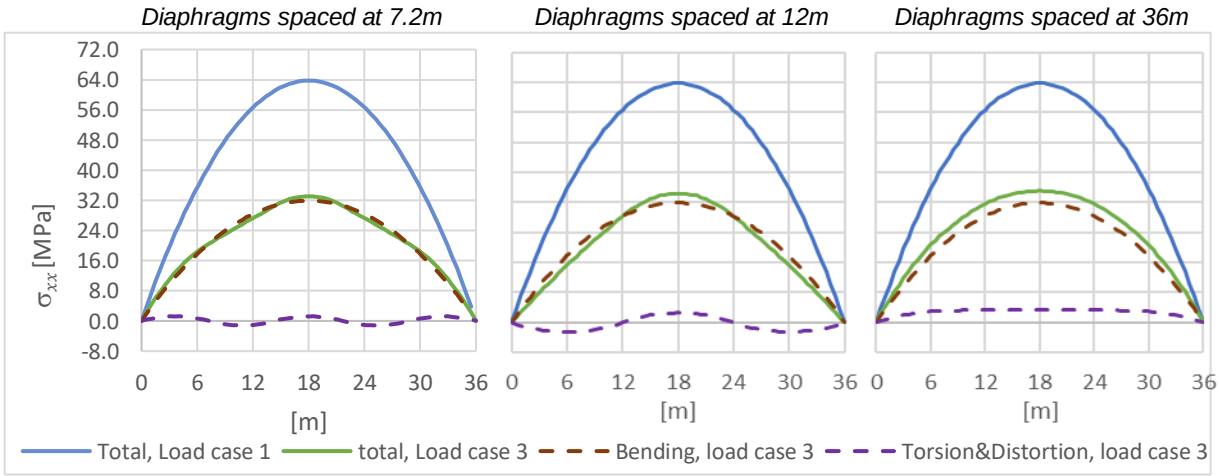

Figure 6.18 – Comparison between maximum longitudinal stresses for load cases 1 and 3

Given this results, for the present box-girder design, all traffic loads should be symmetric with respect to the vertical axis[15].The most unfavourable longitudinal normal stresses are obtained by considering only the effects of bending and, eventually, of symmetric shear lag (see Figure 6.19).

The in-service longitudinal analysis is performed considering the caracteristic design combination, given by (EN 1990-A2 (European Committee For Standardization, 2005a)):

$$\sum_{j\geq 1} G_{k,j} \text{ "+" } Q_{k,1} \qquad (6.1)$$

where G_k and Q_k are the permanent loads and traffic loads, respectively.

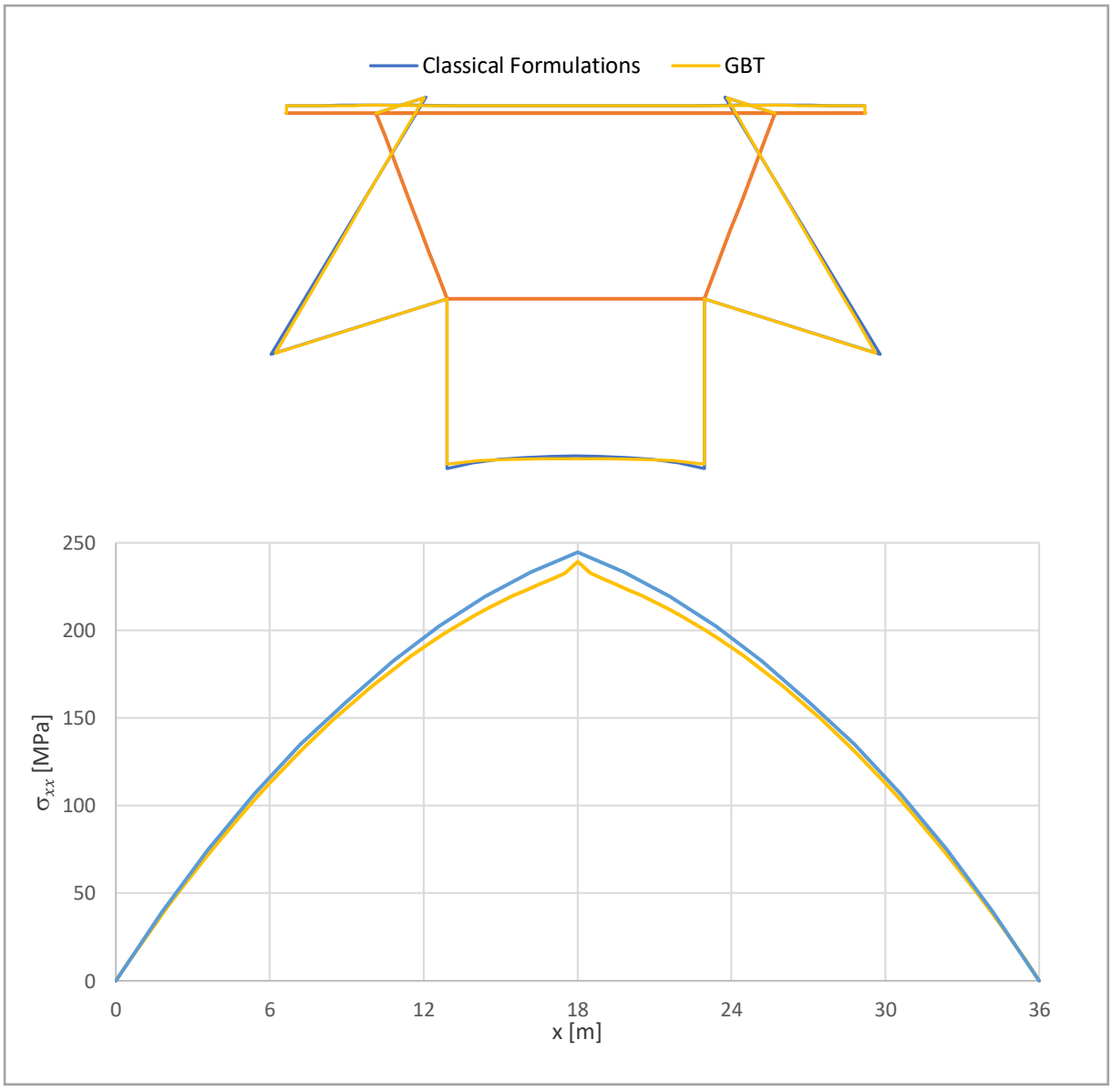

Figure 6.19 – Characteristic stresses at mid-span and longitudinal stress diagram for the web-bottom flange connection obtained by Classical Formulations and GBT approach

[15] For global verifications, the tandem system here replaced by equivalent one-axle loads should be considered circulating centred in its respective notional lane NP EN 1991-2.

The differences in the obtained results come from both shear lag and also bending (see Figure 6.20). In the first numerical example (section 6.2), the bending contributions matched unmistakenly. Here slight differences exist due to the process of homogenisation (the flexural parcel of the classical bending stiffness should be calculated with a thickness ${t_t}^S = \frac{t_t}{\sqrt[3]{n}} \neq \frac{t_t}{n}$).

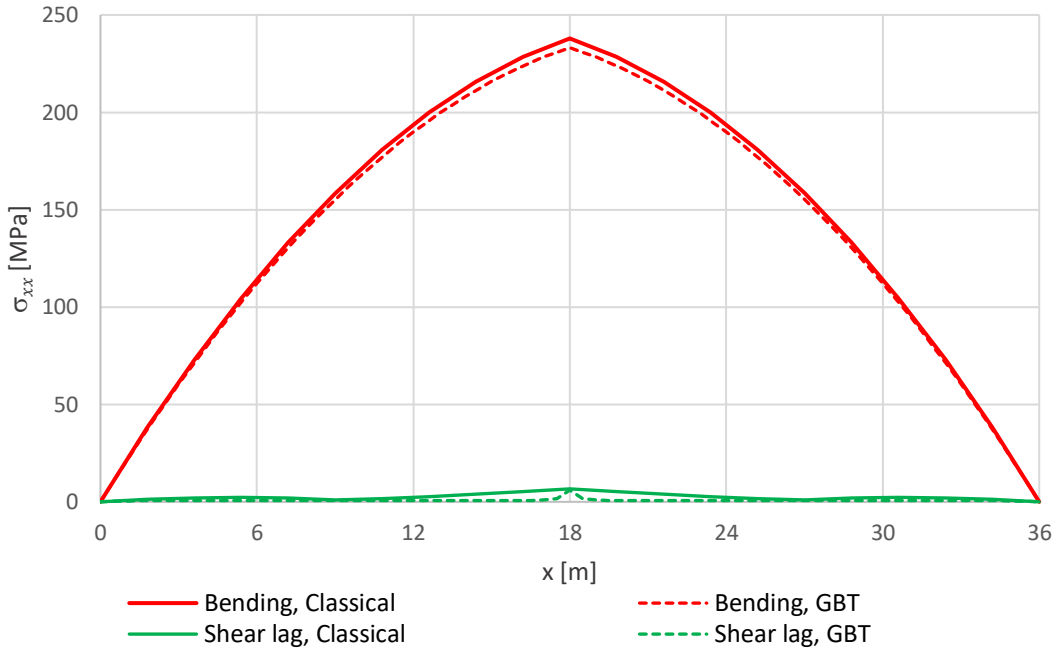

Figure 6.20 – Comparison of bending and shear lag modal participations to the maximum positive stresses

6.4. CRITICAL COMPARISON BETWEEN THE CLASSICAL FORMULATIONS AND GBT

The work presented up to this point aimed to extensively explain two different approaches, one corresponding to the Classical Formulations and another based on GBT-based finite elements. Here, the two are geared towards the longitudinal analysis of both homogenous and composite box-girder bridges.

Having addressed in Chapters 5 and 6 some comparisons in terms of theoretical fundaments and numerical examples, now a more critical comparative overview of the two methods are done, based on the results for the previously two case studies.

Starting with the Classical Formulations, the main advantage is its strong physical meaning, i.e., the separation of the global analysis into simpler, more understandable, sub-analyses of the load-carrying mechanisms. However, it is clear it entails some aspects that can be considered less positive:

a) the first is the level of simplifications that may be required in terms of the definition of the cross-section geometry; With a growing level of geometry complexity, the definition of the classical modes can become very complex (as an illustrative example one cannot consider

the definition of the distortional mode for the composite box-girder bridge analyses in case study 2 including the top steel flange width below the concrete slab).

b) A second drawback has to do with loss of accuracy resulting from some of the simplifying hypotheses assumed, especially regarding the torsion/distortion behaviour.

c) The third inconvenient is the need of several expressions (and coefficients in terms of the shear lag effect) that depend on the type of loading (concentrated or distributed) and boundary conditions. This has to do with the fact that the solutions to the equilibrium equations are obtained analytically and not by means of a finite element analysis.

d) Finally results in terms of longitudinal normal stress distributions are generally slightly higher with respect to results from GBT method.

Nevertheless, from a design point of view, and despite these inconveniences, this approach can still prove to be a fast and insightful tool, very valuable to obtain at least a first estimate of the longitudinal stresses due to bending with shear lag, torsion with warping and distortion.

The Generalized Beam Theory approach presents itself as somewhat of an upgrade of the first method, because it still maintains the possibility of analysing the participation of the several load-carrying mechanisms while considering a simpler, broader and less simplified formulation. Other strong aspects of this formulation are that:

a) Heterogeneous cross-sections, for instance composed by two materials, can be considered without adding any additional simplifications.

b) Also, more complex cross-sections can be considered quite easily, using the GBTUL program.

c) The same can be said for the subset of deformation modes, which can grow far beyond the scope of the Classical Formulations and thus capture other phenomena.

d) From a modal analysis standpoint, it was central to the determination of the effect of intermediate diaphragms to the modal participations of torsion and distortion, but the awareness of an elastically supported continuous beam behaviour comes more in the classical formulation for distortion.

e) About longitudinal normal stress distributions, they are very accurate and in line with shell element model normal stresses.

Referring finally to the designer's point of view, the GBT displacement-based finite element model developed in this work could be appealing, since it has provided results that are in very good agreement with those obtained with shell finite element models and at the same time made it possible to obtain significant insight into the mechanics of the problems addressed.

7. CONCLUSIONS AND FUTURE DEVELOPMENTS

7.1. CONCLUSIONS

The present dissertation revolves around the longitudinal analysis of both concrete and steel-concrete composite box girder decks, through two distinct methods of analysis that allow for a strong perception of the structural behaviours: one concerning the Classical Formulations and another based on the Generalized Beam Theory (GBT).

In Chapter 2, a brief reference was given to common methods used in the determination of longitudinal normal stresses, which among other aspects allowed to clarify the modal abilities of the Classical Formulations and of the GBT, when compared to the finite strip and shell finite element methods.

In Chapter 3, the classical theories for bending, torsion with warping and distortion were explained, including specific rules that enabled the analysis of steel-concrete composite box girders. The non-uniform torsion theory presented in this chapter uncouples the warping displacements from the in-plane rigid-body twist, meaning that it takes into account bi-shear deformation. Distortion is handled through the analogy of a beam on an elastic foundation, which considers the stiffness contributions given by longitudinal bending of the plates and by transverse frame behaviour. The effect of shear lag was also discussed by referring to a simplified methodology involving effective widths, whose accuracy was assessed.

The subdivision of the applied loading into the loads specific to each type of structural response reveals slight simplifications, namely concerning the determination of the distortional loads. Even though, the effect of bi-shear in torsion is taken into account in the calculation of the torsional warping stresses, its influence on distortion is dismissed.

The fundamental formulation of GBT was exposed in Chapter 4, considering the simplification hypotheses that are deemed necessary and sufficient for the analysis of box-girders subjected to standard vertical loads. The deformation field considered included bending, torsion with warping, torsion bi-shear, distortion, distortion bi-shear and both symmetric and anti-symmetric shear lag modes in the top and bottom flanges.

This chapter also encompassed the definition of a GBT-enriched finite element and its implementation in a developed MATLAB program that contains, among other aspects, a simplified interface for load input, the ability to normalize and/or orthogonalize the shear lag deformation modes and to include intermediate diaphragms.

In Chapter 5, a theoretical comparison was established between the two methods. It was possible to clarify some of the complexities found in the Classical Formulations and also discuss the differences found in both cross-section deformation modes and longitudinal equilibrium equations. From this comparison some conclusions were drawn:

1. The definition of the cross-section deformation modes in terms of membrane displacements is equivalent in bending, torsion with warping and distortion. Some minor

differences may occur in composite steel-concrete cross-sections due to the simplifications pertaining to the homogenisation rules.

2. The shear lag effect in these Classical Formulations is semi-empirical and entails a single global symmetric shear lag mode. GBT allows capturing shear lag through more modes, namely symmetric and anti-symmetric modes.
3. The GBT approach allows obtaining equations which are similar to the ones in Classical formulations, but more complex because they consider (i) several wall flexural contributions that are neglected in Classical Formulations and (ii) the coupling of bi-shear and distortion.

The analysis of two numerical examples was conducted in Chapter 6. In the first one, the shear lag modes were compared with shell FEM results and both total and modal results were subject of comparison between the Classical Formulations and GBT results. The second numerical example refers to a composite steel-concrete box girder bridge subjected to standard road traffic loads. It also covers the effect of various intermediate diaphragm configurations in both total and modal stresses. From these case studies, some additional conclusions can be drawn:

4. The longitudinal bending stresses in homogenous box girders are the same for both approaches. Small differences exist in composite steel-concrete box girders due to the simplification rule concerning homogenisation of the cross-section in bending employed in the Classical Formulations.
5. The Classical Formulations' shear lag effect in numerical example 1 does not show ideal agreement with the stress results from a shell finite element model, both in terms of longitudinal and cross-section diagrams. With the GBT approach it was possible to obtain results that agree very well with the shell FEM results. For this outcome, the presence of anti-symmetric shear lag modes was found relevant. For the numerical example 2, the shear lag effects are not as meaningful because the flanges are very narrow.
6. The results of torsion with warping are similar but do not coincide. For distortion, longitudinal stress results are further apart, due to the additional simplifications considered in the Classical Formulations and to the non-inclusion of distortion bi-shear.
7. The added torsional and distortional longitudinal stress profiles (including bi-shear) are similar to those obtained conducting the analysis of a continuous beam on an elastic foundation, when intermediate diaphragms are considered.
8. In light of the torsion/distortion behaviour observed in load case 2, three different load cases for the uniform loading were, covering the most unfavourable design situations: (i) the roadway is fully loaded, (ii) the roadway is loaded only on one side of the plane of symmetry and (iii) the roadway loading between each diaphragm is loaded only on one side of the plane of symmetry, but the side alternates after each span diaphragm.
9. It was observed that in the vicinity of diaphragms a rapid torsional and distortional warping stress variation occurs due to the coupling conditions of torsion, torsion bi-shear, distortion and distortion bi-shear.

Having performed comparisons between formulations and numerical results, at the end of Chapter 6 an overall critical comparison between the two methods led to the general main conclusions concerning the abilities each model as a design tool:

10. The increase in detail in the definition of the cross-section is easy to address in the GBT approach and is not simple in the Classical Formulations. Similarly, in the application of GBT, the existence of heterogeneous cross-section poses no problem, but for the Classical Formulations, some simplified homogenisation rules are required.
11. In overall, the Classical Formulations resort to more simplifications than GBT and this affects the accuracy of results, generally on the safe side.
12. The implementation of a GBT-based finite element avoids the need for several analytical solutions that depend on the type of loading and boundary conditions, as happens in Classical Formulations.
13. The consideration of the shear lag effect in GBT analysis is fairly simple. GBT is also more versatile and naturally more accurate than the use of effective width coefficients.
14. The Classical Formulations comprise a fast and insightful tool, very valuable to obtain a first estimate of the longitudinal stresses due to bending with shear lag, torsion with warping and distortion.
15. The GBT approach shows a great potential as a design tool, because it combines the possibility to analyse the participation of several deformation modes/structural behaviours while being based on a simple, broad and simplified formulation that can produce very accurate results.

7.2. FUTURE DEVELOPMENTS

In light of the promising results shown by the GBT-based finite element approach in the analysis of composite box girders, some of the possible extensions to this work include adding several aspects that need to be considered when analysing a steel-concrete composite bridge deck, namely:

- The influence of the construction stages;
- The existence of longitudinal stiffeners on the bottom flange and on the steel webs;
- The contribution of transverse stiffeners typically adopted in girder decks;
- The consideration in the analysis of the plate instabilities of the webs, due to shear and bending moments, and of the compressed bottom flange near the intermediate supports.

REFERENCES

B.S.I. BS 5400 - Steel, concrete and composite bridges. Part 3: Code of practice for design of steel bridges (2004).

B.S.I. BS 5400 - Steel, concrete and composite bridges. Part 5: Code of practice for design of composite bridges (2005).

Bathe, K. J. (2016). ADINA System. ADINA R&D Inc.

Bebiano, R., Gonçalves, R., & Camotim, D. (2015). A cross-section analysis procedure to rationalise and automate the performance of GBT-based structural analyses. *Thin-Walled Structures*, *92*, 29–47.

Benscoter, S. U. (1954). A theory of torsion bending for multicell beams. *Journal of Applied Mechanics*, *21*(1), 25–34.

Brazão Farinha, J. S., & Correia dos Reis, A. (1993). *Tabelas Técnicas*. P.O.B.

Calgaro, J. A. Virlogeux, M. (1988). *Projet Et Construction Des Ponts: Analyse Structurale Des Tabliers de Ponts*. Paris. Presses de l'Ecole Nationale des Ponts et Chaussées.

Camotim, D., Basaglia, C., & Silvestre, N. (2010). GBT buckling analysis of thin-walled steel frames: a state-of-the-art report. *Thin-Walled Structures*, *48*(10), 726–743

Castro, J. M., Elghazouli, A. Y., & Izzuddin, B. A. (2007). Assessment of effective slab widths in composite beams. *Journal of Constructional Steel Research*, *63*(10), 1317–1327.

Chen, Y. S., & Yen, B. T. (1980). *Analysis of Composite Box Girders, March 1980*. Fritz Laboratory Reports. Paper 447.

European Committee For Standardization. EN 1990:2002-A1. Eurocode - Basis of structural design. (2005).

European Committee For Standardization. NP EN 1990. Eurocódigo - Bases para o projeto de estruturas. Instituto Português da Qualidade (2009).

European Committee For Standardization. NP EN 1991-2. Eurocódigo 1 - Acções em estruturas. Parte 2: Acções de tráfego em pontes. Instituto Português da Qualidade (2005).

Fan, Z. T., & Helwig, T. A (2002). Distortional Loads and Brace Forces in Steel Box Girders. *Journal of Structural Engineering*, *128*(6), 710–718.

Gonçalves, R. (2014). Apresentações Power Point da Unidade Curricular de Lajes e Cascas. Faculdade de Ciências e Tecnologias, Universidade Nova de Lisboa.

Gonçalves, R., Bebiano, R., & Camotim, D. (2014). On the Shear Deformation Modes in the Framework of Generalised Beam Theory. *Thin-Walled Structures*, *84*, 325–334.

Gonçalves, R., & Camotim, D. (2010). Steel-concrete composite bridge analysis using Generalised Beam Theory. *Steel and Composite Structures*, *10*(3), 223–243.

Gonçalves, R., Ritto-Corrêa, M., & Camotim, D. (2010). A new approach to the calculation of

cross-section deformation modes in the framework of generalized beam theory. *Computational Mechanics*, *46*(5), 759–781.

Henriques, D., Gonçalves, R., & Camotim, D. (2015). A physically non-linear GBT-based finite element for steel and steel-concrete beams including shear lag effects. *Thin-Walled Structures*, *90*, 202–215.

Hetenyi, M. (1979). *Beams on elastic foundation: Theory with applications in the fields of civil and mechanical engineering* (11th ed.). The University of Michigan Press.

Kollbrunner, C.F., & Basler, K. (1969). *Torsion in Structures*. Berlin/Heidelberg: Springer-Verlag.

Křístek, V. (2004). A Shear Lag Analysis for Composite Box Girders with Deformable Connectors. *Acta Polytechnica*, *44*(5-6).

Lamas, A. R. G. (1982). *O problema do "shear lag" na análise de estruturas*. Seminário 286. Lisboa.

Maisel, B. I., & Roll, F. (1974). *Methods of analysis and design of concrete box beams with side cantilevers*. Cement and Concrete Association. London. (No. 42.494 Tech Rpt.).

Murray, Noel W. (1984). *Introduction to the theory of thin-walled structures*. Oxford [Oxfordshire] : Clarendon Press

Pedro, J. J. O. (1995). *Distorção em tabuleiros de pontes em caixão. Influência no comportamento longitudinal*. Tese de Mestrado. Universidade Técnica de Lisboa.

Salama, T., & Nassif, H. H. (2011). Effective flange width for composite steel beams. *Journal of Engineering Research*, *8*(1), 28–43.

Schardt, R. (1989). *Verallgemeinerte Technische Biegetheorie (Teoria Generalizada de Vigas)*. Berlin: Springer-Verlag.

Schlaich, J., & Scheef, H. (1982). *Concrete Box-Girder Brides*. Structural Engineering Documents IABSE, Stuttgart.

Silvestre, N., & Camotim, D. (2002). First-order generalised beam theory for arbitrary orthotropic materials. *Thin-Walled Structures*, *40*(9), 791–820.

The MathWorks Inc. (2014). MATLAB (R2014b). *The MathWorks Inc.* Massachussetts.

Vlasov, V. Z. (1961). *Tonkostenye sterjni, 2nd edn.* Moscow, Russia (French translation: "Piéces Longues en Voiles Minces", Éditions Eyrolles, Paris, France, 1962): Fizmatgiz.

Wright, R. N., Abdel-Samed, S. R., & Robinson, A. R. (1968). BEF Analogy for Analysis of Box Girder Bridges. *Journal of the Structural Division*, *94*.

Y.K.Cheung. (1976). *Finite Strip Method in Structural Analysis* (1st ed.). Pergamon Press.

Zienkiewicz, O. C., Taylor, R. L., & Zhu, J. Z. (2005). *The Finite Element Method Set*. Oxford: Butterworth-Heinemann

ANNEX 1. INDIVIDUAL GBT MODE PARTICIPATIONS FOR THE CONCENTRATED LOAD IN NUMERICAL EXAMPLE 1

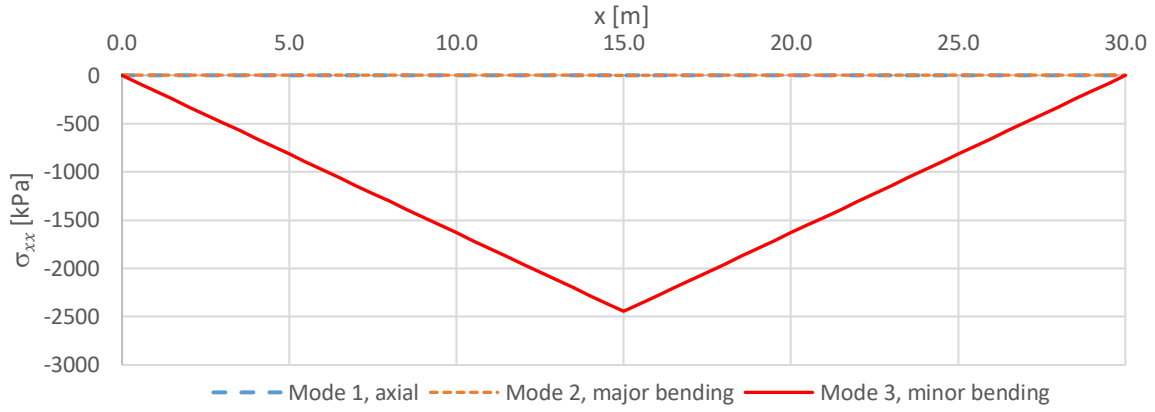

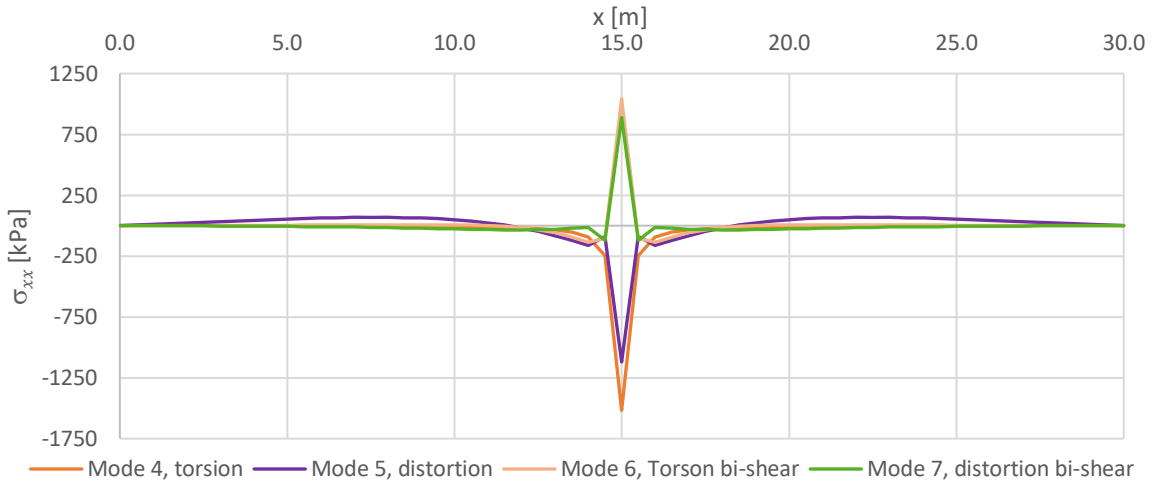

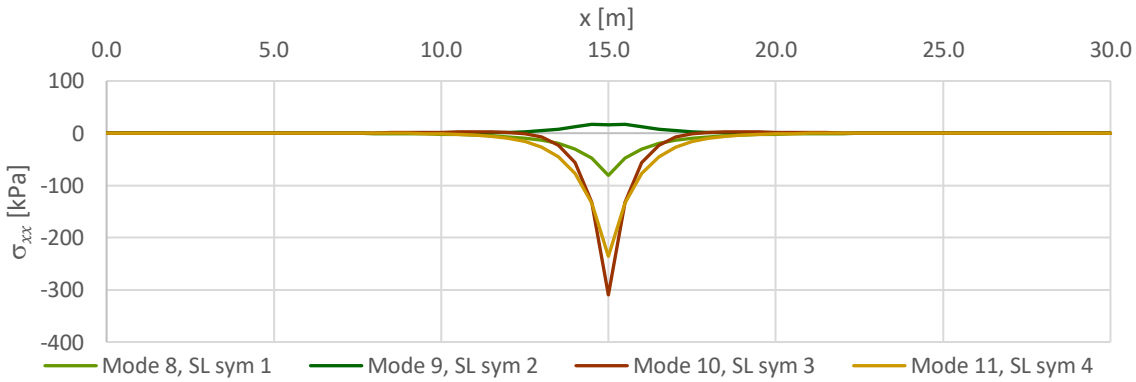

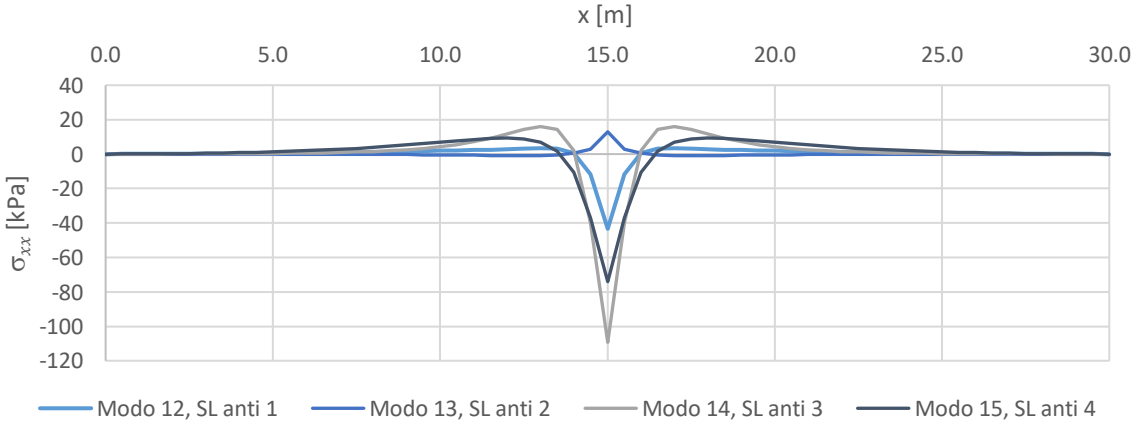

ANNEX 2. CLASSICAL AND GBT STRESS PARTICIPATIONS FOR THE DISTRIBUTED LOAD IN NUMERICAL EXAMPLE 1

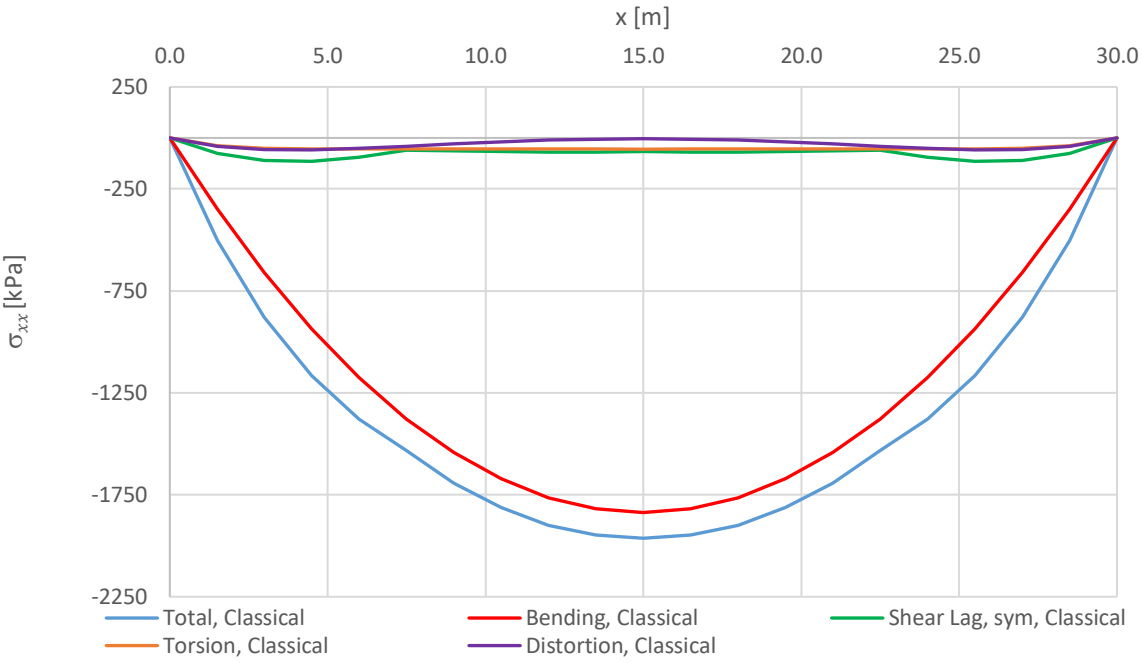

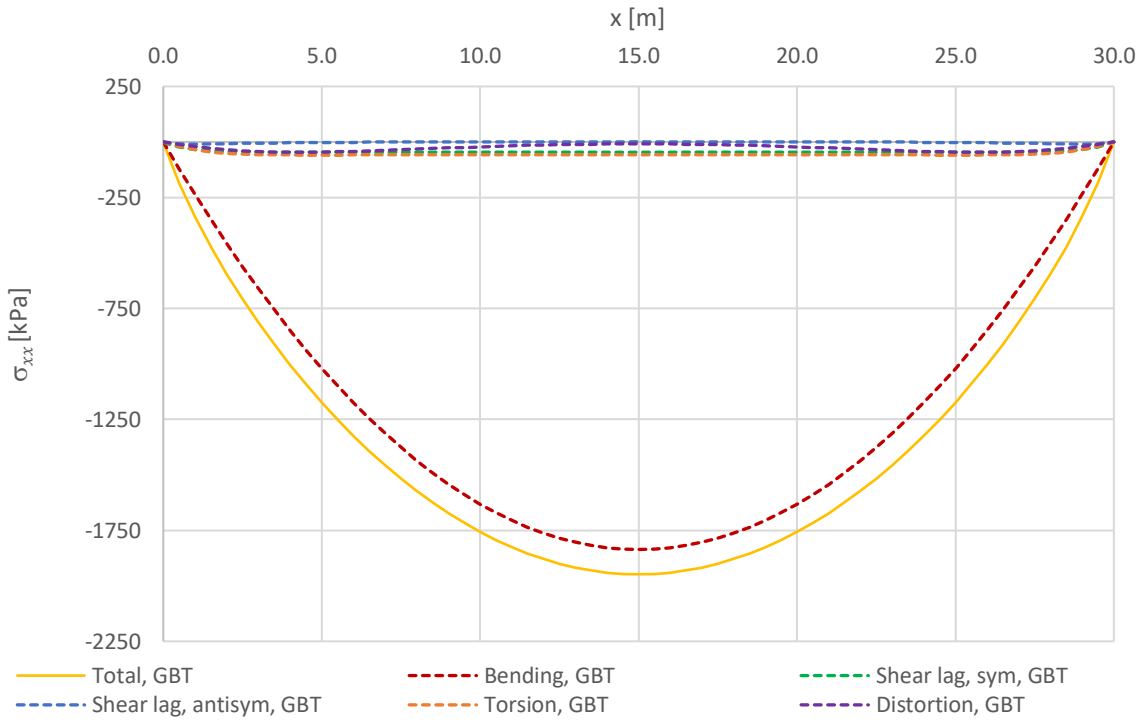

ANNEX 3. COMPARISON OF MODAL STRESS PARTICIPATIONS FOR THE UNIFORM LINE LOAD IN NUMERICAL EXAMPLE 2 FOLLOWING CLASSICAL FORMULATIONS AND GBT APPROACH

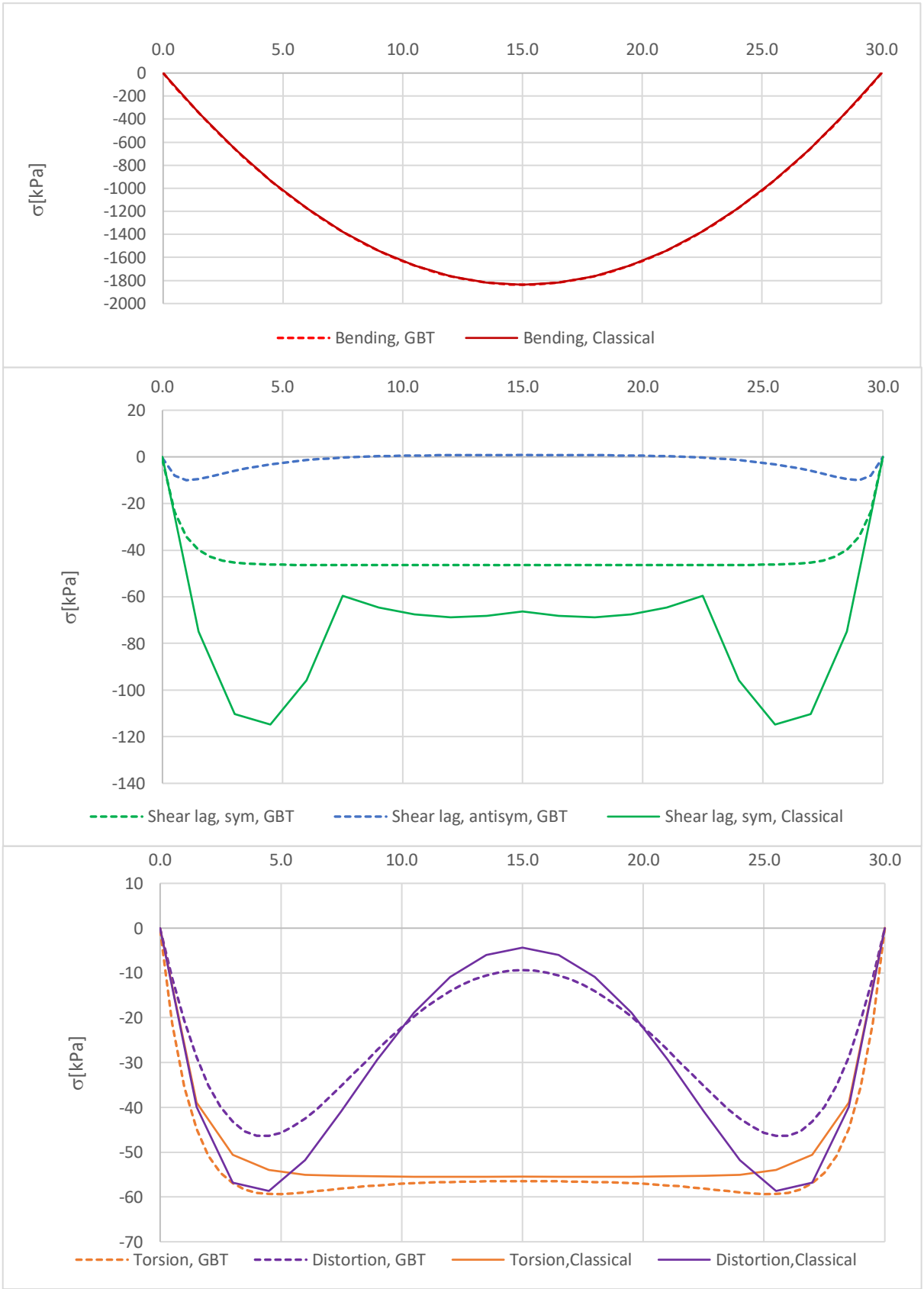

ANNEX 4. INDIVIDUAL GBT MODAL STRESS PARTICIPATIONS FOR THE UNIFORM LINE LOAD IN NUMERICAL EXAMPLE 2

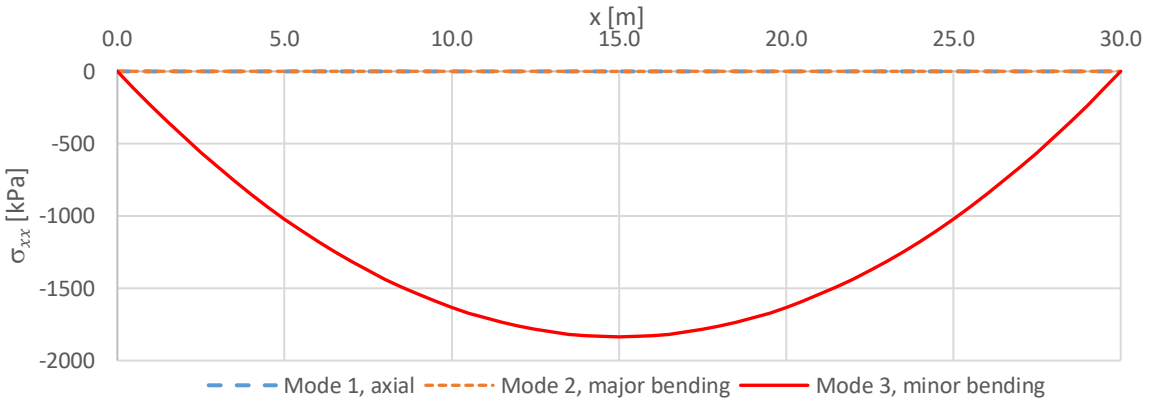

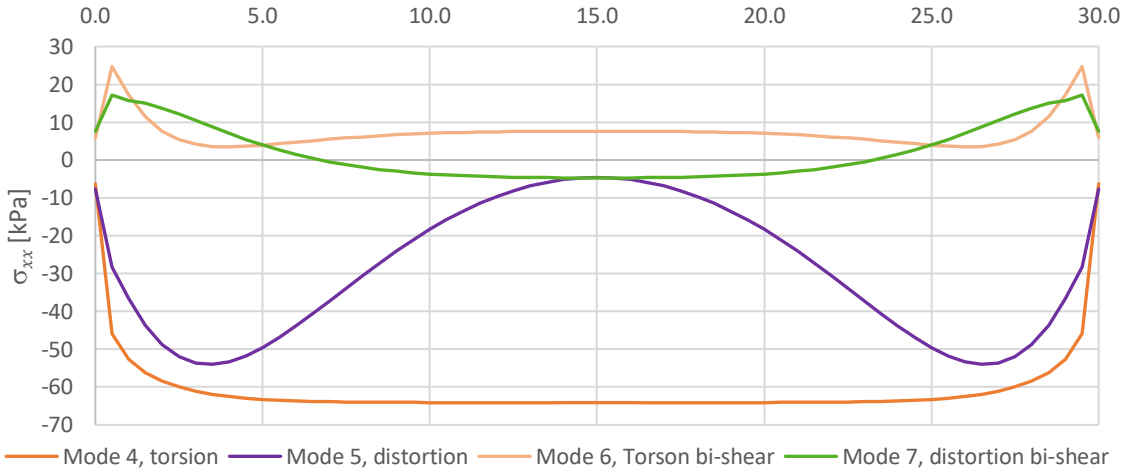

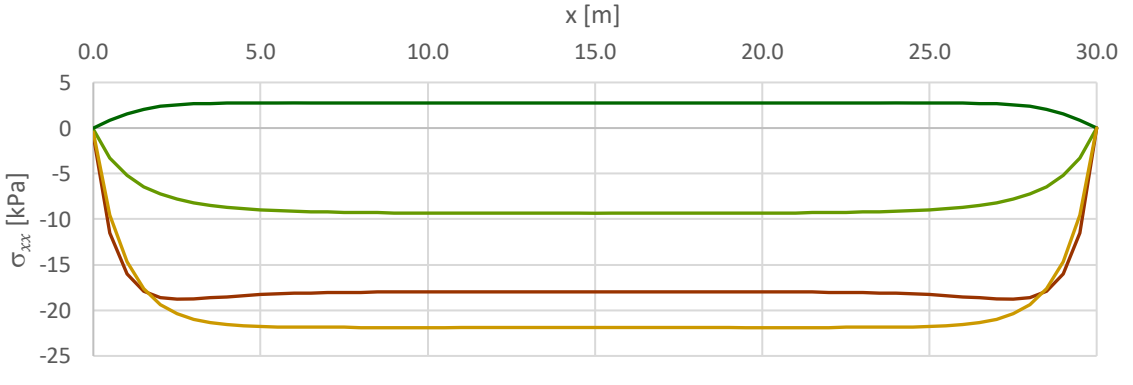

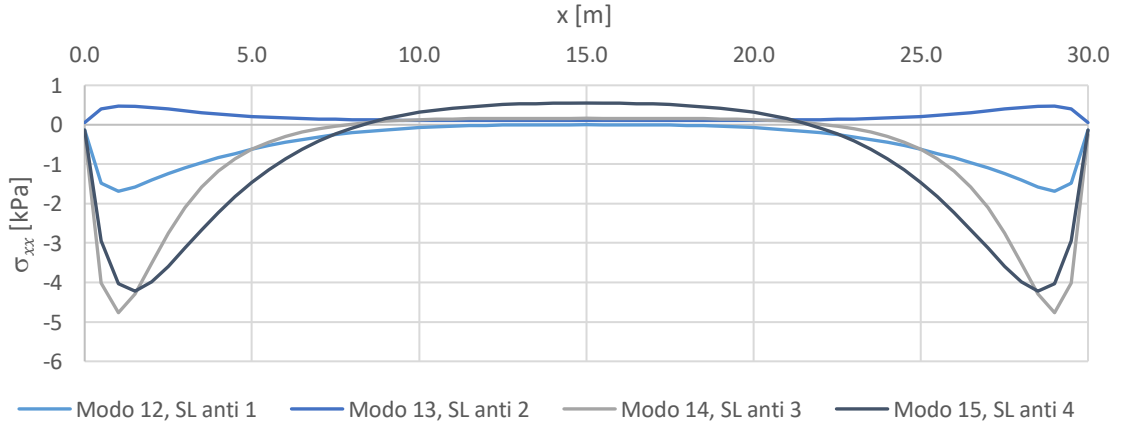

ANNEX 5. COMPARISON OF LONGITUDINAL STRESSES OBTAINED THROUGH CLASSICAL FORMULATIONS FOR NUMERICAL EXAMPLE 1 WITH PUBLISHED RESULTS FROM MAISEL & ROLL (1974)

Problem	Cross-section points (see Figure 3.11)	Stresses in Maisel & Roll [MPa][16]	Stresses in Classical Formulations [MPa]
Bending	1, 2, 5, 6	-2.46	-2.449
	3,4	4.53	4.512
Torsion with warping	1	0.44	0.448
	2	-0.44	-0.448
	3	0.50	0.488
	4	-0.50	-0.488
	5	0.37	0.342
	6	-0.37	-0.342
Distortion	1	0.37	0.362
	2	-0.37	-0.362
	3	1.53	1.521
	4	-1.53	-1.521
	5	-0.73	-0.726
	6	0.73	0.726

[16] The small differences between these published results and those obtained in this work vary solely due to the non-consideration of the reduction to the mid-line in I_{xx} and I_{yy}, and to the small numerical errors which are observed in Maisel & Roll (1974). Replicating the calculations described by the authors, the values are a complete match.